



THE HONG KONG
POLYTECHNIC UNIVERSITY

香港理工大學

Pao Yue-kong Library

包玉剛圖書館

Copyright Undertaking

This thesis is protected by copyright, with all rights reserved.

By reading and using the thesis, the reader understands and agrees to the following terms:

1. The reader will abide by the rules and legal ordinances governing copyright regarding the use of the thesis.
2. The reader will use the thesis for the purpose of research or private study only and not for distribution or further reproduction or any other purpose.
3. The reader agrees to indemnify and hold the University harmless from and against any loss, damage, cost, liability or expenses arising from copyright infringement or unauthorized usage.

IMPORTANT

If you have reasons to believe that any materials in this thesis are deemed not suitable to be distributed in this form, or a copyright owner having difficulty with the material being included in our database, please contact lbsys@polyu.edu.hk providing details. The Library will look into your claim and consider taking remedial action upon receipt of the written requests.

Pao Yue-kong Library, The Hong Kong Polytechnic University, Hung Hom, Kowloon, Hong Kong

<http://www.lib.polyu.edu.hk>

THE FUNCTIONAL ROLE OF
A NOVEL FOXM1/MDM1/110 PROTEIN COMPLEX IN
EMBRYONIC STEM CELLS AND
CANCER STEM-LIKE CELLS

HAO MING

Ph.D

The Hong Kong Polytechnic University

2015

The Hong Kong Polytechnic University

Departmental of Applied Biology and Chemical Technology

**The functional role of a novel
FOXM1/MYH10 protein complex in
embryonic stem cells and cancer stem-like
cells**

Hao Ming

**A thesis submitted in partial fulfillment of the requirements for
the degree of Doctor of Philosophy**

April 2014

Certificate of originality

I hereby declare that this thesis is my own work and that, to the best of my knowledge and belief, it reproduces no material previously published or written, nor material that has been accepted for the award of any other degree or diploma, except where due acknowledgement has been made in the text.

_____ (Signed)

Hao Ming (Name of student)

Abstract

The regulation of self-renewal in stem cells is maintained by promotion of proliferation and inhibition of differentiation, which holds the key answer to the process of ageing and the origin of cancer. In order to investigate the pertinent roles of ageing factors in human embryonic stem (ES) cell self-renewal, FOXM1, FOXO3A and SIRT1 were selected as baits for protein binding partners. From our study, we identified the novel endogenous protein interaction of FOXM1 with MYH10. We confirmed that blebbistatin, a chemical inhibitor of MYH10, can improve human ES cell survival and prevent differentiation with a poor outcome for colony formation in a dosage dependent manner, which is mediated through FOXM1 via inducing BCL-2 protein level and enhancing promoter binding of *OCT4*, respectively. The inhibitions of FOXM1 and MYH10 showed abnormality of both centriole locations and key regulators of mitosis, suggesting the essential roles of FOXM1 and MYH10 in cell-cycle progression in respect to stem cell self-renewal. Genetic knockdown of FOXM1 and MYH10 revealed the essential requirement of these two proteins in pluripotency maintenance as well as a distinctive role for MYH10 in the integrity of stem cell colony.

By applying our findings to CD44^{high}/CD24^{low} breast cancer stem-like cells, we found that FOXM1 and MYH10 are also major players in cancer stem-like cell maintenance. In terms of self-renewing ability, inhibition of MYH10 shows

improved spheroid formation ability in MCF breast cancer stem-like cells associated with Rho/ROCK pathway. This inhibition of MYH10 in turn is dependent on the tissue origin of the breast cancer compared with its isoform.

In conclusion, our findings of the protein complex of FOXM1 and MYH10 contributes to the understanding of the stem cell self-renewing mechanisms in both human embryonic and cancer stem-like cell models.

Acknowledgement

First of all, I would like to express my appreciation to my chief supervisor Prof. Dr. Wong Wing-tak for accepting me in his research group and offering me the opportunity to join PolyU Hong Kong, which would become my memorable adventure in my life.

During this adventure alone in Hong Kong, it is my most grateful to meet Dr. Man Wing-yin, Cornelia as my mentor for her humor and kindness to guide my research at PolyU. What I have learnt from her is not just the knowledge from textbooks but how to be a better person in a humble attitude. Her generous help and suggestions helped me solve the obstacles in my study and life. Her invaluable instructions will be my goals for my future work.

I am glad and thankful to be a member of two research groups. Without their help and accompanies, I can barely finish my research work. I would like to thank Dr. Lee Vien, Ms. Lee Liz and Ms. Chan Flora from Dr. Man's group with whom I spent most of my time to work together. I appreciated all their efforts and professional knowledge for helping my research work. It was a delightful time to work with all of you. I would also like to thank some of the members from Prof Wong's group: Dr. Yung Joseph, Dr. Law Ga-lai, Dr. Gu Yanjuan, Dr Yeung Chi-tong, Dr. Zheng xiangjun, Dr. Zheng Fuling, Dr. Fung Dorothy, Mr. Lo Summy, Mr. Yip Yuk-wang and members from the HKU group. We are a big

family bounded with joys every day.

I would also like to express my thanks to the technicians of the Department of Applied Biology and Chemical Technology, especially Dr. So Pui-Kin, Dr. Wong Gabriel, Mr. Cheng Chor-hing, Mr. Kwan Wing-kong, Miss. Yeung Sarah, Ms. Teo Ivy, Mr. Leung and Mr. Yung for their professional technical supports. Particularly, I would like to appreciate Dr. Shu yuanlan from the animal unit of PolyU Shenzheng and Miss. Yan Clare and Ms. Ho Joyce from PolyU Hong Kong for helping me process the animal studies. Although the animal experiments did not match the expectations, it is your considerations and generous help offered me the opportunity to pursuit my PhD work.

It is time to put a complete end of my three-year PhD study in Hong Kong. There are still many of people I would like to thank for during this journey. Sincerely, I want to thank my grandparents and parents. You are my concrete spiritual supports whenever I was frustrated of loneliness.

Thank you again for all those people who have helped me to live and study in Hong Kong.

Table of Contents

CERTIFICATE OF ORIGINALITY	I
ABSTRACT.....	II
ACKNOWLEDGEMENT.....	IV
TABLE OF CONTENTS.....	VI
ABBREVIATIONS	XI
LIST OF FIGURES AND TABLES	XVIII
CHAPTER 1 INTRODUCTION.....	1
1.1 The origins and mechanisms of pluripotent stem cells.....	1
1.1.1 Brief overview of human embryogenesis.....	1
1.1.2 The derivations of human embryonic stem cells.....	3
1.1.3 The extrinsic signaling for supporting pluripotency.....	4
1.1.4 Developmental state of human embryonic stem cells.....	8
1.1.5 Developmental potential and functional assays to assess the potential.....	10
1.1.6 Induced pluripotent stem cells reverse differentiation potential via epigenetic reprogramming.....	15
1.1.7 Intrinsic circuitry of pluripotency	17
1.2 Stems cells and the pathways to ageing and cancer.....	19
1.2.1 The mechanisms of ageing and stem cell model.....	19
1.2.2 The arising of cancer stem-like cell model during ageing.....	21
1.2.3 The role of FOXM1 in ageing.....	25
1.2.4 The mechanisms of FOXO3A in ageing.....	27
1.2.5 SIRT1 servers as a major ageing factor.....	30
1.3 The functions of non-muscle myosin II family in human embryonic stem cells.....	31
CHAPTER 2 MYH10 INTERACTS WITH FOXM1 IN HUMAN EMBRYONIC STEM CELLS	35
2.1 Introduction	35
2.1.1 H9 human embryonic stem (ES) cells and iPS _{IMR90} induced pluripotent stem (iPS) cells are well-characterized cell lines for stem cell research.....	35
2.1.2 SIRT1, FOXO3A and FOXM1 are pivotal ageing factors for self-renewal in stem cells	37
2.1.3 Non-muscle myosin II (MYH10/MYH9) is essential for the cell-cell contact to support	

stem cell self-renewal.....	38
2.1.4 The association of FOXM1 with E-CADHERIN and beta-CATENIN regulates self-renewal in human ES cells.	39
2.1.5 FOXM1 directly interacts with <i>OCT4</i> promoter to regulate self-renewal.....	40
2.1.6 FOXM1 and MYH10 are both important factors during asymmetric division.	41
2.1.7 Mechanistic action of blebbistatin, the chemical inhibitor of MYH10.	42
2.1.8 Specificity of FOXM1 inhibitor, thiostrepton.	44
2.1.9 The approach to study the function of the novel FOXM1 and MYH10 protein complex in human ES cells.....	44
2.2 Materials and Methods	46
2.2.1 Inhibitors and plasmids	46
2.2.2 Cell culture and transfection	46
2.2.3 Retroviral vector-based shRNA knockdown in human embryonic stem cells	47
2.2.4 Immunoprecipitation (IP) and Mass spectrometry	50
2.2.5 Western blot	50
2.2.6 Immunofluorescence (IF).....	52
2.2.7 Quantitative chromatin immunoprecipitation (ChIP) and data analysis.....	53
2.3 Results	56
2.3.1 Screening novel binding partners with three ageing factors in human ES cells.....	56
2.3.2 Morphological changes in blebbistatin and thiostrepton-treated H9 and iPESIMR90 cells.	65
2.3.2.1 Cell death and cell-cell dissociation in thiostrepton-treated H9 and iPESIMR90 cells.	65
2.3.2.2 Blebbistatin protected dissociated H9 and iPESIMR90 cells from cell death.	66
2.3.2.3 The effects of combined treatments in H9 and iPESIMR90 cells.	67
2.3.3 Reduced pluripotency observed in H9 and iPESIMR90 cells in MYH10 or FOXM1-depleted cells,	74
2.3.3.1 Inhibition of MYH10 by blebbistatin may improve self-renewal.	74
2.3.3.2 Pluripotency was declined during suppression of FOXM1 by thiostrepton.	75
2.3.3.3 Adding blebbistatin failed to rescue the loss of pluripotency triggered by repression of FOXM1 through thiostrepton.	75
2.3.3.4 BCL-2 protein level was restored when blebbistatin was applied with thiostrepton.	82
2.3.4 Adhesive pathway is involved with FOXM1 regulatory role in self-renewal in human ES cells	84
2.3.4.1 ROCK-MYOSIN pathway modulating adhesion via E-CADHERIN and beta-CATENIN in human ES cells is independent of FOXM1 expression.	84
2.3.4.2 FOXM1 is the important downstream of ROCK-Myosin pathway in response of pluripotency after dissociation.	85
2.3.5 Inhibition of the MYH10 and FOXM1 protein complex dysregulates specific mitotic markers during the self-renewal process of human embryonic stem cells.	90
2.3.5.1 Inhibition of MYH10 by blebbistatin altered AURORA B and KIF14 expression levels and affected the localization of CEP170 in ES cells.....	90
2.3.5.2 FOXM1 inhibition downregulated AURORA B and KIF14, and caused centrosomal	

amplification in ES cells.	91
2.3.5.3 The expression levels of AURORA B and KIF14 were restored by blebbistatin treatment in FOXM1-inhibited H9 cells.	91
2.3.6 Genetic knockdown of the MYH10 and FOXM1 complex in H9 human embryonic stem cells.	96
2.3.6.1 Genetic knock-down of MYH10 via retroviral gene transfer.....	96
2.3.6.2 Genetic knockdown of FOXM1 via retroviral gene transfer.....	97
2.3.6.3 Simultaneous knockdown of FOXM1 and MYH10 using shRNAs.	97
2.3.7 Knockdown of the FOXM1 and MYH10 complex affects pluripotency in H9 cells.	103
2.3.7.1 Genetic knockdown of FOXM1 downregulated OCT4, NANOG and SOX2 expression in human H9 cells.	103
2.3.7.2 Genetic knockdown of MYH10 reduced OCT4, NANOG and SOX2 expression in H9 cells.	103
2.3.7.3 Pluripotency is further reduced in double knockdown of MYH10 and FOXM1 H9 cells.....	103
2.3.8 Adhesive pathway was interfered in human embryonic stem cells depleted with FOXM1 and MYH10.	105
2.3.8.1 FOXM1 modulates ROCK1, E-CADHERIN and beta-CATENIN protein levels in H9 cells.	105
2.3.8.2 MYH10 regulates ROCK1, E-CADHERIN and beta-CATENIN expression levels in H9 cells.	106
2.3.8.3 E-CADHERIN was highly upregulated after double knockdown of FOXM1 and MYH10 in H9 cells.	106
2.3.9 Knockdown of the FOXM1 and MYH10 protein complex induced cytokinesis defects	109
2.3.9.1 FOXM1 is required for expression of the mitotic regulators AURORA B kinase and KIF14.	109
2.3.9.2 MYH10 monitors the proper expression of the mitotic regulators AURORA B kinase and KIF14.	109
2.3.10 Summary diagram.....	112
2.4 Discussion	114
2.4.1 MYH10 is a novel protein binding partner with FOXM1 in human embryonic stem cells.	114
2.4.2 Blebbistatin-treated cells exhibited increased viability.	114
2.4.3 Cell-cell interactions were regulated by Myosin and FOXM1 in human ES cells via E-CADHERIN/beta-CATENIN and ROCK axis.....	116
2.4.4 MYH10 exerts distinctive functions from MYH9 in modulating E-CADHERIN mediated adhesion in human embryonic stem cells.....	119
2.4.5 FOXM1 serves downstream of the adhesion pathway to monitor pluripotency in human embryonic stem cells.....	120
2.4.6 FOXM1 and MYH10 monitors the progression of cytokinesis in favor of symmetric division in human embryonic stem cells.....	122

CHAPTER 3 FUNCTIONAL ROLE OF MYH10 IN BREAST CANCER STEM-LIKE CELLS.126

3.1 Introduction	126
3.1.1 The heterogeneity of breast cancer and cancer stem-like cells.....	126
3.1.2 Breast cancer stem-like cells are preferentially maintained in non-adherent spherical culture condition.	127
3.1.3 The functional role of FOXM1 in cancer stem-like cells	128
3.1.4 Non-muscle myosin II plays important role in cancer stem-like cells metastasis.	129
3.1.5 The approach to study the function of FOXM1 and MYH10 in breast cancer stem-like cells.	130
3.2 Materials and Methods.	131
3.2.1 Inhibitors and plasmids.	131
3.2.2 Cell culture and transfection.	131
3.2.3 Cell viability assay.	132
3.2.4 Flow cytometry and Fluorescence-activated Cell Sorting (FACS).	133
3.2.5 Western blot.	134
3.2.6 Immunofluorescence (IF).....	134
3.3 Results	136
3.3.1 Identification of distinctive MYH9 and MYH10 expression in multiple cell lines.....	136
3.3.2 Rho GTPase and ROCK were induced by FOXM1 expression.	140
3.3.3 Expression of MYH10 and FOXM1 is required to maintain CD44 ^{high} /CD24 ^{low} breast cancer stem-like cells.	142
3.3.3.1 Inhibition of FOXM1 reduced the CD44 ^{high} /CD24 ^{low} breast cancer stem-like population.	142
3.3.3.2 Expression of MYH10 is essential for the support of CD44 ^{high} CD24 ^{low} breast cancer stem-like population.	143
3.3.4 MYH10 knockdown improves sphere-forming efficiency in sorted CD44 ^{high} /CD24 ^{low} MCF7 cells.....	150
3.3.5 CD44 ^{high} /CD24 ^{low} cells with MYH10 knockdown show decreased property of cancer stem-like cells.	152
3.3.6 ROCK-MYH10 pathway is responsible for the increased efficiency of MCF7 CD44 ^{high} /CD24 ^{low} sphere formation.....	155
3.3.7 ROCK inhibitor promotes CD44 ^{high} /CD24 ^{low} cancer stem-like population in breast cancer cells, which requires non-muscle myosin II participation.....	158
3.4 Discussion	162
3.4.1 Verification and isolation of CD44 ^{high} /CD24 ^{low} breast cancer cells with cancer stem-like cell characteristics.	162
3.4.2 Justification of the potential role of FOXM1 in promoting the maintenance of cancer stem-like cells in breast cancer.....	163
3.4.3 MYH10 expression is essential to support the cancer stem-like component in breast cancer.	164

3.4.4 Rho kinase inhibitor facilitating mammosphere formation is associated with MYH10 expression.	165
CHAPTER 4 CONCLUSION AND SUGGESTIONS FOR FUTURE STUDY.....	167
4.1 Conclusion.....	167
4.2 Suggestions for future study.....	168
4.2.1 Potential binding of MYH10 with FOXO3A and SIRT1 in human embryonic stem cells.	168
4.2.2 Clarification of a differential function of MYH10 from MYH9 in human embryonic stem cell.....	169
4.2.3 Validation the function of MYH10 and FOXM1 during mitosis for determination of symmetric or asymmetric division.	170
4.2.4 Mechanisms of MYH10 and FOXM1 in cancer stem-like cells.	171
APPENDIX I.....	173
APPENDIX II.....	175
APPENDIX III.....	177
REFERENCES.....	181

Abbreviations

2-D	2-dimentional
2i	Dual inhibition of ERK and GSK3
3-D	3-dimentional
3i	Three inhibitors targeting FGFR, ERK and GSK3
ABCB5	ATP-binding cassette transporter B5
ABCG2	ATP-binding cassette sub-family G member 2
ADP	Adenosine diphosphate
AKT	Protein kinase B
ALDH1	Aldehyde dehydrogenase 1
APC	Allophycocyanin
ATCC	American Type Culture Collection
ATP	Adenosine triphosphate
ATPase	Adenylpyrophosphatase
BCL-2	B-cell lymphoma-2
bFGF	Basic fibroblast growth factor
BMI-1	B lymphoma Mo-MLV insertion region 1
BMP4	Bone morphogenetic protein-4
BSA	Bovine serum albumin
CD	Cluster of differentiation

CDK	Cyclin dependent kinases
CDX2	Caudal-type homeodomain protein-2
CENP F	Centromere protein F
CEP170	Centrosomal protein 170kDa
CEP55	Centrosomal protein 55kDa
C-MYC	v-Myc avian myelocytomatosis viral oncogene homolog
CR	Caloric restriction
CSC	Cancer stem-like cell
Ct	Cycle threshold
DMEM	Dulbecco's Modified Eagle's Medium
DMSO	Dimethyl sulfoxide
DTT	Dithiothreitol
EB	Embryonic body
EC	Embryonic carcinoma
ECL	Enhanced chemiluminescence
EDTA	Ethylenediaminetetraacetic acid
EG	Embryonic germ
EGTA	Ethylene glycol tetraacetic acid
EMT	Epithelial mesenchymal transition
EPCAM	Epithelial cell adhesion molecule
EpiSCs	Epiblast stem cells

ERK	Extracellular signal-regulated kinases
ES	Embryonic stem
ESA	Epithelial -specific antigen
ESRRB	Estrogen-related receptor β
FACS	Fluorescence-activated cell sorting
FGF	Fibroblast growth factor
FOXM1	Forkhead box protein M1
FOXO	Forkhead box protein O
FOXO3a	Forkhead box protein O3A
GAPDH	Glyceraldehyde-3-phosphate dehydrogenase
GCTM-2	Podocalyxin-like precursor isoform-2
GFP	Green fluorescent protein
GP130	Glycoprotein 130
GSK3	Glycogen synthase kinase-3
H3K27me3	Trimethylation of histone H3 lysine 27
H3K4me3	Trimethylation of histone H3 lysine 4
H3K9	Histone H3 lysine 9
H3K9ac	Acetylation of histone H3 lysine 9
H4K16	Histone H4 lysine 16
HDAC	Histone deacetylase complexes
HEPES	4-(2-hydroxyethyl)-1-piperazineethanesulfonic acid
HNF-4	Hepatocyte nuclear factor-4

HRP	Horscradish peroxidase
HSCs	Hematopoietic stem cell
ICM	Inner cell mass
ID	Inhibitor of differentiation
IGF2	Insulin like growth factor-2
IgG	Immunoglobulin G
IP	Immunoprecipitation
iPS	Induced pluripotent stem cells
IVF	<i>In vitro</i> fertilization
JAK	Janus kinase
JARID2	Jumonji- and AT-rich interactive domain-2
JNK	Jun N-terminal kinase
KIF14	Kinesin family member 14
KLF4	Kruppel-like factor-4
LIF	Leukemia inhibitory factor
LIFR	Leukemia inhibitory factor receptor
MALD-TOF	Matrix-assisted laser desorption/ionization time-of-flight
MAPK	Mitogen-activated protein kinase
MEF	Mouse embryonic fibroblast
MEK	MAP kinase-ERK kinase
MET	Mesenchymal to epithelial transition

MLC	myosin light chain
MLCK	myosin light chain kinase
MST1	Mammalian sterile 20-like kinase-1
MYH10	Non-muscle myosin heavy chain 10
MYH14	Non-muscle myosin heavy chain 14
MYH9	Non-muscle myosin heavy chain 9
NAD ⁺	Nicotinamide adenine dinucleotide
N-CAM	Neural cell adhesion molecule
NF- κ B	Nuclear factor kappa-B
NMHCII	Non-muscle myosin heavy chain II
NMII	Non-muscle myosin II
NOD-SCID	Non-obese diabetic severe combined immunodeficient mouse
NP-40	Nonidet P-40 (Octylphenoxypolyethoxyethanol)
Non-muscle myosin II	MYH9/MYH10
OCT4	Octamer-binding transcription factor 4
PAX-6	Paired box protein-6
PBS	Phosphate buffered saline
PcG	Polycomb group protein
PCR	Polymerase chain reaction
PE	R-Phycoerythrin
Pi	Phosphate bound

PI(3)K	Phosphatidylinositol-3-OH-kinase
PIPES	Piperazine-1,2-bis[2-ethanesulfonic acid]
PKB	Protein kinase B
PROS	Prospero
PVDF	Polyvinylidene fluoride
RIF1	RAP interacting factor-1
ROCK	Rho-associated kinase
ROS	Reactive oxygen species
rpm	Rotation per minute
SALL4	Sal-like-4
SD	Standard deviation
SDS	Sodium dodecyl sulfate
SDS-PAGE	Sodium dodecyl sulfate polyacrylamide gel electrophoresis
SHP2	Protein tyrosine phosphatase containing Src Homology 2
shRNA	Short hairpin RNA
siRNA	Small interfering RNA
SIRT1	Sirtuin (silent mating type information regulation 2 homolog)-1
SKP2	S-phase kinase-associated protein 2
SMAD	Mothers against decapentaplegic homolog

	SWI/SNF-related, matrix-associated
SMARCAD1	actin-dependent regulator of chromatin containing DEAD/H box-1
SOX2	SRY-related high mobility group-box protein-2
SSEA	Stage-specific embryonic antigen
STAT3	Signal transducer and activator of transcription-3
TBE	Tris-Borate-EDTA buffer
TBS	Tris-buffered saline
TCF3	T cell factor-3
TEMED	N,N,N',N'-tetramethylethylenediamine
TGF β	Transforming growth factor- β
TWIST1	Twist basic helix-loop-helix transcription factor 1
TUNEL	Terminal deoxynucleotidyl transferase dUTP nick end labeling
UV	Ultra-violet
WNT	Wingless type protein
ZFX	Zinc finger protein, X-linked

List of Figures and Tables

Figure 1.1 Schematic diagram of the developmental events regarding the derivation of cell type and tissues.....	3
Figure 1.2 Extrinsic signaling for pluripotency in mouse and human embryonic cells.	7
Figure 1.3 Models of differential potential for stem cells.....	11
Figure 1.4 Schematic diagram of variants of human FoxM1 protein.....	27
Figure 1.5 Schematic summary of possible pathways involving dissociation induced apoptosis in human embryonic stem cells.....	33
Figure 2.1.1 Schematic diagram for the mechanism of blebbistatin inhibition of non-muscle myosin II.....	43
Figure 2.3.1 Screening novel binding partners with three ageing factors in human embryonic stem cells.....	58
Figure 2.3.2 Mascot analysis of the peptide spectrums from mass spectrometry for FOXM1 and SIRT1 at band 225K.....	60
Figure 2.3.3 Co-immunoprecipitation of MYH10 with FOXM1, FOXO3A and SIRT1 in human embryonic stem cells.....	64
Figure 2.3.4 Inhibition of FOXM1 induced cell death in human embryonic stem cells.....	68
Figure 2.3.5 Characterization of H9 and iPS _{IMR90} cells after chemical inhibitions	

of FOXM1 and MYH10.....	70
Figure 2.3.6 Chemical inhibition of MYH10 with blebbistatin and FOXM1 with thiostrepton.....	72
Figure 2.3.7 MYH10 associated with FOXM1 regulates human embryonic stem cells self-renewal.....	78
Figure 2.3.8 FOXM1 interacted with the <i>OCT4</i> promoter associated with NMIIB.....	80
Figure 2.3.9 Inhibition of MYH10 by blebbistatin can improve the survival of human embryonic stem cells.....	83
Figure 2.3.10 FOXM1 and MYH10 regulates self-renewal through cell-cell interaction.....	88
Figure 2.3.11 Down-regulated FOXM1 and MYH10 interrupted cytokinesis and mitotic exit.....	95
Figure 2.3.12 Specific knockdown of FOXM1 and MYH10 via retroviral gene transfer.....	101
Figure 2.3.13 Depletion of MYH10 and FOXM1 induced the loss of pluripotency.....	104
Figure 2.3.14 Depletion of MYH10 but FOXM1 increased the protein level of E-CADHERIN.....	107
Figure 2.3.15 Depletion of MYH10 and FOXM1 deregulated cytokinesis and mitotic exit.....	111
Figure 3.3.1 Expressions of non-muscle myosin II isoforms are distinctive in	

varied cell types.....	138
Figure 3.3.2 Expression of FoxM1 induced the protein level of Rho GTPase and its effector Rho-associated protein kinase.....	141
Figure 3.3.3 Identifications of CD44 ⁺ /CD24 ⁻ subpopulations in breast cancer cell lines after MYH10 and FOXM1 knock down by flow cytometry.....	148
Figure 3.3.4 Inhibition of MYH10 improves sphere-forming efficiency from CD44 ^{high} /CD24 ^{low} breast cancer stem-like cells.....	151
Figure 3.3.5 Inhibition of MYH10 in CD44 ^{high} /CD24 ^{low} MCF7 spheroids showed reduced characteristics of cancer stem-like cells.....	154
Figure 3.3.6 Expression of MYH10 can suppress the sphere-forming efficiency from breast cancer stem-like cells.....	157
Figure 3.3.7 Identifications of CD44 ⁺ /CD24 ⁻ subpopulations in breast cancer cell lines treated with Y27632 regarding to MYH10/MYH9 level by flow cytometry.....	160
Table 1.1 Comparisons of naïve and primed pluripotent stem cell lines with distinctive phenotypes.....	9
Table 1.2 Major molecular markers for pluripotency and differentiation.....	14
Table 1.3 Surface markers applied for the identification of cancer stem-like cells in different tissues.....	24
Table 2.2.1 Sequences of shRNA sequences for human embryonic stem cell infection.....	49
Table 2.2.2 Primary and secondary antibodies for western blot and	

immunoprecipitation study in human embryonic stem cells	52
Table 2.2.3 Sequences of primers designed for ChIP assay.....	55
Table 2.3.1 List of selected potential interactions between ageing factors discovered by mass spectrometry.....	62
Table 2.3.2 Summary diagram of MYH10 interacts with FOXM1 in human embryonic stem cells.	113
Table 3.2.1 Fluorochrome conjugated antibodies for FACS analysis.....	134
Table 3.2.2 Primary antibodies for western blot analysis in breast cancer stem-like cell research.....	134

Chapter 1 Introduction

1.1 The origins and mechanisms of pluripotent stem cells.

1.1.1 Brief overview of human embryogenesis.

The fundamental processes of life cycle consist of six stages: fertilization, cleavage, gastrulation, organogenesis, metamorphosis and gametogenesis. For human, the period of the primary eight weeks of development was called embryogenesis after fertilization, when the fusion of the male sperm and the female oocyte occur to form the zygote. The first cleavage to 2 cells takes place 24 hours later in a manner of meridional mitotic division, in which the cleavage furrow formation should be accomplished within around 14 minutes to the appearance of 2-cell stage¹. The rotational cleavage happens after about 12 hours and carries the daughter cells into 4-cell stages within around 2 hours¹. A 16-cell morula stage is reached in successive divisions, when the embryo is experiencing compaction to form a compact sphere, and cell adhesion proteins such as E-CADHERIN start to express. The first differentiation event arises at morula stage when the outer rim of the sphere becomes the trophoblast to form the outer layer of the placenta. And the inner cells will ultimately develop to embryo. At embryonic day 5, the morula forms a cavity with fluid from the secretion of trophoblast, which develops into a hollow sphere called blastocyst. The blastocyst hatches from the zona pellucida and gets ready for implantation by attachment

with the endometrium at embryonic day 6-7.

During the second week of human embryogenesis, the implanted blastocyst forms an embryonic disk (egg cylinder in mice) and begins to establish and develop of the placenta to provide the embryo with nutrients from maternal blood for further development. Meanwhile, the inner cell mass (ICM) derived from the morula stage continued to differentiation into two layers of cells: hypoblast and epiblast. The hypoblast will later develop to the primitive endoderm, which will give rise to the wall of yolk sac. Alternatively, epiblast will contribute to all the cells of the three primary germ layers. And a small cavity is formed within the epiblast and eventually filled with amniotic fluid to become amniotic cavity surrounding the fetus.

At the third week of human development, the start of gastrulation is triggered by the differentiation of epiblast into amniotic ectoderm and primitive ectoderm. Later, the primitive ectoderm of the postimplantation blastocyst will generate the ectoderm, mesoderm and endoderm of the gastrula, resulting in the formation of corresponding tissues and organs in the adults. The whole event is strictly monitored and tuned through activation or inactivation of specific genes at the enquiring time in response of cell to cell and to extracellular matrix interactions².

The brief summary of human embryogenesis is illustrated in Fig. 1.1. When not stated otherwise, details refer to references^{3,4}.

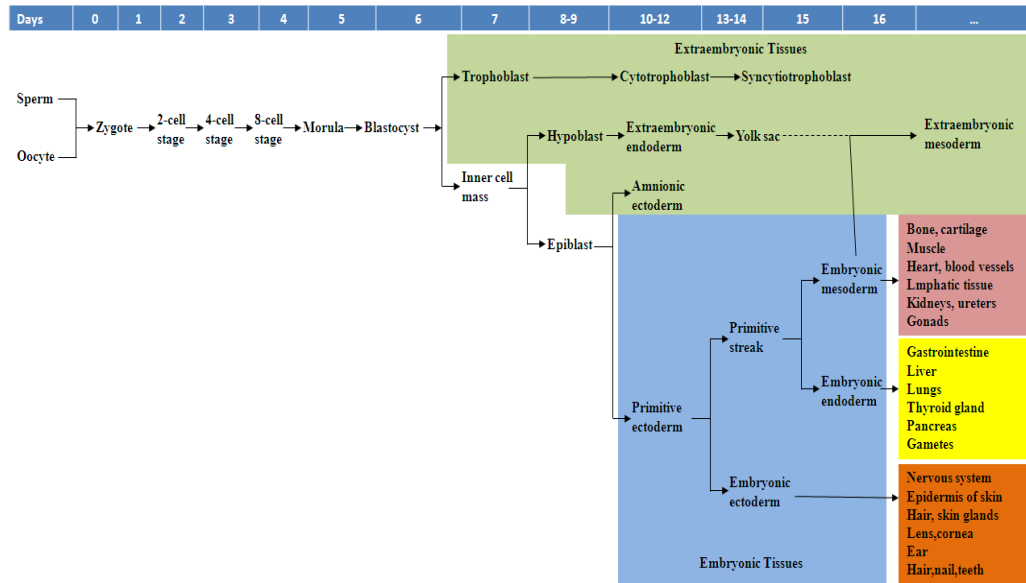


Figure 1.1 Schematic diagram of the developmental events regarding the derivation of cell types and tissues. The approximate duration of each stage was measured with embryonic days after the formation of zygote. The dashed line indicates a possible origin of extraembryonic mesoderm from Yolk sac.

1.1.2 The derivations of human embryonic stem cells.

As allude in 1.1.1, there are certain types of cells, namely embryonic stem (ES) cells, in the early development which harbor the capacities to give rise of all types of cells in the adulthood. However, ES cells only exist transiently in embryos *in vivo* as they undergo differentiation with progressively loss their potentials during development. The attempts of isolation of ES cells benefited from the study of teratocarcinomas in 1950s, which are malignant germ cell tumors that comprise an undifferentiated embryonic carcinoma (EC) component and a differentiated component containing all three germ layer⁵. In 1981, the

derivation of mouse ES cells captured and preserved the pluripotency from *in vivo* blastocyst into *in vitro* laboratory culture condition, which supported with EC-conditioned medium⁶ or with mitotically inactivated mouse embryonic fibroblast (MEF) and serum⁷. Unlike EC cells, mouse ES cells have normal karyotypes and are sufficient to generate chimeras when injected into embryos. Meanwhile, in contrast with their origins from ICM, mouse ES cells can be propagated infinitely *in vitro* owing to their ability of self-renewal.

The derivation of human ES cells seems to be considerably delayed until 1998, when Thomson used embryos from *in vitro* fertilization (IVF) to generate human ES cells⁸. The delay resulted from the differences of ES cells between species and the optimization of human embryo culture medium. Human ES cell lines have been derived from different stages of embryo: morula⁸, later blastocyst⁹, single blastomeres¹⁰ and parthenogenetic embryos¹¹, from which the characteristics varied depending on the timing and techniques of derivations¹². H1, H7, H9, H13 and H14 are five human ES cell lines generated by Thomson from the inner cell mass of human blastocysts via immunosurgery⁸. These five original human ES cell lines can continue to proliferate without commitment for up to 6 months¹³, within which H9 cell line has divided for around two years with over 300 passages¹⁴.

1.1.3 The extrinsic signaling for supporting pluripotency.

It was revealed by *in vitro* study that the hallmarks of ES cells are

pluripotency and self-renewal, which are supported by specific signaling pathways and intrinsic transcription networks. The understanding of critical signaling pathways for pluripotency arose from the process of modifications and identifications of soluble growth factors from defining culture medium and feeder cells. Amongst them, leukemia inhibitory factor (LIF)¹⁵ and bone morphogenetic protein-4 (BMP4)¹⁶ were identified to be the indispensable cytokine to sustain mouse ES cells in undifferentiated condition without serum supply. In LIF pathway, LIF receptor (LIFR) acts with LIF and induces the dimerization with GP130 receptor¹⁷, which subsequently recruits and activates the Janus kinase/signal transducer and activator of transcription-3 (JAK/STAT3)¹⁷, and SHP2/ERK mitogen-activated protein kinase (MAPK) cascade¹⁸. The activation of STAT3 promotes the self-renewal of mouse ES cells while the activation of ERK hinders proliferation. Therefore, a balanced effect of LIF is imposed to mouse ES cell for tuning the state of pluripotency¹⁹. In BMP pathway, BMP4 induces the level of inhibitor of differentiation (ID) protein to prevent commitment by inhibiting ERK activity via the SMAD pathway¹⁶. Although LIF is essential for *in vitro* mouse ES cells derivation and maintenance, there is no apparent requirement for the LIF cascade for *in vivo* mouse development until gastrulation²⁰⁻²². It suggests that additional pathways are involving in maintaining pluripotency. Wingless type (WNT) signaling pathway was found to exert synergistic effect on LIF in preventing differentiation²³. The binding of WNT proteins with FRIZZLED receptors inhibits the activity of

glycogen synthase kinase-3 (GSK3) resulting in the stabilization and nuclear translocation of beta-CATENIN for TCF proteins mediated gene activation for self-renewal²⁴. Based on those findings, a defined condition of the dual inhibition (2i) of FGF4/ERK and GSK3 has been applied to sustain mouse ES cells with chemical inhibitors independent of LIF and BMP through inactivation of ERK signaling²⁵ and promoting WNT pathway²⁴. This approach has also been successfully applied to derive ES cells from non-permissive mouse strains^{26,27}.

As one of the challenges for derivation of human ES cells (refers to 1.1.2), LIF cascade failed to support human ES cells in medium containing serum as how it acted to sustain mouse ES cells^{8,28,29}. There are only very low levels of LIF/LIFR, GP130 and JAK detected in human ES cells³⁰. In contrast, addition of BMP in culture condition will promote trophoblast differentiation in human ES cells³¹ in spite of the fact that BMP pathways are detectable in human ES cells³². Further investigations found that opposing to mouse embryonic cells alternative pathways: basic fibroblast growth factor (bFGF)^{33,34}, transforming growth factor- β (TGF β)³⁵ and insulin-like growth factor 2 (IGF2)³⁶ are major important signaling pathways in the self-renewal of human ES cells. bFGF (FGF2) was the first cytokine identified to be crucial of human ES cell maintenance³⁴. The high level of bFGF produced by human ES cell FGF receptors or supplemented in the culture medium acts with ERK pathway to prevent the spontaneous differentiation into extra-embryonic tissues^{37,38}. It was also suggested that bFGF cooperate with TGF β /ACTIVIN pathway through SMAD2/3 to activate *NANOG*

expression in human ES cells^{35,37}. ACTIVIN was shown to activate bFGF expression^{39,40}, and bFGF reciprocally induce TGFβ/ACTIVIN activity⁴⁰, of which seemed to be redundant when one component was at sufficient dosage in medium^{35,41}. IGF2 inhibits human ES cells from differentiating into endodermal cells via activation of phosphatidylinositol-3-OH kinase (PI(3)K)⁴¹. Current findings have led to understand the relationship between extrinsic factors with their downstream intracellular signal pathways for better manipulation and directing the differentiation of stem cells. A brief summary of extrinsic pathways for mouse and human ES cell self-renewal and differentiation is illustrated in Fig. 1.2. When not stated otherwise, details refer to references⁴²⁻⁴⁴.

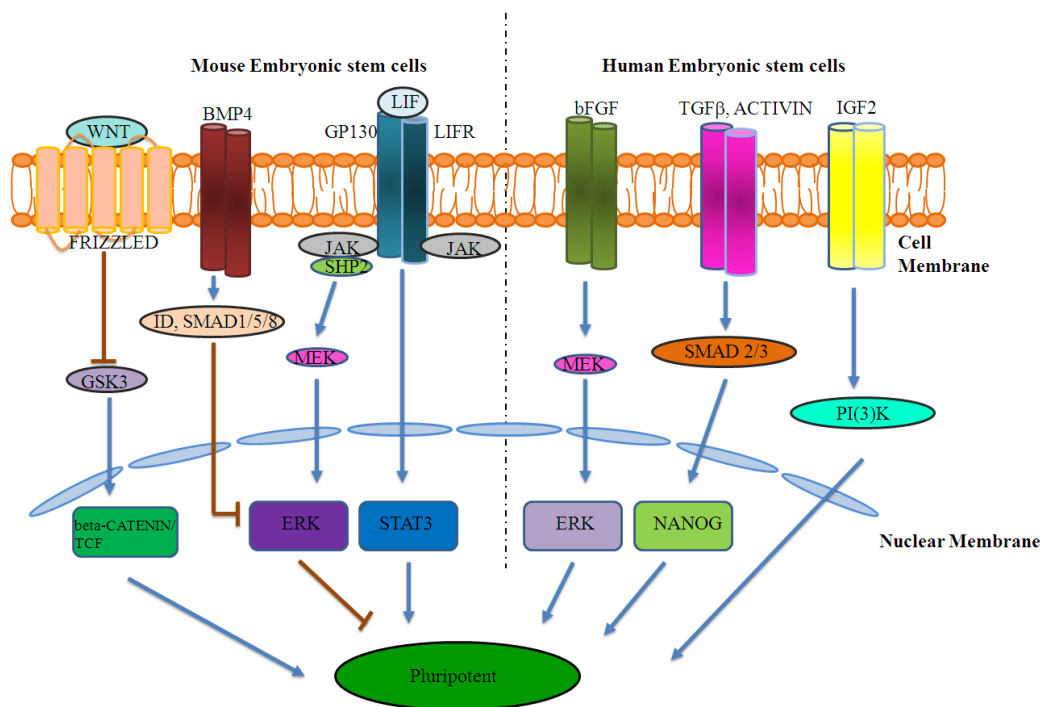


Figure 1.2 Extrinsic signaling for pluripotency in mouse and human embryonic cells. Signaling mediated through members of the leukemia inhibitory factor (LIF), bone morphogenetic protein (BMP4) and Wingless type (WNT) signaling pathway in mouse ES cells (*left*) and basic fibroblast growth

factor (bFGF), transforming growth factor- β (TGF β) and insulin-like growth factor 2 (IGF2) pathways in human ES cell (*right*) convergent into different nuclear targets for regulations of pluripotency. WNT, Wingless type protein. GSK3, Glycogen synthase kinase-3. TCF, Transcription factor. BMP4, Bone morphogenetic protein-4. ID, Inhibitor of differentiation. SMAD, Mothers against decapentaplegic homolog. LIF, Leukemia inhibitory factor. LIFR, Leukemia inhibitory factor receptor. GP130, Glycoprotein 130. JAK, Janus kinase. SHP2, Protein tyrosine phosphatase containing Src Homology 2. MEK, MAP kinase-ERK kinase. ERK, Extracellular signal-regulated kinases. TGF β , Transforming growth factor- β . IGF2, Insulin like growth factor. PI(3)K, Phosphatidylinositol-3-OH-kinase.

1.1.4 Developmental state of human embryonic stem cells.

The major differences (Table 1.1) between mouse ES cells and human ES cells are not only in growth factor requirements (refers to 1.1.3), whereas their colony morphology, proliferation rate, surface-marker level, epigenetic status and especially vulnerability to cellular dissociation all display discrepancy in spite of the fact that they both derived from ICM. Considering the longer period of time for human ES cells in blastocyst stage prior to implantation (3-4 days) than in mouse (~1day), it is plausible to suspect that those two pluripotent stem cell lines are representing distinctive developmental stages during their

derivations.

This idea was proven by the establishment of mouse epiblast stem cells (EpiSCs) from epiblast in early gastrulation embryo, which share signature features with human ES cells but differ from mouse counterpart^{45,46}. The similarities (Table 1.1) between human ES cells and mouse EpiSCs suggested that human ES cells are equivalent to a primitive epiblast or primitive streak progenitor⁴⁷. The mouse ES cells were hence accepted as a naïve ICM-type which is closer to the ground state⁴⁸. It was demonstrated that the developmental potential of mouse EpiSCs is restricted at the post-implantation stage by teratomas but chimera formation after injection into mouse blastocysts⁴⁵. Moreover, naïve human ES cells were attempted to convert by enforcing expression of *KLF4* in human induced pluripotent stem cells exhibiting genetic and epigenetic signatures of mouse ES cells as well as LIF-dependent culture condition and robustness upon dissociation^{49,50}. Knowledge of the original developmental state of different ES cells lines increased our appreciations of understanding the developmental hierarchy and underlying mechanisms.

Pluripotent stem cell lines	Developmental state	Culture condition	Cell surface marker	Alkaline Phosphatase	Female X-Chromosome	Population doubling time	Colony morphology	Sensitive to dissociations	Passed pluripotency test
Mouse ES cells	Naïve	LIF/BMP/3i	SSEA1	Positive	Active	~16 hours	3-D,tight assemblages	No	Teratoma,Chimera, Tetraploid complementation
Mouse EpiS cells	Primed	FGF/ACTIVINA	SSEA1	Negative	Inactive	~18 hours	2-D, flattened sheet	Yes	Teratoma
Human ES cells	Primed	FGF/ACTIVINA	SSEA4/TRA1-60/TRA1-81	Positive	Inactive	~36 hours	2-D, flattened sheet	Yes	Teratoma

Table 1.1 Comparisons of naïve and primed pluripotent stem cell lines with distinctive phenotypes. Differing from its mouse counterpart, human ES cells

resemble to mouse epiblast stem cells with similar culture conditions, morphology and sensitivity to dissociation, indicating its primed epiblast stage. LIF, Leukemia inhibitory factor. BMP, Bone morphogenetic protein. FGF, Fibroblast growth factor. SSEA, Stage-specific embryonic antigen. 3i, Three inhibitors targeting FGFR, ERK and GSK3 (SU5402 for FGFR, PD184352 for ERK, and CHIR99021 for GSK3). 2-D, 2-dimensional. 3-D, 3-dimensional.

1.1.5 Developmental potential and functional assays to assess the potential.

Stem cells are characterized by the ability to self-renew in order to reserve their undifferentiated state once captured from their *in vivo* compartment. More important, in response to certain cues stem cells are endowed with the ability to differentiate into other types of cells from their original of undifferentiated state. The second signature of stem cells is relying on the spectrum of cell types, to which a stem is capable to give rise, and assessed by developmental potential. As illustrated in Fig. 1.1, only the zygote and early blastomeres before 4-cell stage are able to generate the whole organism including extraembryonic tissues, which belong to the unique case of totipotent stem cells⁵¹. Pluripotent stem cells are capable to generate all types of cells *in vitro* except trophoblast lineage. Therefore, embryonic stem cells, embryonic epiblast stem cells and embryonic germ cells (EG) are all fulfill the criteria of pluripotency in spite of their different origins from the embryo. Adult stem cells, like hematopoietic stem cells, residing

in many tissues or organs for replacement of damaged cells are only able to form certain types of cells, which belong to multipotent stem cells. Progenitors only have the capacity to produce one type of cell are unipotent stem cells, such as spermatogonial stem cells. Eventually, the terminally differentiated cells, which loss the ability to generate other types of cells, are confined to nullipotent (Fig. 1.3).

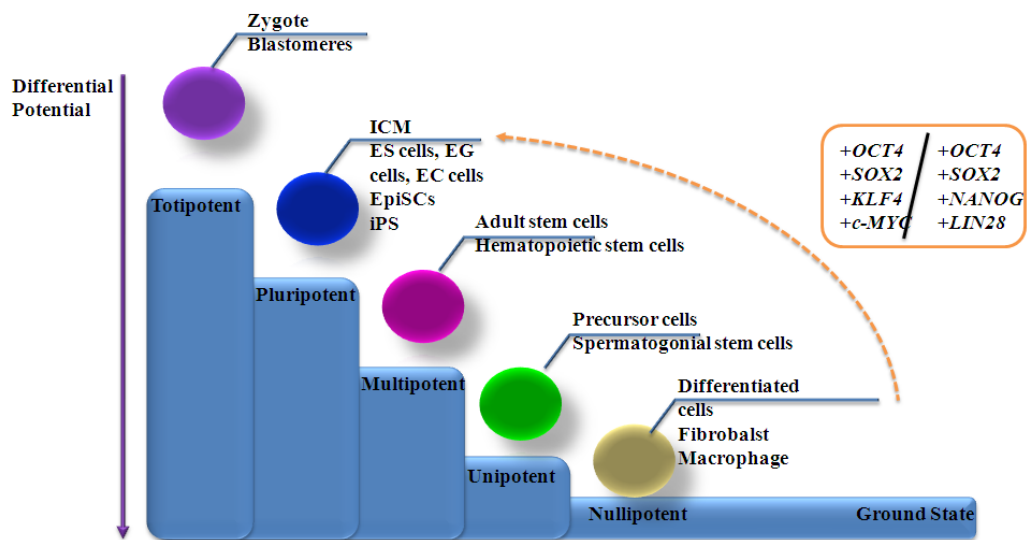


Figure 1.3 Models of differential potential for stem cells. Colored spheres representing cells at differentiation stages. The direction of normal development is reflected by the purple arrow. The orange dashed lines depict the direction of cellular reprogramming with defined factors (box). ICM, inner cell mass. ES cells, ES cells. EC cells, embryonic germ cells. EpiSCs, epiblast stem cells. iPS, induced pluripotent stem cells. *OCT4*, Octamer-binding transcription factor 4. *SOX2*, SRY-related high mobility group-box protein-2. *KLF4*, Kruppel-like factor-4

The developmental hierarchy can be reversed by ectopic expression of certain transcription factors to establish induced pluripotent stem cells (iPS). Details refer to 1.1.6.

The derivations of ES cells from various sources help to establish the functional criteria and characterization of pluripotency. *In vitro* assays, using pluripotent biomarker to discriminate pluripotency to certain degrees regarding on known gene specifically expressed on ES cells (Table 1.2). However, this procedure is not reliable due to the lack of functionality and bias of cell populations⁵².

By definition, pluripotent cells refer to cells owning the potential to give rise of any of the three embryonic germ layers: endoderm, mesoderm and ectoderm. Hence, *in vitro* culture of ES cells into embryonic body (EB), which composed of cells from three germ layers, is the least stringent functional assay. A series of *in vivo* functional tests basing on injection of pluripotent cells into host animal or blastocysts are designed to access the functional contributions of stem cells to different tissues. In physiological condition, sub-renal capsule, intra-muscular and subcutaneous implantations of pluripotent stem cells are capable to form teratomas, which are benign tumors with differentiated cells from all three germ layers, in immunodeficient mouse⁵³. Although it was considered to be the gold standard for assessing pluripotency due to its easy manipulation, there are limitations as lacking evidence for normal development.

Engraftment of stem cells into host blastocyst to form chimera animal circumvented the limitation from teratoma assay. In tetraploid complementation assay, two cells at the two-cell stage of an embryo is fused by electrical shock to form tetraploid cell, which will develop to blastocyst stage and generate extra-embryonic tissues with defects on ICM development. By introducing pluripotent stem cells into tetraploid blastocyst, there will be a high possibility for the pluripotent stem cells to compensate the defected blastocyst and develop into a whole animal. This method excluded the likelihood that host-derived cells can contribute to chimera formation, which appeared to be the most stringent test for pluripotency⁵⁴. Unfortunately, due to the barriers between species, cross-species chimera formation is imprecise and unethical in human trials. Therefore, the most stringent pluripotent test so far for human ES cells and human induced pluripotent stem cells is teratoma formation⁵⁵.

Marker	Expression Cell Type	Marker	Expression Cell Type
Alkaline phosphatase	ES	GATA-4	Endoderm
GCTM-2	ES	HNF-4	Endoderm
NANOG	ES	NESTIN	Ectoderm
OCT4	ES	N-CAM	Ectoderm
SOX2	ES	PAX-6	Ectoderm
SSEA-3/4	hES	VIMENTIN	Ectoderm
Telomerase	ES		
TRA-1-60	hES		
TRA-1-81	hES		
BMP-4	Mesoderm		
BRACHYURY	Mesoderm		

Table 1. 2 Major molecular markers for pluripotency and differentiation.

Common molecular markers to detect and label pluripotent stem cells are listed.

Specific surface markers express on human ES cells were indicated with hES.

The identical markers to detect differentiation of three germ layers were selected.

GCTM-2, Podocalyxin-like precursor isoform-2. OCT4, Octamer-binding transcription factor 4. SOX2, SRY-related high mobility group-box protein-2.

SSEA, Stage-specific embryonic antigen. BMP4, Bone morphogenetic protein-4.

HNF-4, Hepatocyte nuclear factor-4. N-CAM, Neural cell adhesion molecule.

PAX-6, Paired box protein-6.

1.1.6 Induced pluripotent stem cells reverse differentiation potential via epigenetic reprogramming.

In conventional dogma, differentiated cells occupy the terminal of pluripotency, which is a unidirectional dynamic process, and lost their potential to development. The cloning of Dolly the sheep⁵⁶ confirmed that soluble trans-acting factors in mammalian oocyte can reverse the epigenetic status of committed nucleus to a totipotent state⁵⁷. Furthermore, the early attempts on lineage transfer demonstrated that enforcing certain type of transcription factors can induce conversion of cells from different lineages⁵⁸. According to those previous findings, a screen for identifying transcription factors to reprogram differentiated cells into pluripotent cells was conducted in 2003 from a pool basing 24 pluripotent candidates⁵⁹. The core transcription factors for reprogramming were narrowed down to four: *OCT4*, *SOX2*, *KLF4* and *C-MYC*, by generating mouse induced pluripotent stem cells in 2006⁶⁰. One year later, human induced pluripotent stem cells were generated either by expression of *OCT4*, *SOX2*, *KLF4* and *C-MYC*⁶¹ or by *OCT4*, *SOX2*, *NANOG* and *LIN28*⁶² from two individual groups, which are capable to contribute to chimera formation. Subsequent studies showed that some core transcription factors are dispensable, indicating that only limited transcription factors are essential to orchestrate the reprogramming process and maintain the pluripotency^{63,64}. The extremely low efficiency of generation of induced pluripotent stem cells by various methods (0.02-0.1%) infers that the reprogramming is a stochastic

process for the precise timing, balance and level of epigenetic changes rather than enforcing certain transcription factors alone⁶⁵.

Epigenetic modifications were defined as heritable changes in gene expression without the alteration of DNA sequence through DNA or chromatin modifications⁶⁶. The major chromatin modifications occur on various histones including the core histones, H2A, H2B, H3 and H4 via several different modifications involving acetylation, methylation, and phosphorylation. DNA methylation takes place in CpG dinucleotides and is usually related with transcription repression. Besides, there is of great variety of histone modifications in either gene activation or repression. ES cells contain a relative low level of DNA methylation to active those genes which are essential for pluripotency. Those genes are also occupied by active histone modifier such as trimethylation of histone H3 lysine 4 (H3K4me3) or acetylation of histone H3 lysine 9 (H3K9ac). On the other hand, genes require to be suppressed for lineage commitments in ES cells are occupied via the repressive trimethylation of histone H3 lysine 27 (H3K27me3). During development, genes requiring for specific cell lineage determinations are poised with both active and repressive chromatin markers. The poised gene was defined in bivalent histone state⁶⁷.

Among those four transcription factors for transduction into fibroblasts, *OCT4* and *SOX2* are essential for pluripotency reprogramming⁶⁸. In fully committed cells, the developmental potential was suppressed by methylation of *OCT4* and *NANOG* promoters⁶⁹. Depletion of *OCT4* and *NANOG* from ICM or

cells can induce differentiation into trophectoderm and extraembryonic endoderm, respectively^{70,71}. However, *NANOG* was not necessary for reprogramming fibroblast in Yamanaka's reports^{60,61}. It was suggested that *NANOG* may only contribute to stabilize the pluripotent state instead of being the core factors during reprogramming. The continuous viral expression of transduced *OCT4* and *SOX2* genes trigger the sequential epigenetic events in chromatin modifications such as DNA demethylation on the promoters of *OCT4* and *NANOG* resulting in the reprogramming of pluripotency.

1.1.7 Intrinsic circuitry of pluripotency

The gene-expression pattern of pluripotent ES cells is the outcome of transcription regulation, epigenetic modification and signal transduction, of which transcription factors of *OCT4*, *SOX2* and *NANOG* together composing the core transcription regulatory circuitry are the fundamentals of pluripotency and self-renewal. The extensive study of the DNA binding sites of *OCT4*, *SOX2* and *NANOG* through genome wide analysis revealed that these three transcription factors can activate, suppress or poise the expression of a broad variety of target genes to control cell identity during development⁷². Furthermore, these three transcription factors share and co-occupy a great portion of their target genes as well as their own promoters, indicating a self-regulatory circuitry of pluripotency⁷³⁻⁷⁵. This collaboration of master regulators of stemness promotes

the stability of gene expression and surveillance of pluripotency⁵⁵.

OCT4 belongs to the member of the Pit-Oct-Unc (POU) family of transcription factors, which is indispensable for both the derivation and maintenance of ES cells⁷⁶. The expression of *OCT4* is spatiotemporally restricted to early embryos and germ cells *in vivo*⁷⁷. For example, during embryogenesis the expression of OCT4 and Caudal-type homeodomain-2 (CDX2) are mutually exclusive in blastocyst where OCT4 is critical for ICM establishment and CDX2 is necessary for trophectoderm development. These two proteins reciprocally suppress each other's expression *in vivo*⁷⁸. Therefore, the expression of OCT4 *in vitro* in ES cell lines is critical to be sustained within a threshold to prevent differentiation, of which overexpression can cause differentiation into endoderm or mesoderm and reduced expression induces differentiation into trophoblast⁷⁹.

SOX2 is the member of the SRY-related HMG box transcription factors, which shows to be critical in maintenance of self-renewal and prevention of differentiation in human ES cells. Similar to OCT4, the expression of SOX2 in ES cells needs to be kept within an essential range from undifferentiation^{80,81}.

NANOG is a Novel homeodomain transcription factor. Its expression level, similar to OCT4, balanced with the transcription factors GATA4 and GATA6 for differentiation into hypoblast^{70,82}. NANOG overexpression also enables feeder-free growth of human ES cells and improves their cloning efficiency⁸³. The expression of NANOG is necessary for a general suppression of lineage commitment, of which is declined during differentiation⁸⁴.

The regulators of pluripotency are not work alone while the maintenance of undifferentiation requires of the cooperation of the *OCT4-SOX2-NANOG* circuitry. The enhancer region of the *OCT4* gene, for example, is bound with at least 14 transcription factors including, OCT4, SOX2, NANOG, SALL4, TCF3, SMAD1, STAT3, ESRRB, KLF4, KLF2, KLF5, E2F1, N-MYC and ZFX⁸⁵⁻⁸⁷. It was suggested that OCT4 serves as a hub, the anchor node of biological network, for the assembly and regulation of varies protein complexes on the promoters of target genes⁸⁸. The overall outcome from the OCT4-centric module depending on the contributions of their targets on self-renewal, for example, activation of *RIF1*, *JARID2* and *SMARCAD1* are of important factors for telomere length regulation and inactivation *CDX2* are of lineage-specific differentiation⁶⁸.

1.2 Stems cells and the pathways to ageing and cancer

1.2.1 The mechanisms of ageing and stem cell model.

Ageing is the accumulation of the loss of tissue homeostasis and replenishment by a progressive decline in stem cell functions. ES cells are pluripotent cells and are capable to generate all tissues of three germ layers by self-renewal and properly differentiation. Once tissues are fully established, the fundamental role of stem cells turns from tissues building to tissues maintenance, which arise the stem cell models of ageing⁸⁹. Hence, the maintenance of tissues homeostasis and regenerative capacity partially depend on the integrity of adult

stem cells and also contribute to mammalian ageing in terms of stem cells ageing as a result of intrinsic DNA damage⁹⁰. The age-related diseases *per se* derive from the inability of adult stem cells to maintain tissue structure and function⁹¹.

Since ES cells are critical for mammalian development, their genomic integrity must be secured by efficient preventive mechanisms. Indeed, it has been proved that ES cells are readily to eliminate damaged cells from the population by apoptosis with a hypersensitive DNA damage tolerance⁹². And in fact, mouse ES cells are known to be much more sophisticated in apoptosis than differentiated cells after UV-induced DNA damage⁹³. There are likely to be multiple kinds of damage contributing to ageing, which will be regulated by a complex network of maintenance and repair functions.

The risk of self-renewal, however, comes with some danger of the malignant transformation for the organism. The genetic damage may be passed from the stem cells to their daughter cells through self-renewal and can be accumulate in ageing. The accumulation of damage to cellular macromolecules has been postulated to be a cause of cellular attrition with ageing⁹⁴. Unrepaired genomic damage accumulates with ageing inducing the potential fate of transformation, senescence, apoptosis or dysfunction in stem-cell compartments. As time goes by, the depletion and dysfunction of stem-cell compartments cannot match the regenerative needs of a given tissue and will face the organ degenerative failure in ageing. Likewise, when oncogenic DNA damage onset, self-renewing clones with those lesions accumulate and subsequently lead to

cancer. Therefore, cancer and ageing are two related processes due to DNA damage accumulation within self-renewing compartments⁹⁵.

1.2.2 The arising of cancer stem-like cell model during ageing.

Cancer is the disease of accumulations of inherited mutations in genes in normal cells neglecting the growth controlling signals to form a tumor, which is the mixture of heterogeneous lineages of cancer cells, and is the leading cause of death with increasing risks during ageing in human. In analogy to normal tissue, the heterogeneity of tumor consists of cancer cells with hierarchy differing in morphology, proliferation capacity, marker expression and tumorigenicity, with which the stem cell compartment of cancer seem to occupy the apex⁹⁶. The rare population of cancer stem-like cells in tumors displays stem cell-like property, which mimic the self-renewing ability to produce more cancer stem-like cells and give rise to the variety of differentiated cancer cells⁹⁷. It is still controversial for the origin of cancer stem-like cells between the stochastic and hierarchy models. In stochastic model, the features of stemness can be acquired in any types of cells which happen to obtain the malignant mutations in the appropriate endogenous and exogenous factors, and able to process its self-renewal program via dedifferentiation⁹⁸. On the other hand, neoplastic damage may be preferentially accumulated in adult stem cells which hijack the self-renewal pathways for tumorigenic purpose in hierarchy model. The initial of cancer

stem-like cells were proved to be largely depending on the types of human cancers by several studies.

The finding of a single embryonic carcinoma cell is able to undergo self-renewal and multilineage differentiation was the first attempt of experimental demonstration of cancer stem-like cell with a stem cell origin in 1964⁹⁹. Assembling to hematopoietic stem cell, injection of leukemic cells with stem-like phenotype into NOD-SCID mice resulted in leukemia in serially transplantation experiments¹⁰⁰. In solid tumors, similarities of isolation cancer stem-like cells were uncovered from breast cancer^{101,102} as well as brain¹⁰³, colon¹⁰⁴⁻¹⁰⁶, melanoma¹⁰⁷, pancreatic^{108,109}, prostate¹¹⁰, ovarian¹¹¹, hepatic¹¹² and lung¹¹³ cancers with stem-like compartments with a broad spectrum of cell surface markers (refers to Table 1.3). Detail investigations on the gene expression pattern from isolated cancer stem-like cells revealed variations among tumors of same histopathologic type¹⁰⁵, indicating the complexity of cancer initiation in heterogeneous tumors. It was found in animal models that the disruption of stem cell self-renewing property by ectopic expression of *OCT4* can induce neoplastic in normal epithelial tissue¹¹⁴. Mutations of genes controlling asymmetric division, such as *NUMB* and *PROS*, can hinder cell cycle regulation in neuroblasts and contribute to tumorigenesis¹¹⁵.

In spite of the fact that human ES cells sharing similar molecular and cellular signatures with cancer cell lines, such as rapid proliferation rate¹⁴, high activity of telomerase¹⁴ and teratomas formation in transplanted animals⁸, the

overall genetic and epigenetic status appear to be in great analogy^{116,117} as high expression of oncogenes as *C-MYC* and *KLF4*^{118,119}. To be noted, *C-MYC* and *KLF4* are the core transcription members introduced into fibroblast to generate induced pluripotent stem cells⁶⁰. The involvement of *C-MYC* and *KLF4* can remarkably increase the efficiency of induction by promoting stem proliferation with a increased threat of tumor formations^{65,120}. Although the increased risk of aggressiveness in induced pluripotent stem cells may due to the genomic and epigenomic instability during reprogramming as well as the technologies for transductions, the potential tumorigenicity of human embryonic and induced pluripotent stem cells offered us a plausible insight of the rise of tumor in a stem cell model¹²¹.

In the context of normal adult stem cells, a stem cell niche is necessary to support the undifferentiated state with supporting extracellular signals and cell-cell interactions¹²². Current findings suggest that cancer stem-like cells also reside in a similar niche to support their stemness. A cancer stem-like niche may also contribute to trigger the induction of cancer stem-like cell features in differentiated cancer or normal cells. During metastasis, a microenvironment which is in favor of the secondary tumor formations, may recruit the primary tumor for metastasis via the initiation of epithelial mesenchymal transition¹²³. For example, canonical WNT pathway plays important roles in regulation of human embryonic and adult stem cell self-renewal in associated with BMP4¹²⁴. WNT signaling positively induce proliferation of stem cells and migration by

adhesion proteins. BMP4, which was found expressed in the intestinal stem cell niche, counteract with the function of WNT signaling to prevent stem cell expansion¹²⁵. Depletion of the BMP4 receptor accelerates the proliferation of stem cells in the intestine and hair follicle with the consequence of tumor formation^{126,127}.

Collectively, accumulated findings in stem cell biology and cancer research unraveled potential common regulatory mechanisms, which are essential for self-renewal in stem cells and cancer stem-like cells. Fully investigations of the self-renewing mechanism may ultimately resolve the enigma of ageing and the cure of cancer.

Tumour Type	CSC marker	Reference
Breast	CD44 ⁺ /CD24 ^{-/low}	101
Breast	ALDH1 ⁺	102
Brain	CD133 ⁺	103
Colon	CD133 ⁺	104
Colon	EPCAM ^{high} /CD44 ⁺	105
Colon	ALDH1 ⁺	106
Lung	CD133 ⁺	113
Liver	CD90 ⁺	112
Melanoma	ABCB5 ⁺	107
Ovarian	CD133 ⁺	111
Pancreas	CD44 ⁺ /CD24 ⁺ /ESA ⁺	108
Pancreas	CD133 ⁺	109
Prostate	CD44 ⁺ /α ₂ β ₁ ^{high} /CD133 ⁺	110

Table 1.3 Surface markers applied for the identification of cancer stem-like cells in different tissues. ABCB5, ATP-binding cassette transporter B5. EPCAM, epithelial cell adhesion molecule. ESA, epithelial-specific antigen. ALDH1,

Aldehyde dehydrogenase 1.

1.2.3 The role of FOXM1 in ageing.

FOXM1 is one of the Forkhead transcription factors. The human FOXM1 gene locates on chromosome 12p13-3 and is about 25kb¹²⁸. Two exons (Va and VIIa) are alternatively spliced to form three different FOXM1 transcripts, which are named as FOXM1A containing both alternative exons, FOXM1B without either of the exons and FOXM1C retaining the Va exon¹²⁹. FOXM1 is widely expressed in all embryonic tissues, and associated with cell proliferation in dividing cells¹³⁰. The expression of *FOXM1* is found to be crucial in neural stem cell and is subsequently down regulated during differentiation¹³¹. Homozygous knock out of *FOXM1* in mouse resulted in embryonic lethality or defect in myocardium and liver developing at early stage, which suggests the important role of FOXM1 in organogenesis¹³².

The FOXM1 transcription factor is essential for G1/S transition and mitotic progression. Its activity depends upon the activation of cyclin and cyclin dependent kinases (CDK) in that FOXM1 is synthesized and degraded in every cell cycle¹³³. This reveals that the promotion of cell proliferation by FOXM1 requires proper activation by mitogenic cues. The induction of FOXM1 after tissue injury to increase the cell proliferation also suggests its role in tissue regeneration and repair¹³⁴. Furthermore, FOXM1 is one of the most common

overexpressed genes in multiple human tumors ¹³⁵. Due to the acquisition of multiple mutagenic events accumulated during ageing, cells with lower turn-over are easy to accumulate the mutations and transform into cancer. However, since the ongoing stem and progenitor cells are essential to maintain the tissue homeostatic, tumor suppressor may reluctantly attrite stem cell and contribute to ageing ⁸⁹. Therefore, in order to escape the fate of senescence, FOXM1 can support proliferation by stimulating expression of the antioxidant genes to attenuate the induction of Reactive oxygen species (ROS), which are a major source of DNA damage produced by normal metabolism ¹³⁶. On the other hand, FOXM1 is down regulated in quiescent cells ¹³⁷. And the tumor suppressor P53 is required for the down-regulation of FOXM1 to maintain a stable G2 arrest ¹³⁸. Under homeostatic conditions, the need for adult stem cells for proliferation to the self-renewal is restricted, which alleviates the replicative stress in mitosis¹³⁹. The inactive metabolic quiescent state of adult stem cells can spare themselves from oxidative stress ¹⁴⁰. It allows the production of large numbers of differentiated cells from a single stem cell by differential proliferation and balances the long-term homeostasis between the prevention from carcinogenesis ⁹¹.

Nonetheless, regulatory mechanisms underlying the transition of stem cells into old age are less well understood. Study obtained from global gene expression of stem cells purified from young and old mice manifest the important role of epigenetic regulation in stem cell ageing ¹⁴¹. One of the Polycomb group

(PCG) proteins, BMI-1, is essential for maintaining self-renewal in adult hematopoietic stem cell (HSCs)¹⁴², neural stem cell¹⁴³ and leukemic stem cells¹⁴⁴ by repression of the *P16^{Ink4a}-P19^{Arf}* locus to control stem cell cell-cycle and senescence¹⁴⁵. Interestingly, a functional link between FOXM1C and BMI-1 alluded the regulation of self-renewal and senescence by FOXM1 in stem cells¹⁴⁶.



Figure 1.4 Schematic diagram of variants of human FOXM1 protein. Human FOXM1 transcript contains two exons (Va and VIIa) for splicing. Exon Va encodes a 15 amino-acid insertion within the DNA binding-domain of FOXM1 protein. Exon VIIa encodes a 38 amino-acid insertion within the C-terminal transactivation domain of the protein. Differential splicing of Va and VIIa exons generates three FOXM1 isoforms: FOXM1A, FOXM1 B and FOXM1 C. The full length of FOXM1A gene is 801 bp. And the molecular weight of each FOXM1 protein isoform is presented at right side.

1.2.4 The mechanisms of FOXO3A in ageing.

FOXO3A belongs to the member of class O of Forkhead transcription factors. The human genomic location of FOXO3A gene is on chromosome 6q21

and is about 125kb. The FOXO family including FOXO1, FOXO3A, FOXO4 and FOXO6 appear to play important roles in cellular proliferation, metabolism, stress tolerance and indeed longevity¹⁴⁷. FOXO proteins can be detected throughout the mammalian body¹⁴⁸. Among them, FOXO3A is more extensively but highly expressed in brain, spleen, heart and ovary¹⁴⁹. Moreover, in hematopoietic stem cells the importance of FOXO3A in maintaining their quiescent state was highlighted¹⁵⁰. The role of the FOXO family in other adult stem cells is not well studied yet. But the knockout of FOXO3A in mice ovarian follicle resulting in oocyte exhaustion and infertility reveals its role in maintenance of the stem cell niche¹⁵¹.

Posttranslational modifications including phosphorylation, acetylation and ubiquitylation provide pivotal determinations in FOXO family regulations under different cues. Phosphorylation can play both inhibitory and activating roles in FOXO family function. The phosphorylation of FOXO3A by AKT/PKB facilitates to bind of the 14-3-3 chaperone proteins to exclude the FOXO3A from the nucleus to the cytoplasm and prevents its binding with DNA to inhibit its downstream transcription targets¹⁵². Conversely, activation of Jun N-terminal kinase (JNK) or mammalian sterile 20-like kinase-1 (MST1) in response to stress stimulation results in phosphorylation of FOXO family at a distinct set of threonine residues and results in loss of 14-3-3 protein binding and nuclear import with subsequent transcriptional activation¹⁵³. SIRT1-mediated deacetylation of FOXO family appears to regulate subnuclear localization and

alter DNA binding activity by acetylation¹⁵⁴. The cytoplasmic FOXO family will be degraded by proteasome when polyubiquitination occurs after the phosphorylation of FOXO family by AKT/PKB. On the contrary, monoubiquitination of FOXO family in the cytoplasm or nucleus induced by oxidative stress can thereby activate FOXO family¹⁵⁵. Thus, unique combinations of phosphorylation, acetylation, and ubiquitination of FOXO family provide mechanisms to fine-tune FOXOs function¹⁵⁶.

The regulation of FOXO family in hematopoietic stem cells was extensively studied. Recent data indicate that FOXO family members play a critical role in cell cycle, apoptosis and oxidative response in the hematopoietic stem cells compartment and thereby sustain its integrity¹⁵⁷. Deletions of *FOXO1*, *FOXO3*, and *FOXO4* in adult murine bone marrow trend to enforce myeloid and lymphoid lineages skewing accompanied with the deficient in long-term hematopoietic stem cells repopulation¹⁵⁰, eliciting that the FOXO family normally limits the proliferation and mediate dormancy in hematopoietic stem cells. Moreover, ablation of *FOXO3A* alone was sufficient to diminish hematopoietic stem cells function, increase intracellular ROS, disrupt stem cell quiescence, and reduce survival in the hematopoietic stem cells compartment during ageing¹⁵⁸. This finding unravels that oxidative stress contributes to the regulation of proliferation and apoptosis in HSC. Likewise, HSCs that lack the *FOXO* transcription factors show diminished self-renewal and premature exhaustion in response to ROS. And FOXO family may reinforce the tissue maintenance and replacement during

ageing by retaining adult stem cell pools.

Notably among impaired cells in bone marrow and gut epithelium cells with highly proliferative potential, which pose an extreme threat to carcinogenesis because of the propensity from the numerous damaged daughter cells¹⁵⁹. Tumor suppressors such as FOXO3A suppose to be the protective mechanism in such cells to initiate apoptosis in response to oxidative induced DNA damage.

1.2.5 SIRT1 servers as a major ageing factor.

Sirtuins belong to class III histone deacetylase complexes (HDAC), require NAD⁺ as a cofactor. The unconventional use of NAD⁺ infers the links between Sirtuins activity to the cellular redox state and metabolism. Sirtuin 1 is one of the seven mammalian Sirtuin family proteins, which acts in multiple tissues, deacetylating both chromatin and non-histone proteins. Human SIRT1 gene is at 10q21.3 and is around 34kb¹⁶⁰.

Caloric restriction (CR) was proved to slow ageing in lower organisms and rodents by decreasing the activation of senescence in self-renewing compartments. CR produces a more oxidative metabolic state with a higher level of NAD⁺. This in turn activates sirtuins and facilitates survival mechanisms such as senescence and apoptosis inhibition or activation of stress response pathways to extend lifespan¹⁶¹. Mildly increase the *SIRT1* expression in transgenic mouse

model show elusive longevity extension but in a healthier way, such as resistant to diabetes and obesity¹⁶². This indicates the metabolic role of SIRT1 in ageing.

Through deacetylate histone H3 lysine 9 (H3K9) and H4 lysine 16 (H4K16) in human cells may control some aspects of stem cell function^{163,164}. SIRT1 may facilitate the maintenance of self-renewal by silencing of differentiation genes. Since after initiation of differentiation, precisely spatial and temporal modifications need to be determined in specific lineage to active necessary differential genes and repress pluripotent genes¹⁶⁵. It underscores the potential of extend lifespan and to avoid cell and organism senescence through SIRT1 in adult stem cells.

In animal models, the depletion of SIRT1 from mouse ES cells results in mild negative effect on pluripotency. However, the overexpression of SIRT1 can induce pluripotency gene expression^{166,167}. Knock down of *SIRT1* in human ES cells does not seem to cause the shift of gene expression pattern from pluripotency to differentiation¹⁶⁸. It was proposed that SIRT1 may regulate development indirectly through its target, such as P53 deacetylation, which was supported by *SIRT1* knock out mouse can survive with hyperactive P53¹⁶².

1.3 The functions of non-muscle myosin II family in human embryonic stem cells.

Three different genes in mammalian cells MYH9 (non-muscle myosin

heavy chain 9), MYH10 (non-muscle myosin heavy chain 10) and MYH14 (non-muscle myosin heavy chain 14) encode NMHCIIA, NMHCIIIB and NMHCIIIC, respectively. No heterodimer formation between the three NMHCII formations were documented¹⁶⁹. MYH9 and MYH10 but not MYH14 are readily detectable in human ES cells¹⁷⁰.

Non-muscle myosin II (NMII) serves as a key mediator of cell migration, adhesion, polarity and proliferation, due to the binding of NMII with actin filaments and acting as a motor sliding on actin filaments to generate contraction in those processes. The process is triggered by the binding of myosin light chain (MLC), which is activated by phosphorylation through kinases, such as Rho-associated kinase (ROCK) or Myosin light chain kinase (MLCK)¹⁷¹.

One of the most discernible characteristics of human ES cells is their tight associations with each other to form compact colonies during proliferation⁸, which is shared by the epiblast epithelium of the human embryo and varies from the mouse ES cells⁴⁵. Accordingly, the development of compact colonies is considered as a reliable readout from derivation of human induced pluripotent stem cells^{61,62}. The proliferation and survival of cells in epithelial structures are well orchestrated *in vivo*. The disruption of such structure in stem cells, induces excessive membrane blebbing and results in substantial cell death due to the hyperactive actin-myosin contraction¹⁷². The actin-myosin based cytoskeleton is a dynamic system essential for contraction motility, and tissue organization

173,174

It is plausible that NMII may function as a part of the molecular sensor to monitor the changes at physical and molecular levels during developmental processes. In fact, the process by which the ICM is reshaped into the epiblast involves a dramatic rearrangement and the ROCK/myosin system may equip the epiblast cells to undergo a rapid movement to promote the development (refers to 2.1.3 and Fig. 1.5)¹⁷².

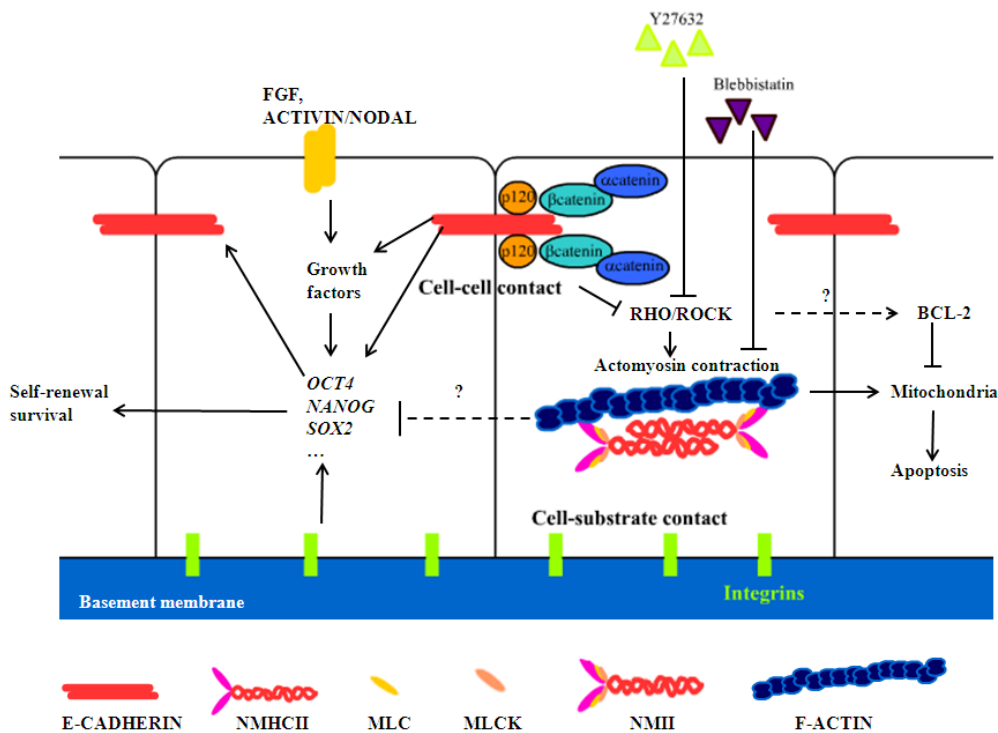


Figure 1.5 Schematic summary of possible pathways involving dissociation induced apoptosis in human embryonic stem cells. In the support of growth factors, human ES cells establish the circuit for pluripotency and self-renewal via OCT4-SOX2-NANOG core transcription factors (refers to 1.1.7). The pluripotency was postulated to be monitored by cell-cell interactions and cell-substrate contact. Dissociated human ES cells expressing less E-CADHERIN and induce Rho/ROCK activity to increase the mechanical

tension from actomyosin contractions, which cause apoptosis via mitochondria pathway and differentiation through unknown mechanisms. The small molecular Y27632 (refers to 2.1.3) and blebbistatin (refers to 2.1.7) can prevent the apoptosis by inhibition the activity of ROCK and non-muscle myosin heavy chain, respectively. BCL-2 level (refers to 2.1.3) is related to the anti-apoptotic effect induced by blebbistatin with unknown mechanisms. NMHCII, non-muscle myosin heavy chain II. MLC, myosin light chain. MLCK, myosin light chain kinase. NMII, non-muscle myosin II.

Chapter 2 MYH10 interacts with FOXM1 in human Embryonic

Stem cells

2.1 Introduction

2.1.1 H9 human embryonic stem (ES) cells and iPS_{IMR90} induced pluripotent stem (iPS) cells are well-characterized cell lines for stem cell research.

One of the arising challenges for biological research is to solve the problem of mammalian ageing, with respect to decline in tissue homeostasis and organ function. This ageing process is complicated and may be driven by a number of factors including genetics, environment, or behaviors¹⁷⁵. As mentioned in section 1.2.1, the progression of ageing is a consequence of the loss of homeostasis and organ functions. In mammalian tissues, adult stem cells undergo self-renew and differentiation to maintain the homeostasis. Therefore the ability of self-renew and differentiation, which was originated from ES cells, may hold the key answers to solve this old ageing question. Hence, human ES cells were selected for the basic models in this project.

The H9 human ES cell line, was one of the 14 cell lines originally derived from inner cell mass of human blastocysts (refers to 1.1.2) in 1998⁸. H9 is also the most characterized and widely used cell line among the other 600 cell lines. The use of H9 accounted for 83.3% of the published literature on human ES cell research up to 2009¹⁷⁶. A global detailed study analyzed 59 independently

derived human ES cell lines, including H9 cells, showed a common expression pattern of stem cell markers with only very subtle phenotypic differences¹⁷⁷. H9 ES cells, was characterized with a normal female karyotype within 32 passages^{8,177}. The H9 cell line was, therefore, selected as a reliable ES cell model for this project.

Comparing with their fully committed origin, transducing a specific set of transcription factors to somatic fibroblasts enables these somatic cells to be reprogrammed into an embryonic state with the ability of self-renewal.⁶⁰ These cells are called Induced Pluripotent Stem (iPS) cells. iPS cells exhibit morphological and functional similarities to ES cells⁶¹. iPS_{IMR90} cells were reprogrammed from IMR90 fetal fibroblast cells with the transduction of *OCT4*, *SOX2*, *NANOG* and *LIN28*(refers 1.1.6), Compared with H1, H7, H9, H13 and H14 human ES cell lines, iPS_{IMR90} cell line does have similar gene expression pattern revealed by microarray analysis⁶². iPS_{IMR90-4}, from this study, is one of the 4 clones originated from iPS_{IMR90} is hence comparable with H9 cell line in genetic background. The successful reprogrammed iPS cells undergo phenotypic changes and form flat colony with tight cell-cell interactions similar to human ES cells lines⁶². This acquired phenotype from iPS is essential for the viability and pluripotency in human ES cells as well, which provide us an alternative model to study the mechanisms of self-renewal.

2.1.2 SIRT1, FOXO3A and FOXM1 are pivotal ageing factors for self-renewal in stem cells

In the context of ageing as mentioned in 1.2.3-1.2.5, stem cell-ageing is related to its intrinsic self-renewing mechanisms. The specific factors and the roles of these factors involved in stem cell-ageing are still not fully understood. Hence, the focus of this project is the identification of novel ES cell ageing factors and the mechanistic roles of these new factors in ES cells ageing¹⁷⁸.

SIRT1 was well-characterized in its function to prolong lifespan in metazoans and rodent models^{161,179}. It was reported that SIRT1 may induce NANOG protein expression in mouse ES cells, indicating its role in regulating pluripotency¹⁶⁶. It is therefore reasonable to select SIRT1 as one of the ageing factors corresponding to stem cell self-renewal in this study.

It has been revealed that ES cells would age when they were induced to oxidative stress¹⁸⁰. FOXO3A is hence postulated to be another ageing factor for its role in regulating the level of reactive oxygen species (ROS)¹⁵⁰. Considering the contribution of FOXO3A in cellular senescence and in the maintenance of hematopoietic stem cell homeostasis *in vivo*¹⁵⁸, it is reasonable to investigate FOXO3A on the self-renewing properties of ES cells in this current study.

The determination of self-renewal, asymmetric division to be precise is driven by mitotic division *per se*. We hypothesized that mitotic fidelity was compromised during ES cell ageing and may be inextricably linked to specific ageing factors associated with mitotic fidelity. FOXM1, a Forkhead transcription

factor, which is indispensable for mitotic progression¹³⁰ is believed to be an ageing factor for ES cells. Evidence was supported by its function in organogenesis¹³², tissue regeneration¹³⁴, oxidative stress¹⁴⁶ and carcinogenesis¹³⁶(refers to 1.2.3). To uncover the underlying molecular mechanisms of how stem cells age, we have used FOXM1 to examine the novel roles of its key protein interactors or pathways during mitotic division of ES cells.

2.1.3 Non-muscle myosin II (MYH10/MYH9) is essential for the cell-cell contact to support stem cell self-renewal.

As eluded in section 1.1.4, human ES cells as well as human iPS cells are highly vulnerable after dissociation¹⁸¹. This feature has pointed in the direction of cell-cell interaction, being essential in ES cells self-renewal and survival.

Viability could be enhanced in dissociated human ES cells by the chemical inhibitor of Rho-associated kinase (ROCK) (Y27632)¹⁸². This ROCK inhibitor is commonly used to improve lipofectamine mediated transfection¹⁸³. The cause of apoptosis in dissociated human ES cells was found due to its hyperactivated actomyosin contraction induced blebbing¹⁸⁴. Inhibition of ROCK activity by Y27632 was able to suppress the blebbing, via the mitochondrial pathway by BCL-2 (B-cell lymphoma-2) family¹⁷². Non-muscle myosin II (MYH9/MYH10) was therefore identified as one of the direct downstream effectors of the ROCK pathway for actomyosin contraction in dissociated human ES cells¹⁸⁴. In support

of that, an alternative inhibitor, namely blebbistatin, targeting non-muscle myosin II (refers 2.1.7) was also proven to enhance the survival of dissociated human ES cells¹⁷⁰. However, the downstream of the actomyosin contraction is not yet fully understood. MYH9 was shown to regulate colony integrity and to support survival while the function of MYH10 was barely understood¹⁸⁵. Evidence indicated that specific isoform of MYH10 (refers to 1.3) was involved in different functions in response to different signals involved in survival and apoptosis in ES cells¹⁸⁶. There are contradictory results from recent studies on whether pluripotency may be retained through inhibition of non-muscle myosin II by blebbistatin in dissociated human ES cells^{170,185}. For example, elevated transcript levels of *OCT4* and *NANOG* and their protein expression levels were observed when blebbistatin was applied in the range of 2.5 to 5 μ M¹⁷⁰. While the concentration of blebbistatin was raised up to 10 μ M, the protein expressions of *OCT4*, *NANOG* and even *SOX2* were significantly diminished¹⁸⁵. These findings alluded that MYH9 and/or MYH10 may interact with other factors or pathways through unidentified mechanism(s) to regulate self-renewal in ES cells.

2.1.4 The association of FOXM1 with E-CADHERIN and beta-CATENIN regulates self-renewal in human ES cells.

The expression of E-CADHERIN has long been characterized as one of the undifferentiated markers in human ES cells¹⁸⁷. The extracellular domain of E-CADHERIN stabilized the interactions between the adjacent cell membrane

for colony formation, while the cytoplasmic domain provides a docking site for multiple adaptor proteins such as, p120-CATENIN and beta-CATENIN¹⁸⁸. It was elaborated that beta-CATENIN can coordinate with either adhesion complex or WNT (Wingless type protein) signaling proteins¹⁸⁹. For example, the loss of E-CADHERIN mediated cell adhesion can promote beta-CATENIN nuclear translocation¹⁹⁰. The nuclear translocation of beta-CATENIN, which will activates WNT targets including BMP, C-MYC and CYCLIN D1¹⁹¹. Interestingly, it was indicated that FOXM1 could directly interact with beta-CATENIN to promote the nuclear accumulation of beta-CATENIN, which in turn facilitates the self-renewal in neural stem/progenitor cells by transactivation of those WNT target genes¹⁹². On the other hand, FOXM1 is crucial for embryonic development because of the fact that FOXM1 knockout mouse suffered from severe defects in development^{193,194}. When FOXM1 was proven to be able to transactivate the promoter of E-CADHERIN, it was postulated to improve cell-cell interactions and might be important during embryogenesis.¹⁹⁵ It is hence logical to study the functional role of FOXM1 in association with the network of adhesive pathways. The mechanisms are yet to be explored in human ES cells.

2.1.5 FOXM1 directly interacts with *OCT4* promoter to regulate self-renewal.

In ES cells, pluripotency was found to be regulated by transcription factors such as *OCT4*, *SOX2*, and *NANOG*. FOXM1 was identified to be one of the

transcription factors which bind on *OCT4* promoter. The binding of FOXM1 to *OCT4* promoter positively regulates pluripotency in murine ES cells¹⁹⁶. Nevertheless, the functional role of FOXM1's binding on *OCT4* promoter is still to be understood. In human ES cells, it is not known whether FOXM1 would have occupancy on OCT4 promoter.

2.1.6 FOXM1 and MYH10 are both important factors during asymmetric division.

Self-renewal in ES cells is governed by asymmetric division. Actomyosin network generates intracellular forces to drive the polarization in a spatiotemporal resolution¹⁹⁷. For example, the asymmetric cortical accumulation of non-muscle myosin II results in the asymmetric force distribution¹⁹⁸. The force distribution can further decide the asymmetric spindle position¹⁹⁹. The physical segregation of two distinctive daughter cells, known as cytokinesis, is achieved through the ingression and subsequent abscission of the plasma membrane by the formation of cleavage furrow with actomyosin contraction²⁰⁰. At the stages of polarization and cytokinesis, MYH10 actively participates in and monitors asymmetric division associated with specific factors such as AURORA kinase B (AURORA B)²⁰¹ and the kinesin family member 14, KIF14²⁰². Detailed evidence was exemplified that CEP170, a marker for mature centrioles²⁰³, is modulated through myosin and kinesin networks²⁰⁴.

FOXM1 is a critical transcription factor for G1/S and G2/M transition

during mitosis ²⁰⁵. FOXM1 may also upregulate multiple targets such as CYCLIN B1, SKP2 and CEP55 for cell cycle progression²⁰⁶⁻²⁰⁸. The loss of FOXM1 may trigger chromosome mis-segregation, and may lead to mitotic dysregulation during ageing ¹³⁰. FOXM1 also safeguards cytokinesis through AURORA B, SURVIVIN and CENP F ¹³⁰.

Considering the common events where MYH10 and FOXM1 were involved during cellular adhesion and proliferation, it is conceivable to deduce that there may be crosstalk between MYH10 and FOXM1 to regulate human ES cells self-renewal.

2.1.7 Mechanistic action of blebbistatin, the chemical inhibitor of MYH10.

MYOSIN 10 (MYH10), which belongs to non-muscle myosin II (refers to 1.3) shares same enzymatic activities on conserved head domain, with catalytic sites with ATPase activity ¹⁷¹. Similar to all other myosin II isoforms, MYH10 exerts ATPase activity is dependent on ACTIN binding ²⁰⁹. In the ACTIN-MYOSIN ATPase cycle, MYH10 binds to ATP and hydrolyses ATP into ADP-P_i in the absence of ACTIN. The binding of ACTIN accelerates the release of P_i and triggers the motility of MYH10 along ACTIN ²¹⁰. However, (-)-blebbistatin (1-phenyl-2-pyrrolidinone) as a cell membrane permeable small molecular, can prevent the P_i release from the MYOSIN-ADP-P_i complex. It, therefore, will block MYH10 in a dissociated state prior to the binding of ACTIN

²¹¹. (Fig. 2.1.1) Blebbistatin shows rapid inhibition of the ATPase activity of MYH10 at an IC_{50} of around 2 μ M of blebbistatin ²¹². H9 human ES cells showed poor colony formation and reduced pluripotency after 10 μ M of blebbistatin treatment. This effect induced by blebbistatin is reversible in H9 cells. When H9 cells were pretreated with 3 to 5 days of 10 μ M of blebbistatin, prolong culture of H9 cells without blebbistatin will restore colony integrity and the protein level of pluripotent markers. The specificity of blebbistatin is not only against myosin 10, but also myosin 9 and myosin 14 due to the conserved enzymatic domain²¹³.

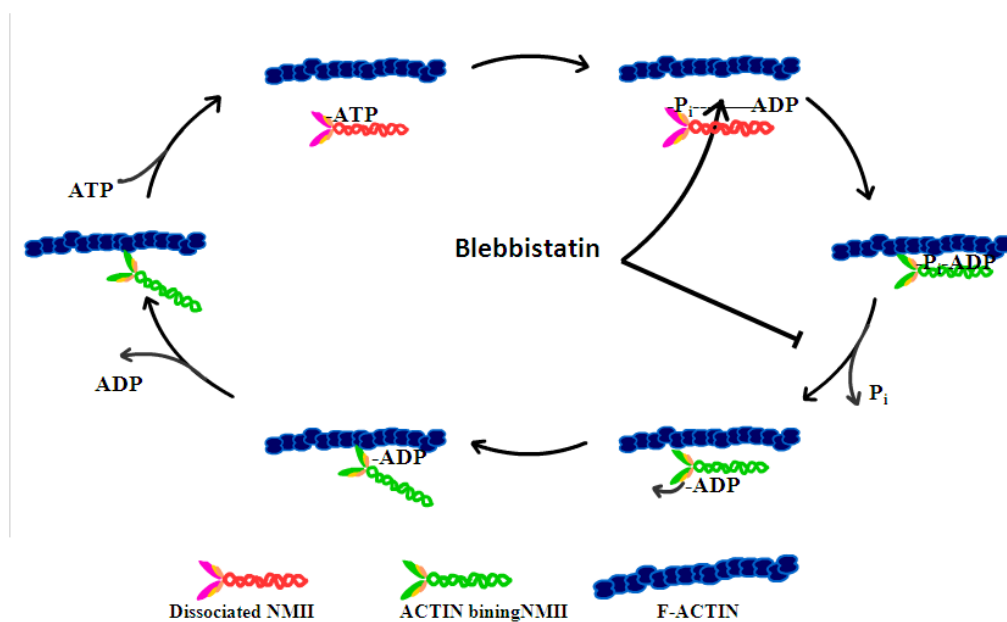


Figure 2.1.1 Schematic diagram for the mechanism of blebbistatin inhibition of non-muscle myosin II. In the cycle of myosin ATPase, dissociated myosin (red) binds with ATP, hydrolyses it to ADP-P_i, and interacts with ACTIN to release the P_i. During this moment, blebbistatin can competitively binds with the active site of ADP-P_i to prevent the binding with ACTIN and inhibit P_i releasing.

2.1.8 Specificity of FOXM1 inhibitor, thiostrepton.

FOXM1 belongs to the forkhead box transcription factor family, which is highly expressed in all embryonic tissues and dividing cells (refers to 1.2.3) ¹³⁰. It has been reported that this natural product, thiostrepton derived from *Streptomyces azureus*, exhibits the ability to suppress the expression of FOXM1 at a concentration of 10 μ M in MCF7 breast cancer cells²¹⁴. However, the mechanism(s) behind this finding remains controversial. Evidence was shown that thiostrepton directly binds with FOXM1 protein to interfere with its genomic target sites as well as its own promoter. Subsequent suppression of the transcript and protein levels of FOXM1 can thus be detected ²¹⁵. Thiostrepton was also identified as a proteasomal inhibitor, and has the same function with other proteasomal inhibitors such as bortezomib, MG132, MG115 and lactacystin. In this scenario, the mechanism of which may be due to the repression of FOXM1 through stabilization of the negative regulators of FOXM1^{216,217}.

2.1.9 The approach to study the function of the novel FOXM1 and MYH10 protein complex in human ES cells.

Identification of the physical interaction between FOXM1 and MYH10 should be further verified by immunoprecipitation.

To understand if this novel protein complex would affect pluripotency in human ES cells, there is a need to know whether FOXM1 or MYH10 could

bind on *OCT4* promoter. This will be achieved by chromatin immunoprecipitation (ChIP) assay.

To understand the functional role(s) of the MYH10/FOXM1 protein complex in self-renewal of ES cells, there is a need to study the upstream factors and the downstream effectors in FOXM1 and/ or MYH10 depleted cells. For example, in this chapter, we have investigated on the E-CADHERIN mediated Rho-ROCK-MYOSIN pathway. The effect of FOXM1 on the Rho-ROCK-Myosin pathway in association with E-CADHERIN will also be studied in thiostrepton-treated ES cells (refers to 2.1.8).

To investigate the connection between FOXM1 and adhesion induced cell survival in human ES cells, it is crucial to inhibit the ATPase activity of MYH10 by blebbistatin (refers to 2.1.7). It is important to look at the morphology and the self-renewal function of the ES cells in combined treatments; whether thiostrepton and blebbistatin will have a synergistic or antagonistic pattern could be revealed in the combined treatments studies.

The concept of asymmetric division was greatly acknowledged from the studies of the embryos of model animals such as *Caenorhabditis elegans* and *Drosophila melanogaster*²¹⁸. Very limited knowledge of the asymmetric event in human ES cells was explored. Another goal of this chapter is to investigate whether this novel protein complex would exert any effects on ES cells asymmetric division/ mitotic control (refers to 2.1.6)

2.2 Materials and Methods

2.2.1 Inhibitors and plasmids

Blebbistatin (-) and Y27632 were purchased from Sigma-Aldrich and thioestrepton was obtained from Tocris Bioscience.

pcDNA3-*FOXMI* was generously provided from Prof. Erick Lam from Imperial College London.

2.2.2 Cell culture and transfection

Human ES cell H9 in GFP and induced pluripotent stem cell iPS_{IMR90-4} were obtained from WiCell research institute. Cells were routinely maintained under feeder-independent condition on Matrigel (BD Biosciences) –coated 6-well plates (IWAKI) supplied with defined medium, mTeSR1 (StemCell Technologies). Medium was replaced daily until the next passage to keep cells in an undifferentiated condition. For subculture, culture medium was replaced with 1ml of 2mg/ml dispase (Invitrogen) for 5 minutes at 37° C. When the colony edges begin to curl up, dispase was aspirated and cells were gently washed with 1mL DMEM/F12 (Invitrogen) for 3 times. Subsequently, cells were gently scraped off from the plates in 2 ml of culture medium and split onto new plates.

Human breast cancer MCF7 and fibroblast IMR90 were purchased from American Type Culture Collection (ATCC) and cultured under ATCC

recommendations. Briefly, cells were grown in DMEM (Invitrogen) supplied with 10% FBS (Hyclone), 1% sodium pyruvate (Sigma), 0.6% L-glutamate (Sigma) and 1% penicillin and streptomycin (Invitrogen). For subculture, medium was replaced with sterilized PBS (Invitrogen) for wash once when cells reached 70-80% confluence. Cells were detached with trypsin-EDTA (Invitrogen) before neutralized with complete DMEM culture medium. Cell pellet was collected at 800 rpm for 3 minutes at room temperature and resuspended into required volume for subculture.

All cells were maintained in a humidified incubator (Thermo) supplied with 5% carbon dioxide at 37° C.

For liposome-mediated transfection, IMR90 cells were transfected with 0-2 µg of DNA plasmids with 5 µl FuGENE HD transfection reagent (Roche Diagnostics) per T25 flask (Corning) according to the manufacture's protocol. Transfection conditions with MCF7 cells were optimized for maximal efficiency with 3-4 µg of DNA plasmids against 9-12 µl X-tremeGENE HP transfection reagent (Roche Diagnostics) per T25 flask. Medium was replaced 24 hours after each transfection and cells were collected for protein levels analysis after 48 hours.

2.2.3 Retroviral vector-based shRNA knockdown in human embryonic stem cells

Specific shRNA sequences were designed targeting *FOXMI* and *MYH10*

according to previous publications (Table 2.2.1). PAGE purified oligonucleotides (Tech Dragon Limited) were constructed into pSIREN RetroQ vectors according to manufacturer's instructions (Clontech). Successful insertions were confirmed by DNA sequencing with U6 forward primer (5'-GGGCAGGAAGAGGGCCTAT-3').

In details, shMYH10 oligonucleotide sequence was constructed into pSIREN vector for transfection into MCF7 cells (refers to 2.2.2) to identify efficient suppressing constructs. shMYH10 clone 2 was selected as it could efficiently suppress MYH10 expression (Appendix I A, 7th column). For retroviral production, GP2-293 cells were transfected with pSIREN-shMYH10 plasmid together with envelope vectors by the CalPhos Mammalian Transfection Kit (Clontech) followed the manufacturer's protocol after optimization in the ratio of 5µg pSIREN-shMYH10 plasmid together with 2.5µg pVSV-G, 2.5µg pAmpho and 2.5 µg p10A1 (Appendix I B, 4th column). The viral volume for initial infection was determined as 300 µl (Appendix I B, 4th column). In order to improve the efficiency of knockdown, 1 T25 of GP2-293 cells with 50-60% confluence were transfected with 8µg pSIREN-shMYH10 alone before antibiotic selection to establish stable cell lines. Transfected GP2-293 cells were plate in selection medium containing varied concentration (1-3 µg/ml) of puromycin (Sigma) for titration. Healthy colonies of packaging cells were isolated and propagated before transfection of envelope vectors in the ratio determined as mentioned above. The optimal concentration for selection was found to be

3µg/ml of puromycin for 8 days (Appendix I C, 4th column).

Subsequently, the mixture of 300 µl viral supernatant and 1.7 ml of mTeSR1 with 8 µg/ml polybrene (Santa Cruz) was applied to a 6-well culture plate of H9 cells in 70% confluence for the initial infection. Infected H9 cells were replaced with fresh medium containing 1µg/ml puromycin after 24 hours for further selection. Stable H9 cells transduced with shRNA targeting MYH10 were maintained in 1µg/ml puromycin-supplemented media for further analysis

Similarly, shFOXM1 oligonucleotide sequence was constructed and confirmed. Clone 3 was selected and used in the following experiments denoted as shFOXM1 in short (Appendix I A, 3rd column). Establishment of stable virus producing cell line of shFOXM1 and infection procedures were followed by the same conditions determined from assays of knockdown MYH10.

Same strategies were applied to construct shControl plasmid for external negative control.

shRNA name	Target sequence (5'-3')	Publication
shControl	TGCGTTGCTAGTACCAAC	Clontech
shFoxM1	CACGCAAGTAGTGGCCATC	219
shMYH10	GGAAGAAGCUCGACGCGCA	184

Table 2.2.1 Sequences of shRNA sequences for human embryonic stem cell infection.

2.2.4 Immunoprecipitation (IP) and Mass spectrometry

Cells were lysed with RIPA buffer (refers to Appendix II) containing protease and phosphate inhibitors cocktail (Sigma). Protein concentrations were determined by Bio-Rad Dc Protein assay kit (Bio-Rad) and 200 µg of protein was incubated with 2 µg antibodies against FOXM1, SIRT1, FOXO3A and MYH10 (Table 2.2.2) at 4° C overnight, respectively. 50% protein A and protein G agarose beads mixture (CalBioChem) were added into the protein samples for 2-hour incubation at 4° C, and subsequently rinsed with RIPA buffer properly. Samples were separated with 10% SDS-PAGE gel, followed by coomassie blue (refers to Appendix II). The coomassie blue stained gel bands were manually excised, destained, dehydrated and digested with sequencing-grade trypsin (Promega). The peptides were submitted for analysis by Matrix-assisted laser desorption/ionization time-of-flight (MALD-TOF) Mass Spectrometry. The resulting peaks were analyzed by Masslynx (Waters) and uploaded to the online Database (Matrixscience) for comparison. Protein candidates were verified with corresponding molecular weight and selected candidates were further confirmed with co-immunoprecipitation.

2.2.5 Western blot

5-20 µg of protein was fractionated by 10% SDS-PAGE (refers to Appendix II) and transferred onto a PVDF membrane (Bio-Rad) with 110mA current at 4° C

overnight. The membrane was blocked in 5% w/v nonfat dry milk (Carnation) or 2% w/v Bovine Serum Albumin (BSA, USB) according to the manufacturer's protocols of each primary antibody (refers to Table 2.2.2). Primary antibodies with the indicated dilutions in blocking buffer (refers to Table 2.2.2) were incubated with the sliced membrane at 4° C overnight, and followed with incubation of corresponding secondary antibodies conjugated with HRP (refers to Table 2.2.2) at room temperature for 1 hour. The blots were developed using ECL plus western blotting detection reagent (GE Healthcare). Primary and secondary antibodies are listed below for immunoprecipitation and western blot analysis.

Antibody	Catalog No.	Company	MW	Species	Dilution
KIF14	ab3746	Abcam	190KD	Rabbit	1:1000
E-CADHERIN	ab15148	Abcam	120KD	Rabbit	1:500
beta-CATENIN	ab6302	Abcam	94KD	Rabbit	1:3000
α-TUBULIN	ab6160	Abcam	55KD	Rat	1:1000
OCT4	ab19857	Abcam	43KD	Rabbit	1:3000
SOX2	ab59776	Abcam	40KD	Rabbit	1:3000
NANOG	ab21624	Abcam	38KD	Rabbit	1:1000
AURORA B	611083	BD Transduction	41KD	Mouse	1:1000
GAPDH	AP0063	Bioworld	37KD	Rabbit	1:3000
MYH9	3403	Cell Signaling	230KD	Rabbit	1:1000
MYH10	3404	Cell Signaling	230KD	Rabbit	1:1000
FOXO3A	9467	Cell Signaling	97KD	Rabbit	1:1000

BCL-2	2876	Cell Signaling	28KD	Rabbit	1:500
ROCK1	Sc-6056	Santa Cruz	160KD	Goat	1:500
SIRT1	Sc-19857	Santa Cruz	120KD	Goat	1:500
FOXMI	Sc-502	Santa Cruz	100KD	Rabbit	1:3000
Goat-HRP	Sc-2020	Santa Cruz	/	Donkey	1:3000
Mouse-HRP	Sc-2005	Santa Cruz	/	Goat	1:3000
Rabbit-HRP	Sc-2004	Santa Cruz	/	Goat	1:3000
Rat-HRP	Sc-2956	Santa Cruz	/	Chicken	1:3000

Table 2.2.2 Primary and secondary antibodies for western blot and immunoprecipitation study in human embryonic stem cells. MW: Molecular Weight.

2.2.6 Immunofluorescence (IF)

H9 or iPS_{IMR90} cells, cultured under freed- free conditions on 35mm petri dishes (MatTek) were washed once with cold PBS, fixed with 3.7% paraformaldehyde (Sigma) for 20 minutes at room temperature and permeablized with 0.05% Triton X-100 (Sigma) and 0.5% BSA in PBS at 4° C overnight. Samples were incubated with primary antibodies (refers to Table 2.2.2) at 4° C overnight followed by 3-4 washes with PBS and a 1-hour incubation with Alexa Fluor 488 (or 555)- conjugated secondary antibody (Invitrogen) at room temperature. Nuclei were counter stained with Hoechst (Invitrogen) for 5

minutes. Phase-contrast and fluorescent images were collected with 20X0.5 NA EC Plan Neofluar Ph2/ 60X1.4 NA EC Plan Neofluar DIC objective (Carl Zeiss) on an Axio Observer Z1 microscope (Carl Zeiss). All the images were collected with a cooled charge-couple device camera ORCA-R2 (Hamamatsu) at room temperature and processed with MetaMorph (Molecular Devices).

2.2.7 Quantitative chromatin immunoprecipitation (ChIP) and data analysis

For the putative FoxM1 binding sites on *OCT4*, *SOX2* and *NANOG* promoters, -5000bp of corresponding promoter regions upon ATG transcription initial site were searched with FoxM1 consensus binding sequence²²⁰ (A(T/C)AAA(T/C)AA) by BLAST (NIH). Putative binding sites were schemed in Fig. 2.3.8A and designed primers for ChIP verification were listed in Table 2.2.3.

2×10^6 H9 cells were chemically cross-linked with 1.42% formaldehyde (Sigma) for 15 minutes at room temperature and subsequently quenched with 125mM glycine (Affymetrix). Cells were scraped with plastic police and washed with cold PBS. Resuspended cells in IP buffer (refers to Appendix II) with protease inhibitors, were sheared with sonication to solubilize cross-linked DNA with a 15-second long pulse at 50% maximum power output for 8 times. The resulting chromatin fragments were incubated with 2 μ g anti-FoxM1 antibody (refers to Table 2.2.1) or normal rabbit IgG antibody (Santa Cruz) at 4° C for at

least 2 hours. 40µl of Protein A agarose beads (CalBiochem) were properly washed with PBS and added into the DNA-protein complexes for additional 1-hour incubation at 4° C. Subsequently, beads were washed 5 times with cold IP buffer without inhibitors. 100µl of Chelex 100 (Bio-Rad) was added and boiled for 10 minutes to reverse the crosslink. The input DNA were reversed after sonication without incubation of antibody and treated for reversal crosslink concurrently with other samples. DNA were then treated with proteinase K (Invitrogen) and precipitated with ethanol. DNA samples were amplified with designed primers (refers to Table 2.2.3) by PCR and separated by 1% agarose gel (Biowest). The visualization was performed with Molecular Imager ChemiDoc XRS system (Bio-Rad) and was processed in Quantity One (Bio-Rad). For quantitative analysis, DNA samples in triplicate were amplified by PCR with designed primers (refers to Table 2.2.3) and Power SYBR Green PCR master mix (Applied Biosystems) using a 7900HT fast real-time PCR system according to manufacturer's protocol (Applied Biosystems). Each cycle threshold (Ct) value was determined by SDS 2.3 software (Applied Biosystems), and normalized with percent of input²²¹.

Primer	Sequence	Size
<i>NANOG</i>	Forward: 'AGTTCTCATTTATGCCCAT3'	200bp
Site A	Reverse: 5'GGAATCTTTGGTGGTTGG3'	
<i>NANOG</i>	Forward: 5'TGCCTTTACCCAAACTGT3'	222bp

Site B	Reverse:5'GTAGATCAAATAGACCAAAA3'	
<i>OCT4</i>	Forward: 5'ATCTCAGCTCACTGCACCCT3'	191bp
Site A	Reverse:5'GCAGTTCGAGACCAGCCT3'	

Table 2.2.3 Sequences of primers designed for ChIP assay.

2.3 Results

2.3.1 Screening novel binding partners with three ageing factors in human ES cells.

The rationale of studying ageing factors in the regulation of ES cells self-renewal has been stated in sections 1.2.3-1.2.5. FOXM1, FOXO3A and SIRT1 were selected as baits to identify novel binding partners from human ES cells. Protein extracts of H9 cells (refers to 2.1.2) were subjected to immunoprecipitation; and the immunoprecipitated proteins were denatured and separated by SDS-PAGE gel. The ensuing coomassie blue staining of the gels displayed numerous primary protein binding targets of the three ageing factors respectively (Fig. 2.3.3.1A-C FOXM1, FOXO3A and SIRT1). Among those, discernible bands were excised from the gel by slicer according to the molecular weight (Fig. 2.3.1). The mass spectral readout for the band excised (refers to 2.2.4) from the FOXM1 pull at the molecular weight of 225KD (Fig. 2.3.1 A, *left*) was collected (Fig. 2.3.2 A). Online analysis for the peptide spectrum from Fig. 2.3.2A led to the discovery of MYH10 as the potential binding partner for FOXM1 at the molecular weight of 225KD (Fig. 2.3.2 B). Similarly, when the peptide spectrum (Fig. 2.3.2 C) derived from the SIRT1 pull at the molecular weight of 225KD (Fig. 2.3.1 B, *left*) was submitted to Matrixscience for analysis, the result appeared to be MYH10 as well with a high score for 80 (Fig. 2.3.2 D). The peptide readout from mass spectrum for FOXO3A at the same position (Fig. 2.3.1 C, *left*) was unfortunately unreadable (data not shown). The rest of the

candidates with high scores and matched molecular weights were enumerated (Table 2.3.1).

Endogenous interaction between MYH10 and FOXM1 (Fig. 2.3.3 A & B, *last columns*) was first confirmed by co-immunoprecipitation in both H9 cells (Fig. 2.3.3 A & B, *left*) and iPS_{IMR90} cells (Fig. 2.3.3 A & B, *right*). Using the same co-IP method, we revealed that MYH10 endogenously interact with FOXO3A (Fig. 2.3.3 C & D, *last columns*) as well as with SIRT1 (Fig. 2.3.3 E & F, *last columns*) in H9 cells (Fig. 2.3.3 C & D, *left*) and iPS_{IMR90} cells (Fig. 2.3.3 E & F, *right*).

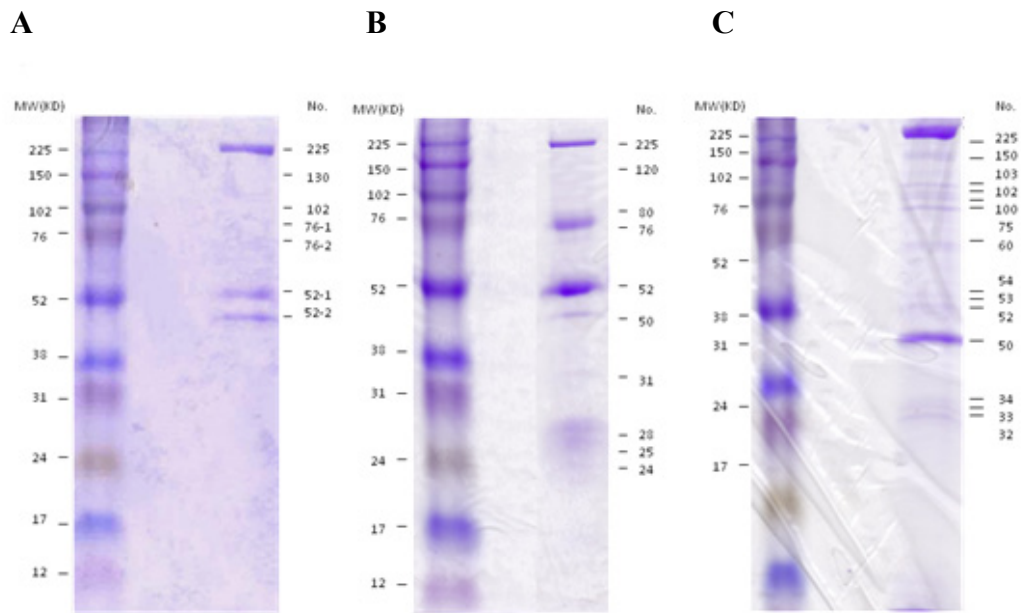
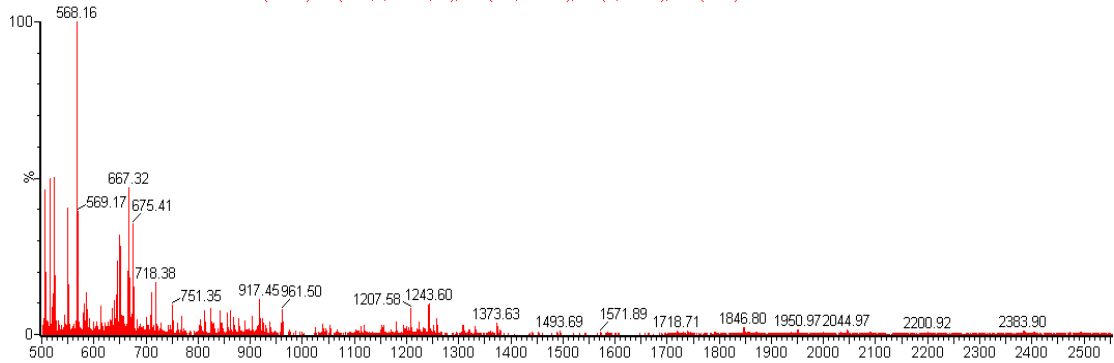


Figure 2.3.1 Screening novel binding partners with three ageing factors in human ES cells. (A) Proteins were pulled out by immunoprecipitation with anti-FOXM1 antibody in H9 cells. The immunoprecipitates were separated by SDS-PAGE gel electrophoresis and subsequently stained with coomassie blue. (B, C) Anti-SIRT1 and FOXO3A antibodies were used to pulled out novel binding targets

A

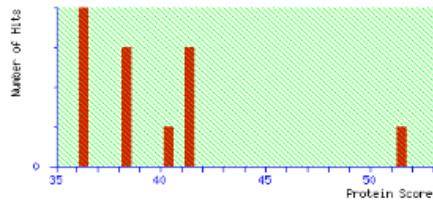
Kin-Dr Man-24122010 FOXMI 225k 62 (1.033) Cn (Cen,4, 80.00, Ht); Sm (SG, 2x3.00); Sb (5,40.00); Cm (1:87)

**B****Mascot Search Results**

User : FoxM1 225k
Email : hm_ein@hotmail.com
Search title :
Database : SwissProt 2010_12 (523151 sequences; 184678199 residues)
Timestamp : 11 Jan 2011 at 06:37:54 GMT
Top Score : 52 for **MYH10_RAT**, Myosin-10 OS=Rattus norvegicus GN=Myh10 PE=1 SV=1

Mascot Score Histogram

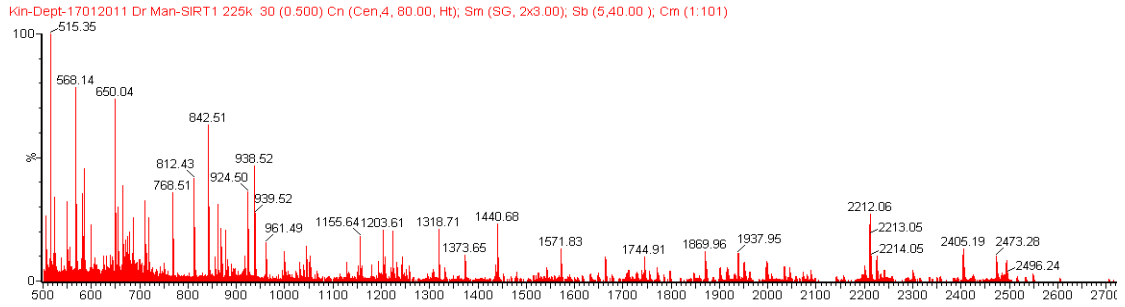
Protein score is $-10 \cdot \log(P)$, where P is the probability that the observed match is a random event. Protein scores greater than 70 are significant ($p < 0.05$).

**Concise Protein Summary Report**

Significance threshold p < Max. number of hits

- [MYH10_RAT](#) **Mass:** 228824 **Score:** 52 **Expect:** 3.7 **Matches:** 12
 Myosin-10 OS=Rattus norvegicus GN=Myh10 PE=1 SV=1
[MYH10_MOUSE](#) **Mass:** 228855 **Score:** 51 **Expect:** 3.8 **Matches:** 12
 Myosin-10 OS=Mus musculus GN=Myh10 PE=1 SV=2
[ZNF620_HUMAN](#) **Mass:** 48472 **Score:** 46 **Expect:** 13 **Matches:** 5
 Zinc finger protein 620 OS=Homo sapiens GN=ZNF620 PE=2 SV=1
[ZNF620_PONAB](#) **Mass:** 48631 **Score:** 46 **Expect:** 14 **Matches:** 5
 Zinc finger protein 620 OS=Pongo abelii GN=ZNF620 PE=2 SV=1
[KAD_METNO](#) **Mass:** 21109 **Score:** 44 **Expect:** 21 **Matches:** 4
 Adenylate kinase OS=Methylobacterium nodulans (strain ORS2060 / LMG 21967) GN=adk PE=3 SV=1
[KAD_METPB](#) **Mass:** 21340 **Score:** 42 **Expect:** 32 **Matches:** 4
 Adenylate kinase OS=Methylobacterium populi (strain ATCC BAA-705 / NCIMB 13946 / BJ001) GN=adk PE=3 SV=1
[MYH10_BOVIN](#) **Mass:** 228958 **Score:** 42 **Expect:** 33 **Matches:** 11
 Myosin-10 OS=Bos taurus GN=MYH10 PE=2 SV=2
[MYH10_HUMAN](#) **Mass:** 228858 **Score:** 42 **Expect:** 33 **Matches:** 11
 Myosin-10 OS=Homo sapiens GN=MYH10 PE=1 SV=3

C



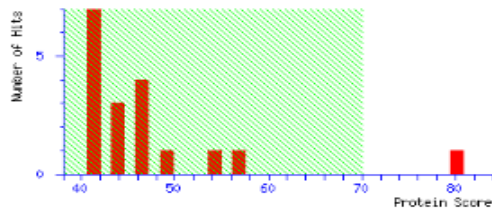
D

Mascot Search Results

User : Sirt1 225K Jan/18
Email : hm_ein@hotmail.com
Search title :
Database : SwissProt 2011_01 (524420 sequences; 185205850 residues)
Timestamp : 18 Jan 2011 at 10:20:20 GMT
Top Score : 80 for **MYH10_HUMAN**, Myosin-10 OS=Homo sapiens GN=MYH10 PE=1 SV=3

Mascot Score Histogram

Protein score is $-10 \cdot \log(P)$, where P is the probability that the observed match is a random event. Protein scores greater than 70 are significant ($p < 0.05$).



Concise Protein Summary Report

Format As **Concise Protein Summary** [Help](#)
 Significance threshold p < Max. number of hits

- [MYH10_HUMAN](#) **Mass:** 228858 **Score:** 80 **Expect:** 0.005 **Matches:** 12
 Myosin-10 OS=Homo sapiens GN=MYH10 PE=1 SV=3

Figure 2.3.2 Mascot analysis of the peptide spectrums from mass spectrometry for FOXM1 and SIRT1 at band 225K. (A) Peptide spectrum of the band stained at molecular weight 225KD from the FOXM1 pull was presented after analysis with Masslinx. (B) Human MYH10 was identified by matching the spectrum of 225KD band from FOXM1 pull with the Matrixscience online database (C) Result from Masslinx showed the peptide spectrum from SIRT1 binding pull at the same molecular weight 225KD. (D) The matched

spectrum from Matrixscience displayed human MYH10 again for potential SIRT1 binding partner at molecular weight 225KD with a very high score.

Protein Name	Score	Binding	Function
Ring finger protein 29	29	FOX M1	Unknown
LAMIN-B2	22	FOX M1	Nuclear stability, chromatin structure and gene expression
MYH10 (Myosin-10)	52/80	FOX M1, SIRT1	Creating a contractile force and kinetic energy transduction
Protein phosphatase 1E	40	SIRT1	Cell division, glycogen metabolism, muscle contractility and protein synthesis
DYNEIN	67	SIRT1	Force production and ATPase activity
MYH9 (Myosin-9)	50	SIRT1	Creating a contractile force and kinetic energy transduction
NF- κ B inhibitor epsilon	40	SIRT1	Inhibition of DNA-binding of NF- κ B

Table 2.3.1 List of selected potential interactions between ageing factors discovered by mass spectrometry. Summary of potential interaction partners identified by mass spectrometry, including MYH9 and 10, Protein phosphatase, LAMIN, DYNEIN and NF- κ B inhibitor, annotated with scores and functions.

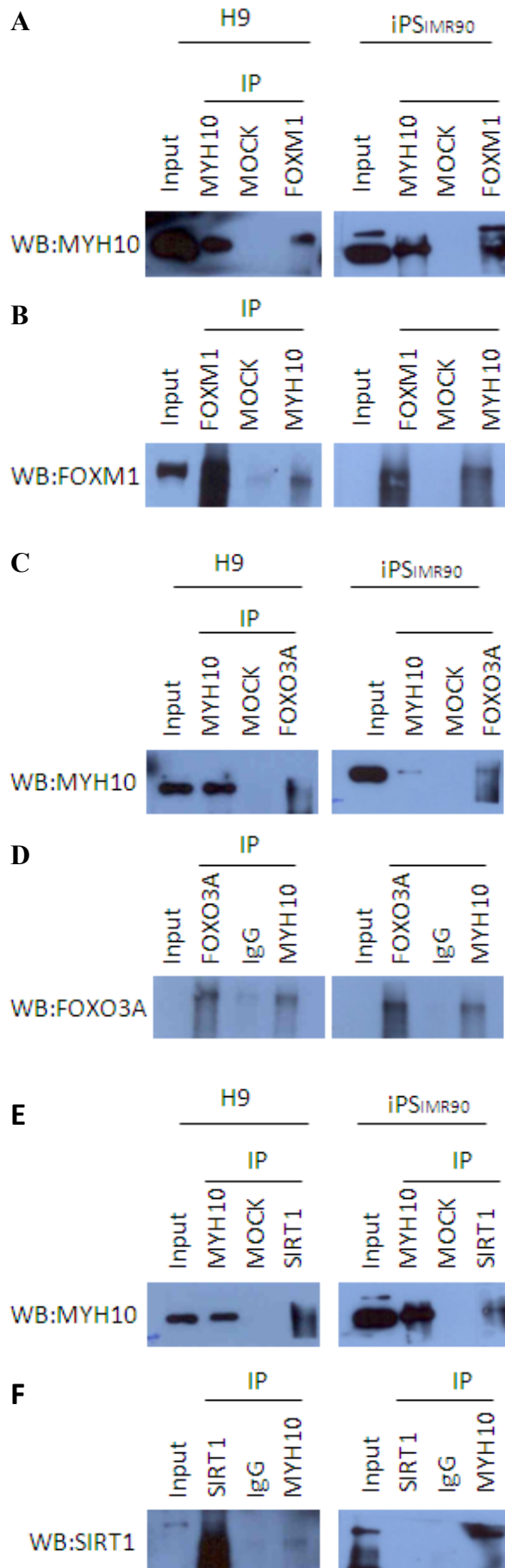


Figure 2.3.3 Co-immunoprecipitation of MYH10 with FOXM1, FOXO3A and SIRT1 in human ES cells. (A) Protein extracts of H9 (*left*) and iPS_{IMR90} (*right*) cells were subjected to immunoprecipitation with anti-MYH10 antibody for positive control, control IgG for mock, and anti-FOXM1 antibody for probe, followed by western blotting analysis with anti-MYH10 antibody. (B) Reciprocal IP experiment using anti-FOXM1 antibody for positive control, control IgG for mock and anti-MYH10 antibody, followed by western blotting analysis with anti-FOXM1 antibody. (C) Anti-MYH10, control IgG and anti-FOXO3A antibodies were used as positive control, mock and probe respectively for immunoprecipitation analysis in both H9 (*left*) and iPS_{IMR90} (*right*) cells. Western blotting analysis was performed with anti-MYH10 antibody. (D) Anti-FOXO3A, control IgG and anti-MYH10 antibodies were selected as positive control, mock and probe respectively for co-immunoprecipitation. Anti-FOXO3A antibody was used for western blotting analysis. (E) Immunoprecipitation performed in H9 (*left*) and iPS_{IMR90} (*right*) cells with anti-MYH10 antibody for positive control, control IgG for mock, and anti-SIRT1 antibody for probe, followed by western blotting analysis with anti-MYH10 antibody. (F) Co-immunoprecipitation was performed with anti-SIRT1 antibody for positive control, control IgG for mock and anti-MYH10 antibody for probe. Anti-SIRT1 antibody was then used for western blotting analysis.

2.3.2 Morphological changes in blebbistatin and thiostrepton-treated H9 and iPSIMR90 cells.

2.3.2.1 Cell death and cell-cell dissociation in thiostrepton-treated H9 and iPSIMR90 cells.

It was reported that FOXM1 could be directly targeted by thiostrepton at cellular level ²¹⁵. This natural small molecule can significantly inhibit the protein level of FOXM1 in MCF7 breast cancer cells at a concentration of 5 μ M after 24 hours of treatment ²¹⁴. The efficiency of FOXM1 inhibition was also revealed in IMR90 cells for the same concentration and treatment time (Fig. 2.3.4, A). Even after transiently expression of FOXM1 in IMR90 cells, the inhibition of FOXM1 by thiostrepton can still be achieved at 5 μ M after 24 hours. To investigate the effect of thiostrepton on inhibition of FOXM1 in the human ES cells of H9 cells, the H9 cells were treated with various doses of thiostrepton from 0 to 10 μ M, followed by measurements of cellular viabilities at different time points from 6 hours to 48 hours by phase contrast microscope (Fig. 2.3.4, C-F). However, using the same concentration of thiostrepton reported on MCF7 cells, the exposure of H9 cells to thiostrepton was observed to induce cell death and cell-cell dissociation after a short period of treatment for only 6 hours. H9 cells were observed to be still viable through microscope, with intact colony, at 0.5 μ M for 48 hours (Fig. 2.3.5, C). Downregulation of FOXM1 was verified by Western Blotting analysis with this particular condition of treatment (Fig. 2.3.6A, 2nd row). This set of data reveals the importance of FOXM1 in stem cells survival. And

this specific treatment condition was selected in the following experiments.

2.3.2.2 Blebbistatin protected dissociated H9 and iPSiMR90 cells from cell death.

The motor function of MYH10 on ACTIN can be blocked by blebbistatin²¹². This chemical compound can effectively repress the ATPase activity of MYH9 or MYH10 in human ES cells¹⁷⁰. Blebbistatin treated human ES cells formed dissociated colonies in which cells were spread out with lose cell-cell contacts¹⁸⁵. Interestingly, blebbistatin may enhance ES cells survival under this cell-cell dissociation condition^{184,222} (refers to 2.1.7). Similarly, we also observed that H9 ES cells treated with 5 μ M blebbistatin for 4 days may prevent colony formation without affecting viabilities (Fig. 2.3.5, 2nd column). Protein expression of MYH10 was not downregulated due to the fact that blebbistatin only inhibits the ATPase activity of MYH9, MYH10 or MYH14 (refers to 2.1.7 and Fig. 2.3.6A, 1st row). We verified the observation on the effect of blebbistatin to induce cell-cell dissociation in ES cells by immunofluorescence (IF) staining. Our IF data revealed the loss of MYH10 staining located at the cell-cell junctions after blebbistatin treatment (Fig. 2.3.6C, 2nd column). In order to compensate the inhibition of the ATPase activity of MYH10 by blebbistatin (refers 2.1.7), the protein expression of MYH10 was found to be induced in a dosage dependent manner (Fig. 2.3.7C, 1st column).

2.3.2.3 The effects of combined treatments in H9 and iPSIMR90 cells.

Taken together, the combined treatments with both the chemical inhibitors for the mentioned conditions were observed to disrupt colony integrity with reduced cell viability (Fig. 2.3.5, 4th column). The protein level of FOXM1 was initially induced by 5 μ M blebbistatin treatment for the first 48 hours in combined treatment. From our Western blotting analysis, the additional 48 hours treatment of 0.5 μ M thiostrepton was not sufficient to suppress the induced FoxM1 protein level by blebbistatin compared with cells treated with 0.5 μ M thiostrepton alone (Fig. 2.3.6A, 3rd vs. 4th column). The protein level of FOXM1 was shown to be reduced after 0.5 μ M thiostrepton treatment for 2 days in the presence of blebbistatin treatment (Fig. 2.3.6B, i). However, prolonged treatment of thiostrepton can induce massive cell death and this was reflected in the decreased protein level of loading control, TUBULIN (Fig. 2.3.6B, ii). The dislocation of MYH10 at the cell-cell junctions was also an evident revealed by immunofluorescence staining (Fig. 2.3.6C, 4th column). Compared to treatment with blebbistatin alone, the combined treatment showed profound cell-cell dissociation with increased cell death (Fig. 2.3.5B&D). Comparing with thiostrepton single treatment, the FoxM1 protein level was elevated in the combined treatment and thus may promote cell viability (Fig. 2.3.9, 4th column).

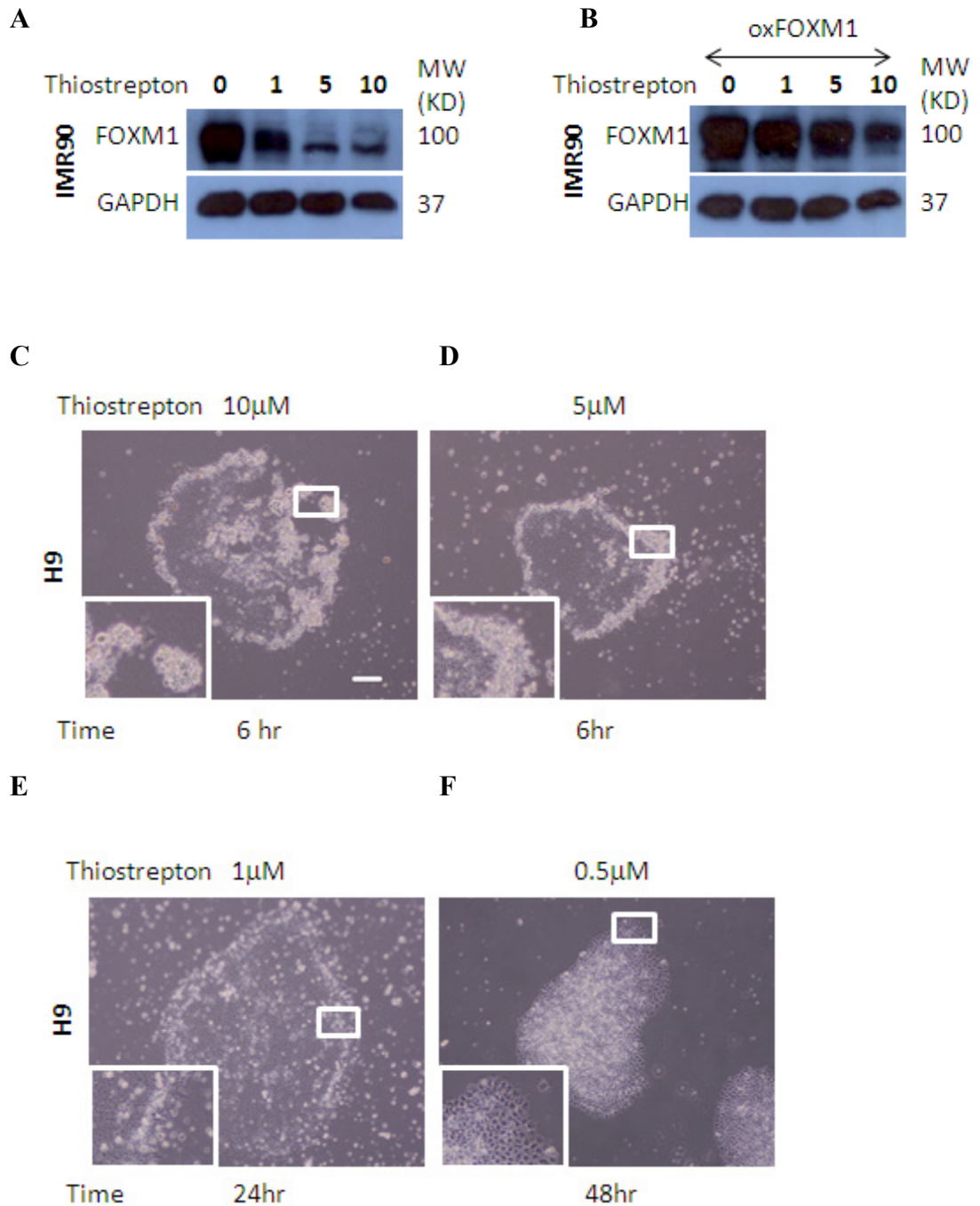


Figure 2.3.4 Inhibition of FOXM1 induced cell death in human ES cells. (A)

Western blot analysis of FOXM1 from IMR90 cells treated with thiostrepton in increasing dosages, revealed a dose-dependent expression pattern of FOXM1 **(B)**

Western blot analysis of FOXM1 from IMR90 cells which was transfected with 2μg pcDNA3-FOXM1 prior to thiostrepton treatments in increasing dosages.

(C-F) H9 cells treated with various concentrations of thiostrepton were captured upon the time with phase contrast microscope at 100X magnification when cell death and dissociation occurred. H9 cells were treated with 10 μ M for 6 hrs, 5 μ M for 6 hrs, 1 μ M for 24 hrs, or 0.5 μ M thiostrepton for 48 hrs respectively (Scale bar = 100 μ m).

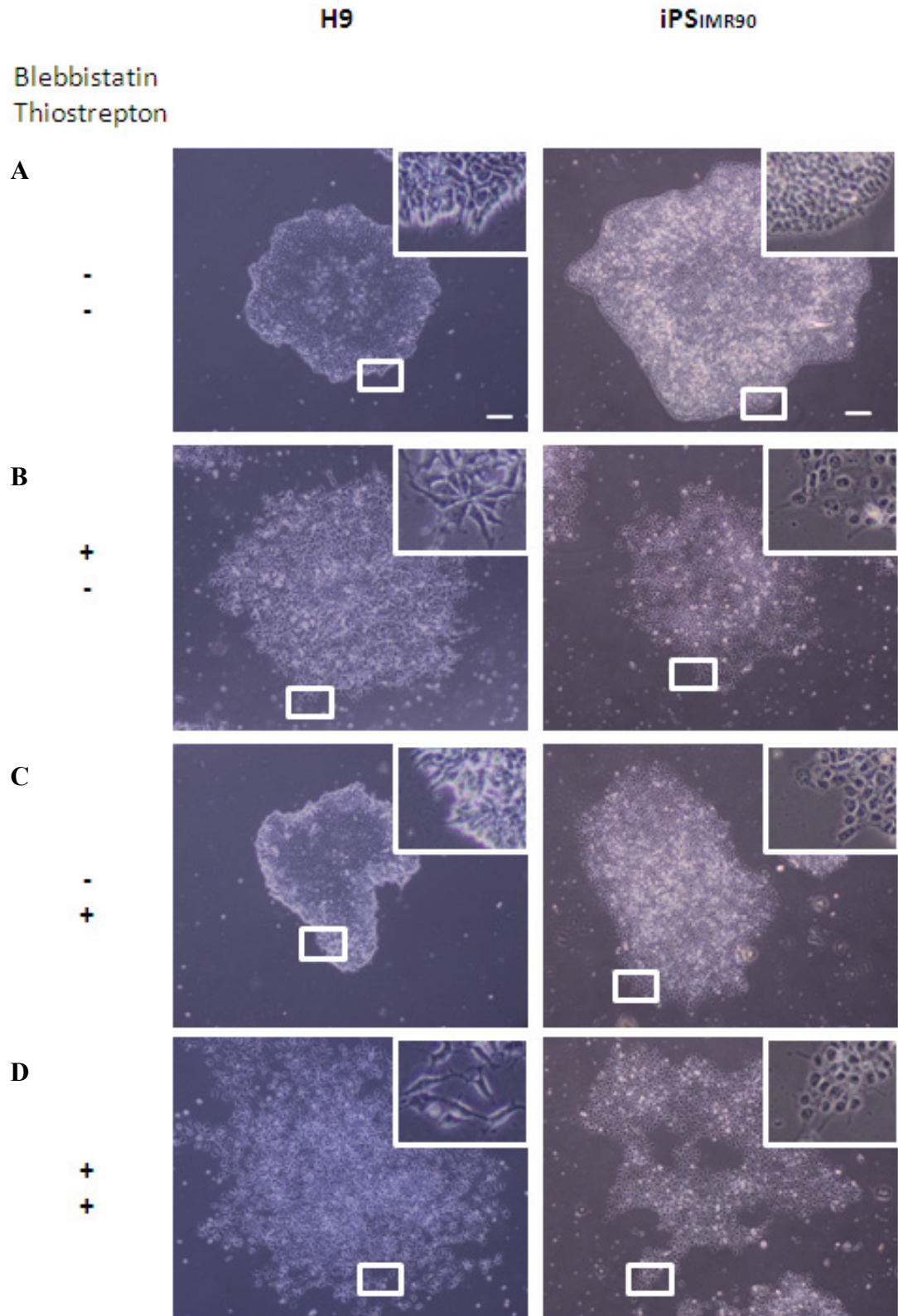


Figure 2.3.5 Characterization of H9 and iPS_{IMR90} cells after chemical inhibitions of FOXM1 and MYH10. Representative phase-contrast images of H9 (upper panels) and iPS_{IMR90} (lower panels) grown with 5 μ M blebbistatin or

0.5 μ M thiostrepton treatment. **(A)** Cells were cultured without any inhibitors. **(B)** Cells were treated with 5 μ M blebbistatin for 4 days. **(C)** Cells were treated with 0.5 μ M thiostrepton for 2 days. **(D)** Cells were treated with 5 μ M blebbistatin for 4 days; and 0.5 μ M thiostrepton was added on the 3rd day after blebbistatin treatment. (Scale bar=100 μ m)

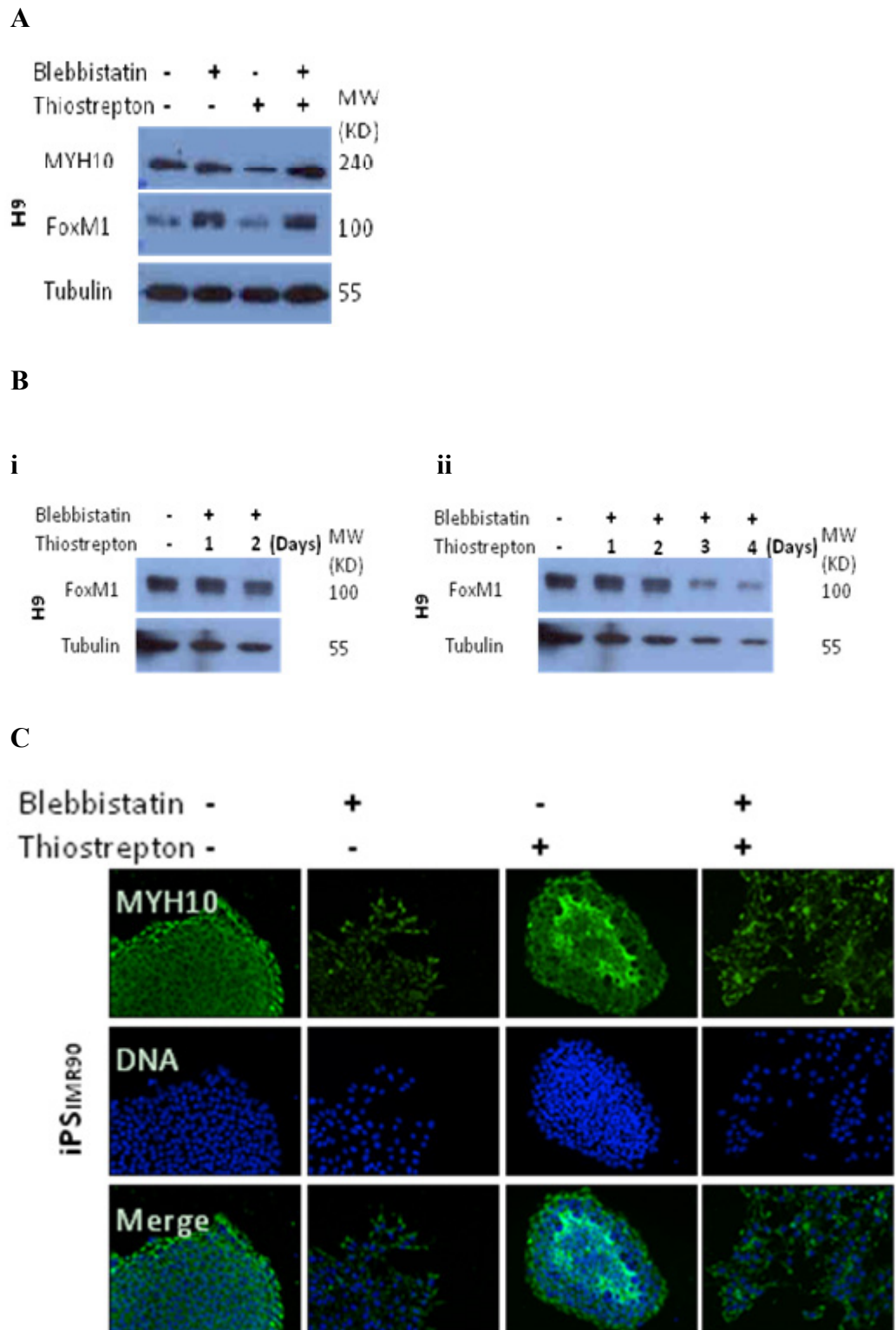


Figure 2.3.6 Chemical inhibition of MYH10 with blebbistatin and FOXM1 with thiostrepton. Inhibition of MYH10 induced upregulation of FOXM1.

(A) Western blot analysis of MYH10 and FOXM1 expression levels in H9 cells

treated with 5 μ M blebbistatin or 0.5 μ M thiostrepton. **(B)** Western blot analysis of FOXM1 in the presence of 5 μ M blebbistatin when 0.5 μ M thiostrepton was added in a time dependent manner for 1 to 4 days. (i) Thiostrepton was added 48 hours after blebbistatin treatment for additional 1 to 2 days. (ii) Same western blot with prolonged treatments of thiostrepton was displayed. **(C)** Dislocation of MYH10 observed at the cell-cell junctions of iPS_{IMR90} colony after chemical inhibition of FOXM1 and MYH10. Fluorescent images of iPS_{IMR90} cells stained with antibody against MYH10 treated with 5 μ M blebbistatin or 0.5 μ M thiostrepton.

2.3.3 Reduced pluripotency observed in H9 and iPSiMR90 cells in MYH10 or FOXM1-depleted cells,

2.3.3.1 Inhibition of MYH10 by blebbistatin may improve self-renewal.

The master pluripotent proteins OCT4, NANOG and SOX2 are often highly expressed in human ES cells. In this study, we found that ES cells treated with blebbistatin resulted in the formation of poorly aggregated colonies. However, augmented self-renewing ability was detected by upregulation of the pluripotent transcription factors via Western blotting result from dissociated H9 cells treated with 5 μ M blebbistatin (Fig. 2.3.7A, 2nd column). When H9 cells were treated with blebbistatin in a dosage dependent manner, the enhancement of pluripotency was found to be within the range of 2.5 to 5 μ M blebbistatin for 4 days (Fig. 2.3.7, C). The pluripotent markers declined slightly at 10 μ M blebbistatin treatment (Fig. 2.3.7C, 4th column). And cells can poorly survive at the condition of 20 μ M blebbistatin for 24 hours or further (Fig. 2.3.7B, 4th column). The fluctuation of pluripotency in response with the dosage of blebbistatin is highly associated with the expression of FOXM1 when the peaks of FOXM1 and pluripotent makers were reached at 5 μ M blebbistatin treatment (Fig. 2.3.7C, 2nd row).

2.3.3.2 Pluripotency was declined during suppression of FOXM1 by thiostrepton.

The inhibition of FOXM1 by thiostrepton can trigger dramatic cell death as well as downregulation of some important master regulatory pluripotency markers such as OCT4, NANOG and SOX2 (Fig. 2.3.7A, 3rd column).

2.3.3.3 Adding blebbistatin failed to rescue the loss of pluripotency triggered by repression of FOXM1 through thiostrepton.

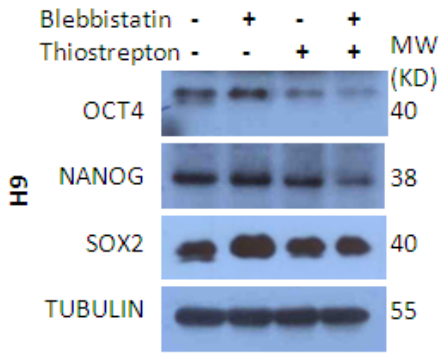
We showed that the presence of blebbistatin can improve ES cell viability (Fig. 2.3.5, 4th column), but failed to prevent loss of stemness induced by thiostrepton (Fig. 2.3.7A, 4th column).

The homogeneous staining of OCT4 from our results indicates that there are no dynamic heterogeneities in gene expression of *OCT4* from our cultured human ES cells with or without chemical inhibitory treatments.(Fig. 2.3.7, D). Therefore, overall elevation of OCT4 staining was observed when the ES cells were treated with 5 μ M blebbistatin for 4 days (Fig. 2.3.7D, 2nd column). This set of data was in line with the Western blotting result in retrospect (Fig. 2.3.7A, 2nd column). The decline of OCT4 staining after 0.5 μ M thiostrepton treatment alone or with 5 μ M blebbistatin (Fig. 2.3.7D, 3rd & 4th column) once again represented the observation from our Western blot data as shown in Fig. 2.3.7A, 3rd & 4th column.

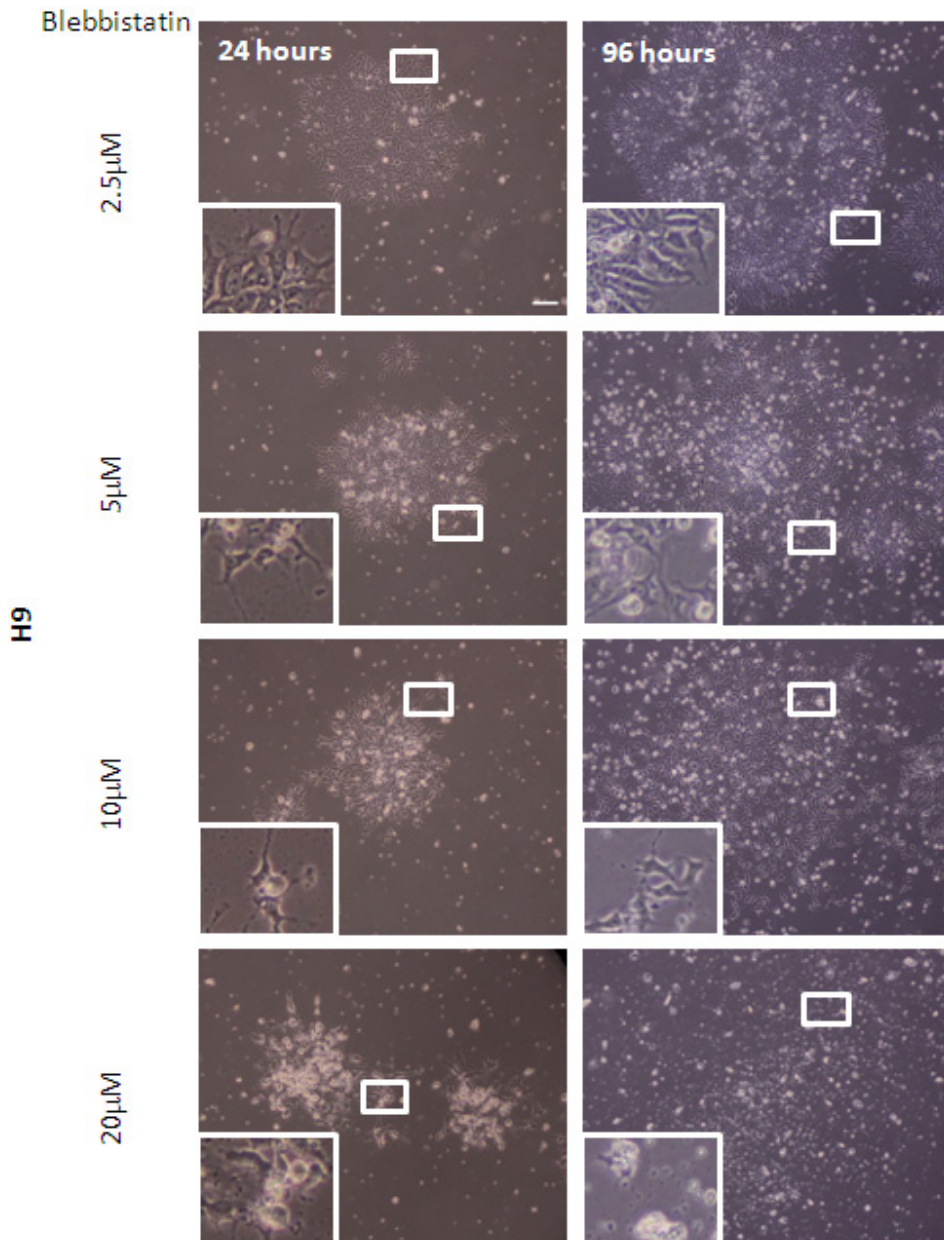
To further investigate the mechanisms involved in the maintenance of pluripotency and self-renewal associated with MYH10 and FOXM1,-5kb

promoter regions of the human *OCT4*, *NANOG* and *SOX2* were screened for the FOXM1 DNA consensus binding sites. Multiple FOXM1 putative binding sites were found at the regions of either *NANOG* or *OCT4* but *SOX2* promoters (Fig. 2.3.8A). The region of -4243 to -4231 bp on *OCT4* promoter was positively confirmed by CHIP assays, in which the transcription factor, FOXM1, can indeed bind to the *OCT4* promoter in H9 ES cells (Fig. 2.3.8B). This finding was elicited by our qPCR result as well. As shown in Fig. 2.3.8C, *column 2*, the FOXM1 occupancy on *OCT4* promoter was enhanced under blebbistatin treatment. This enhancement, which is a consequence of the elevated FOXM1 level induced by blebbistatin (Fig. 2.3.6A, *2nd column*), results in the increased of OCT4 (Fig. 2.3.7A, *2nd column, row 1*), NANOG (Fig. 2.3.7A, *2nd column, 2nd row*) and SOX2 protein levels (Fig. 2.3.7A, *2nd column, 3rd row*). There is little effect of thiostrepton alone on FOXM1's binding on OCT4 promoter in H9 cells (Fig. 2.3.8C, *column 3*), however, the levels of all stemness markers OCT4, NANOG and SOX2 were declined slightly (Fig. 2.3.7A, *3rd row*). The binding was declined when two inhibitors were both applied, suggesting the ability of self-renewal was compromised in this condition (Fig. 2.3.8 C, *column 4*). This piece of data is in line with our finding that the protein levels of OCT4 (Fig. 2.3.7A, *4th column, row 1*), NANOG (Fig. 2.3.7A, *4th column, row 2*), and SOX2 (Fig. 2.3.7A, *4th column, row 3*) were dramatically reduced.

A



B



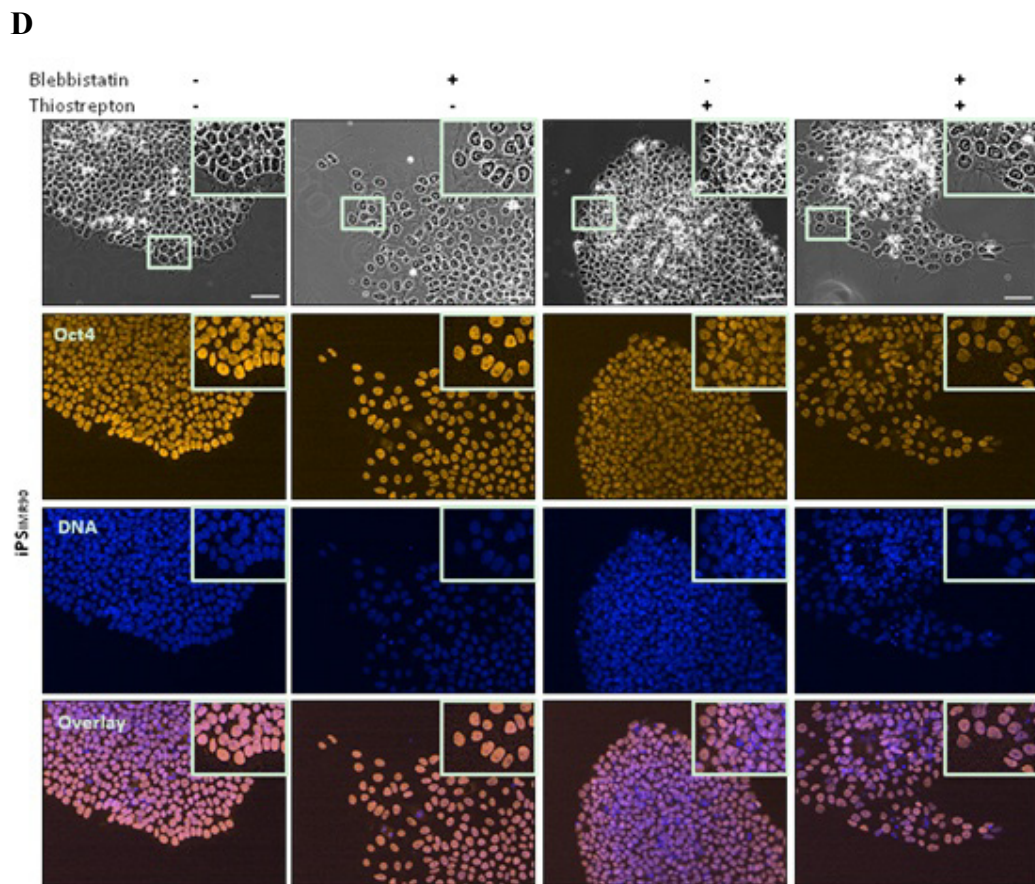
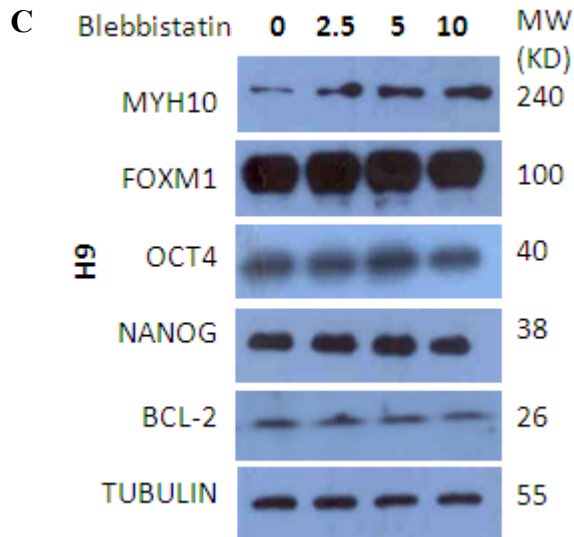


Figure 2.3.7 MYH10 associated with FOXM1 regulates human embryonic stem cells self-renewal. (A) Elevated FOXM1 promotes self-renewal and expressions of the markers for stemness. Western blot analysis of OCT4, NANOG and SOX2 protein in H9 cells treated with 5 μ M blebbistatin or 0.5 μ M

thiostrepton. **(B)** H9 cells treated with 2.5 to 20 μM blebbistatin were displayed after 24 hours (*upper panel*) or 96 hours (*lower panel*) respectively. **(C)** Dosage dependent levels of MYH10, FOXM1 and pluripotent markers in H9 cells treated with varied concentrations of blebbistatin. Western blot analysis of MYH10, FOXM1, OCT4, NANOG and SOX2 proteins in H9 cells treated with 0 to 10 μM blebbistatin. **(D)** Homogeneous expression of OCT4 in iPS_{IMR90} cells after chemical inhibition. Immunofluorescence staining of OCT4 in iPS_{IMR90} cells in the presence or absence of blebbistatin or thiostrepton (Scale bar=100 μm).

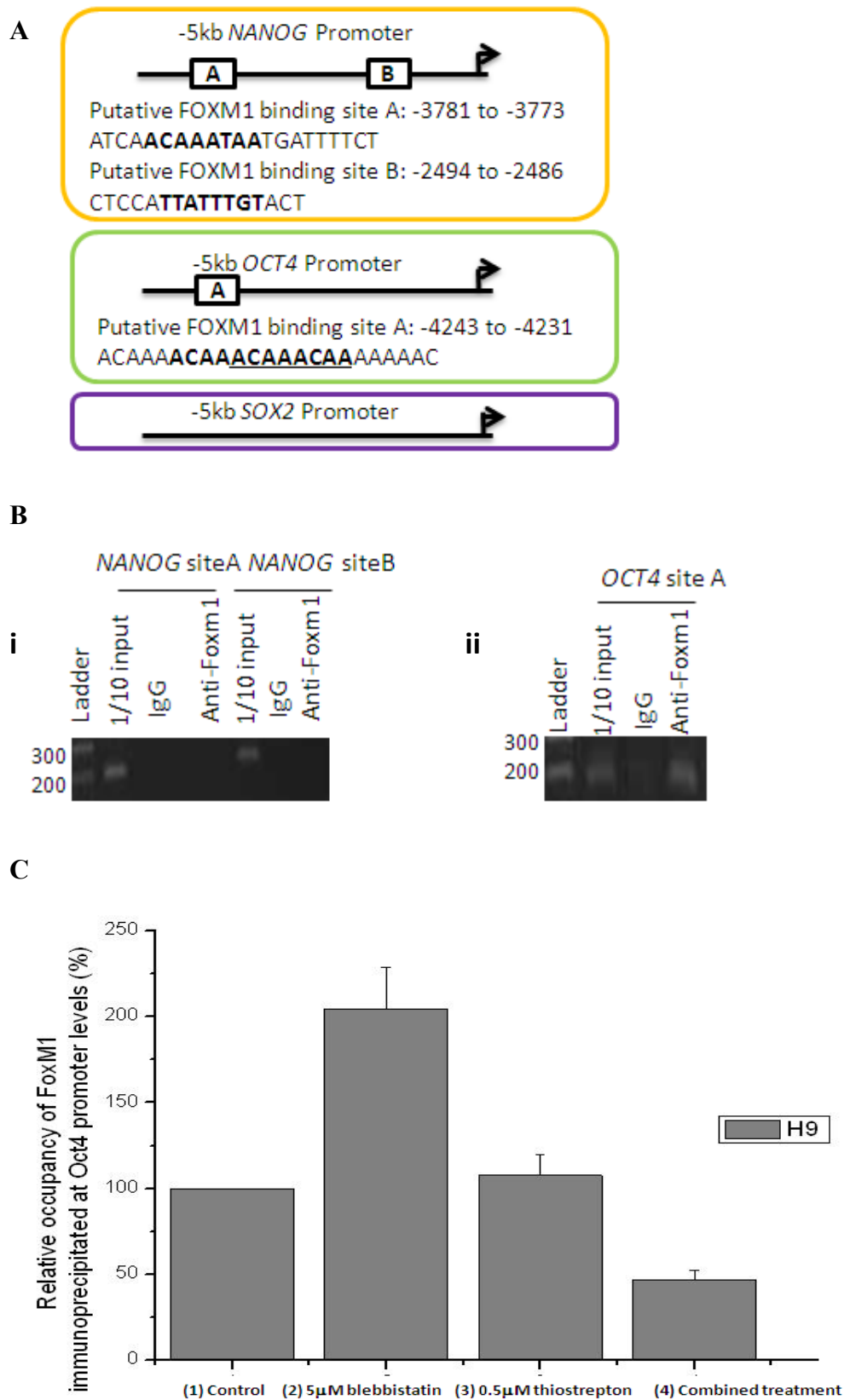


Figure 2.3.8 FOXM1 interacted with the OCT4 promoter associated with NMIIB. (A) Schematic of FOXM1 putative promoter binding sites on *NANOG*

and *OCT4* in human ES cells. The predicted positions of putative FOXM1 binding site in -5kb human *OCT4*, *NANOG* and *SOX2* promoters by gene sequence analysis and the positions of primers designed for ChIP assays. ChIP assay revealed the direct binding of FOXM1 on *OCT4* promoter. **(B)** ChIP assays were used to show direct binding of FOXM1 to endogenous *OCT4* promoter regions instead of *NANOG* in H9 cell line. The predicted size of the PCR product on *OCT4* promoter was 191kb. **(C)** ChIP-qPCR analysis of FOXM1 occupancy on the *OCT4* promoter. The different chemical inhibitors treated H9 cells were subjected to ChIP assays, and followed by qPCR analysis for the relative occupancy of FOXM1 at *OCT4* promoter. The treatment for each column is indicated as follow: (1) control H9 cells without any treatment; (2) H9 cells treated with 5 μ M blebbistatin for 4 days; (3) H9 cells treated with for 2 days; (4) Combined treatment stated at (2) and (3) were applied to H9 cells.

2.3.3.4 BCL-2 protein level was restored when blebbistatin was applied with thiostrepton.

Previously, we detected an increase in the viability of H9 and iPS_{IMR90} ES cells treated with blebbistatin (Fig. 2.3.5, *2nd column & 4th column*), we confirmed that such increase was associated with the increased level of anti-apoptotic BCL-2 protein (refers to 2.1.3), the upregulation of which is known to prevent apoptosis (Fig. 2.3.9, *2nd column*).

In contrast, the protein level of BCL-2 in ES cells treated with thiostrepton was reduced (Fig. 2.3.9, *3rd column*), indicating the apoptotic effect of thiostrepton-treated ES cells.

The combined treatment scenario, the elevated BCL-2 protein level (Fig. 2.3.9, *4th column*) circumvented the apoptotic trigger from thiostrepton; we noticed a decrease in stemness exemplified by the reduction of NANOG and OCT4 expression levels (Fig. 2.3.7A, *4th column*).

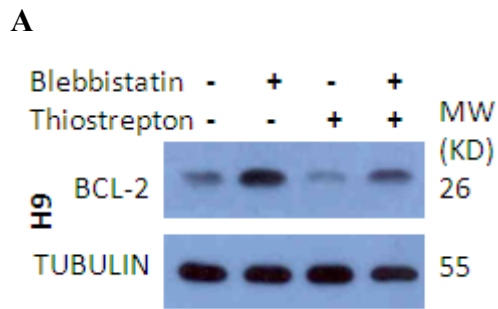


Figure 2.3.9 Inhibition of MYH10 by blebbistatin can improve the survival of human embryonic stem cells. (A) Inhibition of MYH10 can enhance the viability of human ES cells by upregulating BCL-2. Western blot analysis of BCL-2 in H9 cells treated with 5 μ M blebbistatin or 0.5 μ M thiostrepton.

2.3.4 Adhesive pathway is involved with FOXM1 regulatory role in self-renewal in human ES cells.

2.3.4.1 ROCK-MYOSIN pathway modulating adhesion via E-CADHERIN and beta-CATENIN in human ES cells is independent of FOXM1 expression.

As alluded in section 1.3, the dissociation of human ES cell colony is most likely due to the inhibition of NMMII by blebbistatin¹⁷², which results in the loss of E-CADHERIN at the cell-cell junctions and reduction in the recruitment of beta-CATENIN to trigger ROCK activation^{172,185}. The increased ROCK activation will induce the actomyosin contraction for apoptosis, from which was prevented by blebbistatin treatment in human ES cells (refers to Fig. 1.5)¹⁷². Therefore, the protein levels of E-CADHERIN and beta-CATENIN were reduced while the protein level of ROCK1 was increased in dissociated H9 colonies under blebbistatin treatment (Fig. 2.3.10A, 2nd column). We also observed that E-CADHERIN and beta-CATENIN were mis-localized from their normal residence at the cell-cell junctions in those poorly formed colonies induced by blebbistatin (Fig. 2.3.10B & C, 2nd column). Notably, the protein level of FOXM1 was induced by blebbistatin treatment (Fig. 2.3.6A, 2nd column).

Meanwhile, suppression of FOXM1 by thiostrepton also reduced the protein levels of E-CADHERIN as well as beta-CATENIN, along with upregulation of ROCK1 (Fig. 2.3.10A, 3rd column). But compared with blebbistatin treatment, there is nearly no effect on colony dissociation after

inhibition of FOXM1 by thioestrepton. Although the staining of E-CADHERIN and beta-CATENIN at cell-cell junctions was punctated after thioestrepton treatment, the colonies of iPSIMR90 were remained intact (Fig. 2.3.10B & C, 3rd column). These results suggested that FOXM1 may weaken cell-cell association by downregulation of E-CADHERIN.

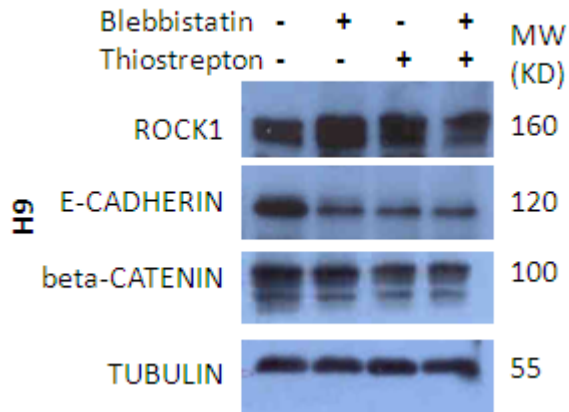
As the result from the combined treatment, the loss of E-CADHERIN together with beta-CATENIN were augmented while ROCK1 was slightly enhanced (Fig. 2.3.10A, 4th column). Collectively, the protein level of FOXM1 is independent of the state of colony dissociation induced by blebbistatin in human ES cells. However, suppression of FOXM1 may alternatively destabilize the cell-cell interactions by modulation of the protein levels of ROCK, E-CADHERIN and beta-CATENIN.

2.3.4.2 FOXM1 is the important downstream of ROCK-Myosin pathway in response of pluripotency after dissociation.

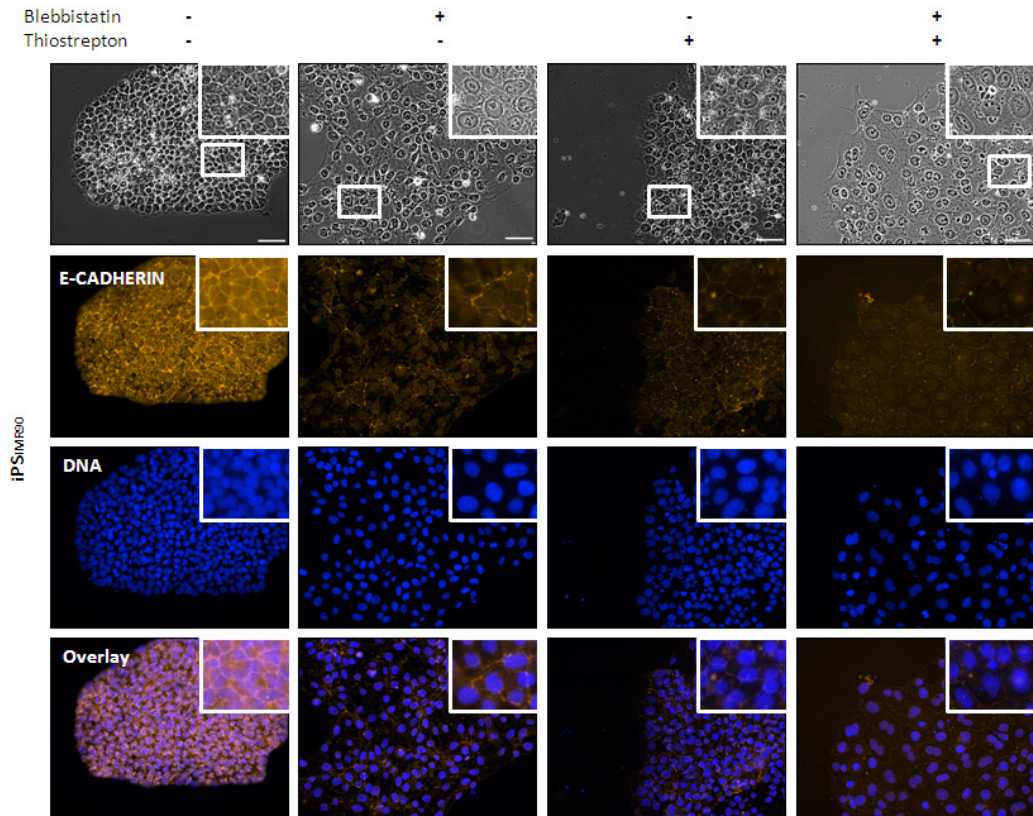
To investigate the aforementioned role of FOXM1 regulating ROCK expression other than colony dissociation in human ES cells, H9 cells were treated with 10 μ M Y27632 and 5 μ M blebbistatin for 4 days and 0.5 μ M thioestrepton for 2days. The result displayed an increasing trend of FOXM1 compared with control cells treated with blebbistatin and thioestrepton (Fig. 2.3.10c, 2nd row). But the protein levels of OCT4 (Fig. 2.3.10c, 3rd row), NANOG (Fig. 2.3.10c, 4th row) and SOX2 (Fig. 2.3.10c, 4th row) were found to

be further decreased when the activity of ROCK was inhibited by Y27632 in the presence of blebbistatin and thiostrepton. These results indicated that FOXM1 was the effector of ROCK-Myosin pathway for pluripotency in response to dissociation.

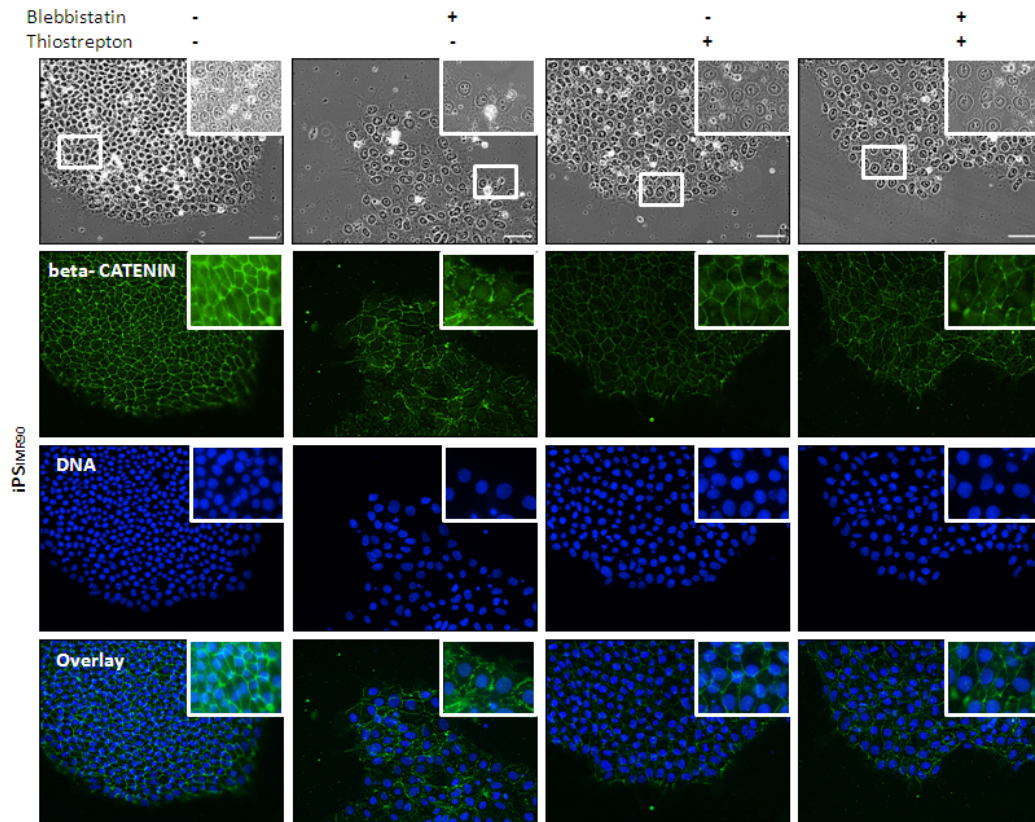
A



B



C



D

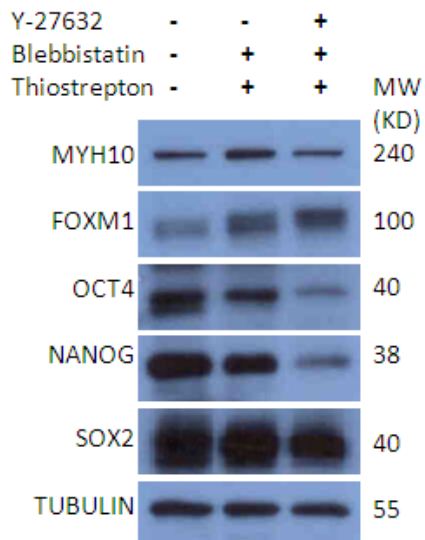


Figure 2.3.10 FOXM1 and MYH10 regulates self-renewal through cell-cell interaction. (A) FOXM1 and MYH10 modulates self-renewal via adhesive molecules. Cellular protein levels of ROCK1, E-CADHERIN and

beta-CATENIN in the presence or absence of blebbistatin or thiostrepton. **(B)**

Inhibition of FOXM1 and MYH10 disrupted E-CADHERIN adhesion in iPS_{IMR90} cells. Immunofluorescence staining of E-CADHERIN in iPS_{IMR90} cells treated with or without blebbistatin or thiostrepton (Scale bar=100 μ m). **(C)**

Inhibition of FOXM1 and MYH10 altered beta-CATENIN adhesion in iPS_{IMR90}. Immunofluorescence staining of beta-CATENIN in iPS_{IMR90} cells treated with or without blebbistatin or thiostrepton (Scale bar=100 μ m).

(D) The role of ROCK1 with FOXM1 and MYH10 in determination of stemness.

Western blot analysis of MYH10, FOXM1, OCT4, NANOG and SOX2 treated with or without Y27632, blebbistatin or thiostrepton.

2.3.5 Inhibition of the MYH10 and FOXM1 protein complex dysregulates specific mitotic markers during the self-renewal process of human embryonic stem cells.

2.3.5.1 Inhibition of MYH10 by blebbistatin altered AURORA B and KIF14 expression levels and affected the localization of CEP170 in ES cells.

To investigate the role of MYH10 in the self-renewal process in ES cells, the expression levels of AURORA B (a member of the chromosome passenger complex), and KIF14 (the central spindle kinesin interacting factor) were analyzed by Western Blotting analysis after blebbistatin inhibition (Fig. 2.3.11A, 2nd column). The cleavage furrow position is determined by mitotic spindle, myosin localization and other mechanisms during asymmetric division²²³, which can be observed from cleavage furrow ingression by microscope. Although cleavage furrow ingression was not affected under 5 μ M treatment of blebbistatin (Fig. 2.3.11B, 2nd column), the elevation of AURORA B and KIF14 protein levels suggested that the regulators associated with contractile ring and central spindle factors were altered. To explore whether asymmetric division may be affected other than cleavage furrow position by MYH10 inhibition, CEP170 as a marker for mother centriole (refers to 2.1.6) was observed with IF staining during mitosis in iPS_{IMR90} under blebbistatin treatment (Fig. 2.3.11C, 2nd column). No significant defects were observed before telophase. However, an increase signal of CEP170 at the midbody was detected at cytokinesis (Fig. 2.3.11C, 2nd column,

3rd panel arrows). These results suggest that 5 μ M blebbistatin treatment did not hinder the position of cleavage furrow but improved the migration of mother centriole to the midbody during cytokinesis for self-renewal.

2.3.5.2 FOXM1 inhibition downregulated AURORA B and KIF14, and caused centrosomal amplification in ES cells.

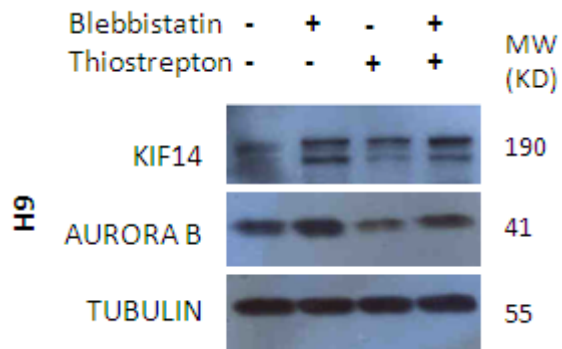
In parallel, thiostrepton was applied to H9 and iPS_{IMR90} cells to study the function of FOXM1 during mitosis in human ES cells. AURORA B and KIF14 were downregulated as a result of FOXM1 inhibition by thiostrepton (Fig. 2.3.11A, *3rd column*). Meanwhile, loss of MYH10 at the cleavage furrow indicative for cytokinesis failure (Fig. 2.3.11B, *3rd column*). The defect in cytokinesis may induce chromosome instability if the cell still commits to divide under this condition (Fig. 2.5&2.7A, *3rd column*). Supernumerary centrosomes were also found in iPS cells treated with thiostrepton by staining of CEP170 protein during mitosis (Fig. 2.3.11C, *3rd column, arrows*).

2.3.5.3 The expression levels of AURORA B and KIF14 were restored by blebbistatin treatment in FOXM1-inhibited H9 cells.

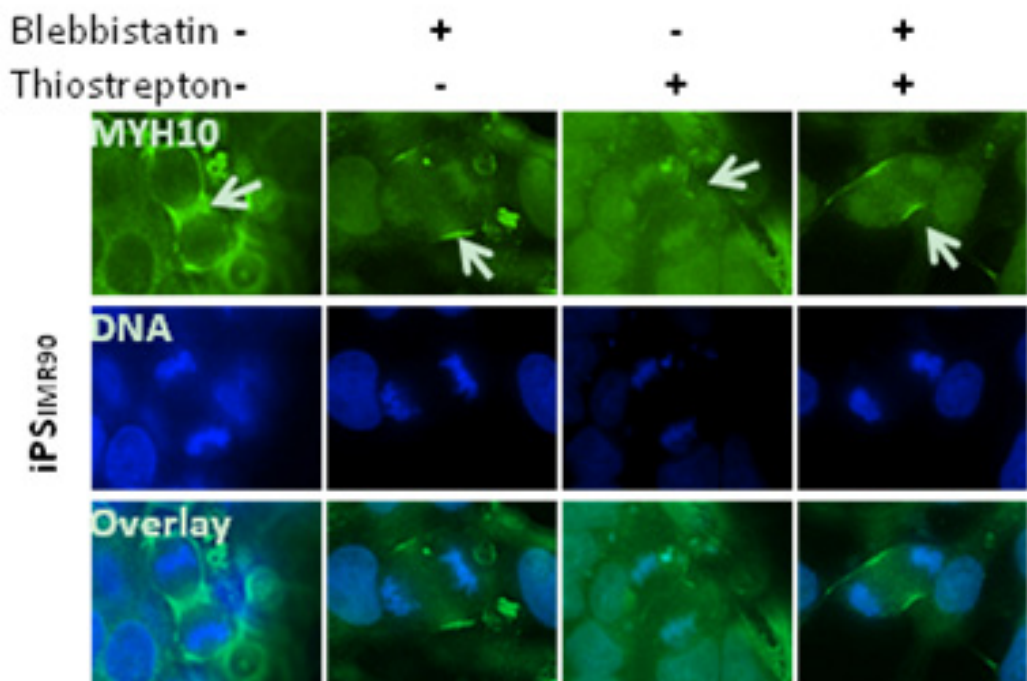
To investigate whether the induction of FOXM1 protein level by blebbistatin treatment (Fig. 2.3.6A, *2nd column*) can rescue the defects caused by thiostrepton treatment during mitosis (Fig. 2.3.11A-C, *3rd columns*), we found that the addition of blebbistatin circumvented the suppression of AURORA B

and KIF14 in FOXM1-inhibited H9 cells (Fig. 2.3.11A, 4th column). We further observed the recruitment of MYH10 back to the cleavage furrow with this rescue (Fig. 2.3.11B, 4th column).

A



B



C

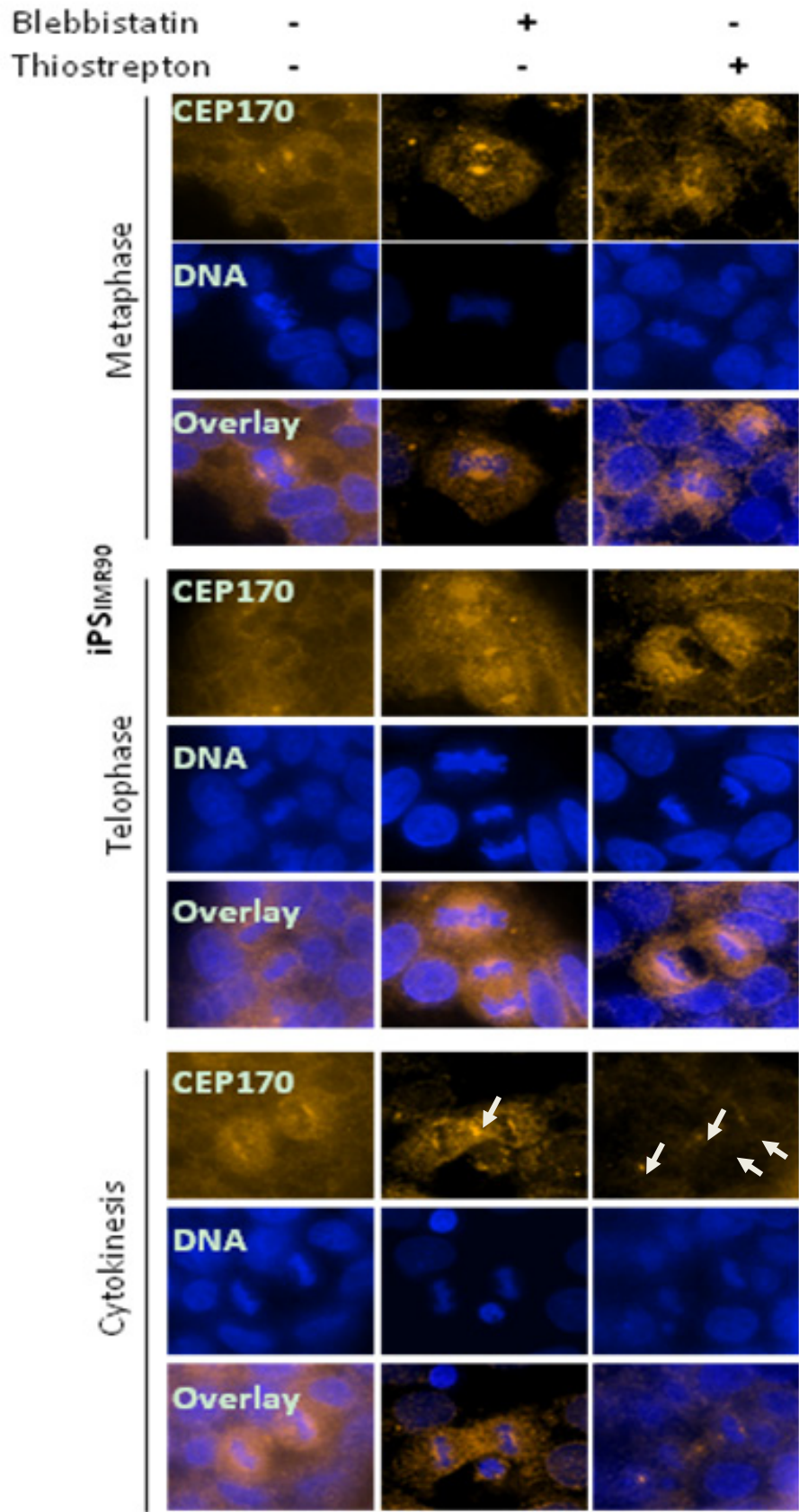


Figure 2.3.11 Downregulated FOXM1 and MYH10 interrupted cytokinesis and mitotic exit. (A) Altered cytokinesis markers after FOXM1 and MYH10 inhibition. Western blot analysis of KIF14 and AURORA B protein in H9 cells treated with 5 μ M blebbistatin or 0.5 μ M thiostrepton. (B) Blebbistatin treatment restored the recruitment of MYH10 at the cleavage furrow after the inhibition of FOXM1 by thiostrepton. Immunofluorescence staining of MYH10 during telophase in iPS_{IMR90} treated with or without blebbistatin or thiostrepton. (C) The marker of centrioles (CEP170) revealed cytokinesis malfunction during FOXM1 and MYH10 inhibition. Immunofluorescence staining of CEP170 in iPS_{IMR90} treated with or without blebbistatin or thiostrepton during different stages of mitosis.

2.3.6 Genetic knockdown of the MYH10 and FOXM1 complex in H9 human embryonic stem cells.

2.3.6.1 Genetic knock-down of MYH10 via retroviral gene transfer.

Unlike blebbistatin treatment in which both MYH9 and MYH10 activities were affected (refers to 2.1.7), genetic knockdown is necessary for our studies to exclude the non-specific inhibitory effect from chemical inhibitor and investigate the solo interaction between MYH10 and FOXM1. Hence, specific knockdown of MYH10 was achieved (refers to 2.2.3) and shown by Western blot analysis. The protein level of MYH9 was not affected after cells were infected with shMYH10. (Fig. 2.3.12B, 2nd row). Meanwhile, the protein level of FOXM1 was dramatically reduced after MYH10 knockdown (Fig. 2.3.12B, 3rd row).

We observed phenotypic differences when H9 cells were treated with blebbistatin, compared with MYH10-depleted H9 cells. H9 cells were observed to be tightly associated in shMYH10 cells, in comparison with the dissociated ES cells from blebbistatin-treated cells (Fig. 2.3.5B VS. Fig. 2.3.12D, 4th column). Pointed protrusions were observed to be localized at the peripheries of the colonies (Fig. 2.3.12D, 4th column inset).

The results from our immunofluorescence staining also revealed reduced MYH10 signal intensities at both the cell-cell junctions and at the cleavage furrows, after MYH10 was depleted (Fig. 2.3.12E, 2nd column). In addition, the FOXM1 signal intensity was suppressed from the nuclei (Fig. 2.3.12F, 2nd column).

2.3.6.2 Genetic knockdown of FOXM1 via retroviral gene transfer.

We detected specific depletion of FoxM1 after H9 cells were transduced with shRNA, without affecting other forkhead members such as FOXO3A (Fig. 2.3.12A, 2nd & 3rd columns). We did not detect a reduction of MYH10 protein level after FOXM1 knockdown (Fig. 2.3.12A, 1st column). We also observed phenotypic differences between H9 cells treated with thiostrepton and with FOXM1 depletion. We found that H9 cells depleted with FOXM1 were much healthier with no obvious cell death compared with cells treated with thiostrepton (Fig. 2.3.5C VS. Fig. 2.3.12D, 3rd column). No colony dissociation was found in H9 cells depleted with FOXM1. Cell protrusions were also observed to be localized at the peripheries of the colonies (Fig. 2.3.12D, 3rd column inset).

We revealed a reduction of FOXM1 immunofluorescence signals at the nuclei. In contrast, the staining intensity of FoxM1 at the protrusions was enhanced (Fig. 2.3.12F, 3rd column). We further noted that the staining intensity of MYH10 at the cell-cell junctions and at the cleavage furrows was slightly reduced after FOXM1 knockdown (Fig. 2.3.12E, 3rd column).

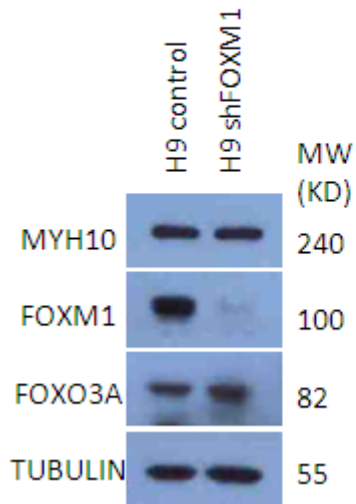
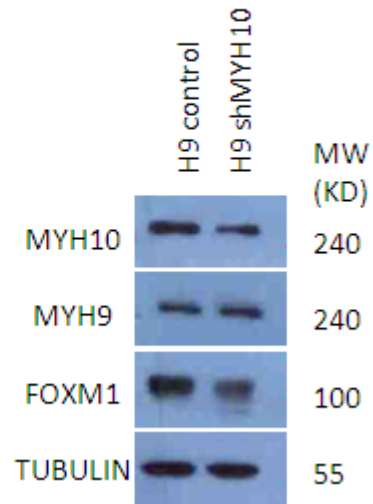
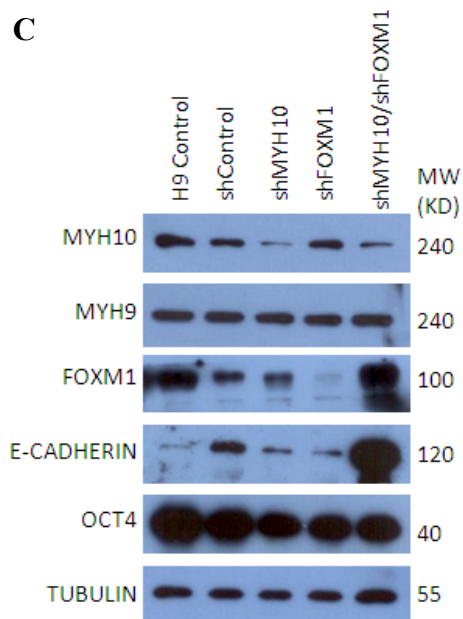
2.3.6.3 Simultaneous knockdown of FOXM1 and MYH10 using shRNAs.

Simultaneous knockdown of MYH10 and FOXM1 in H9 cells also showed efficient suppression of the protein level of MYH10 instead of MYH9. (Fig. 2.3.12C, 1st row). Meanwhile, the protein level of FOXM1 was slightly

induced (Fig. 2.3.12C, 3rd row). A negative control for shRNA with a scrambled sequence was constructed (refers to 2.2.3) and displayed to exclude the non-specific targeting during infection (Fig. 2.3.12C, 2nd column).

H9 cells co-transduced with shFOXM1 and shMYH10 displayed tight colonies with excessive protrusions at the peripheries (Fig. 2.3.12D, 4th column).

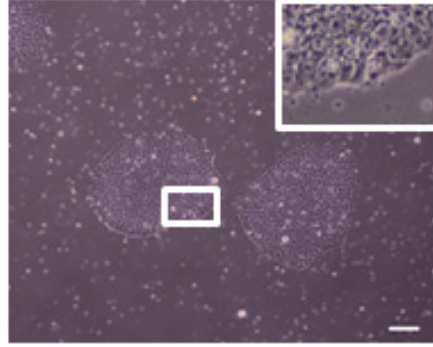
Immunofluorescence staining using MYH10 antibody revealed undefined cell-cell junctions and cleavage furrows (Fig. 2.3.12E, 4th column). Unlike the single knockdown of FOXM1 or MYH10 where the staining of FOXM1 was preferentially located in nuclei, simultaneous knockdown of FOXM1 and MYH10 displayed more staining of FOXM1 at the protrusions (Fig. 2.3.12F, 4th column).

A**B****C**

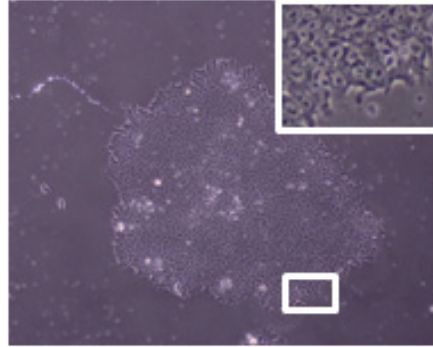
D

H9

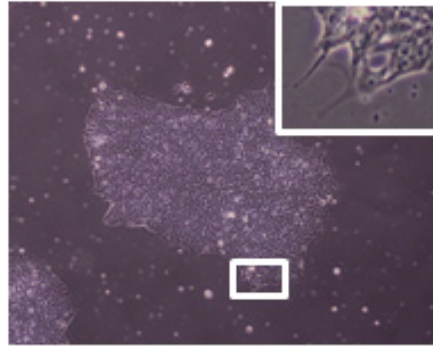
Control



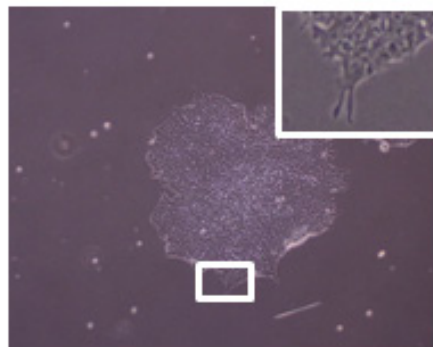
shControl



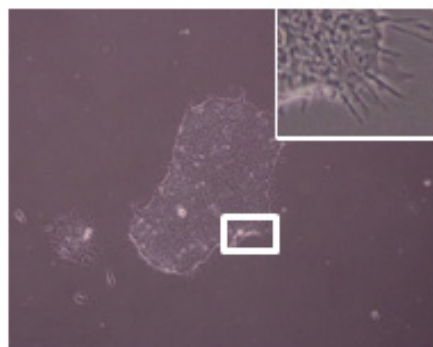
shFOXM1



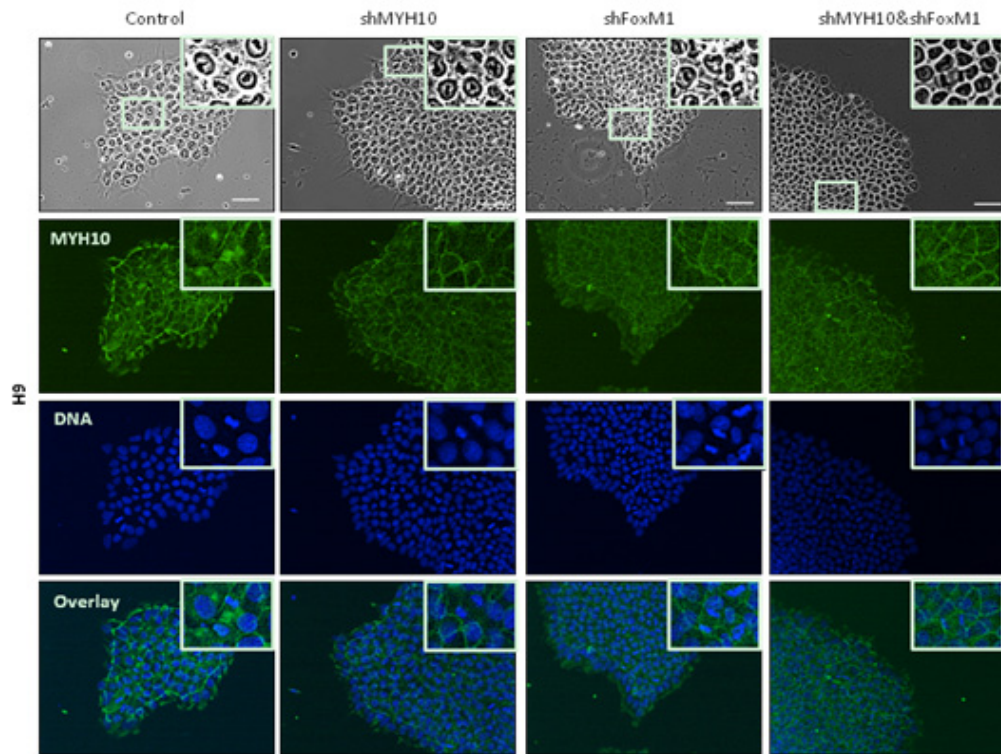
shMYH10



shFOXM1 & shMYH10



E



F

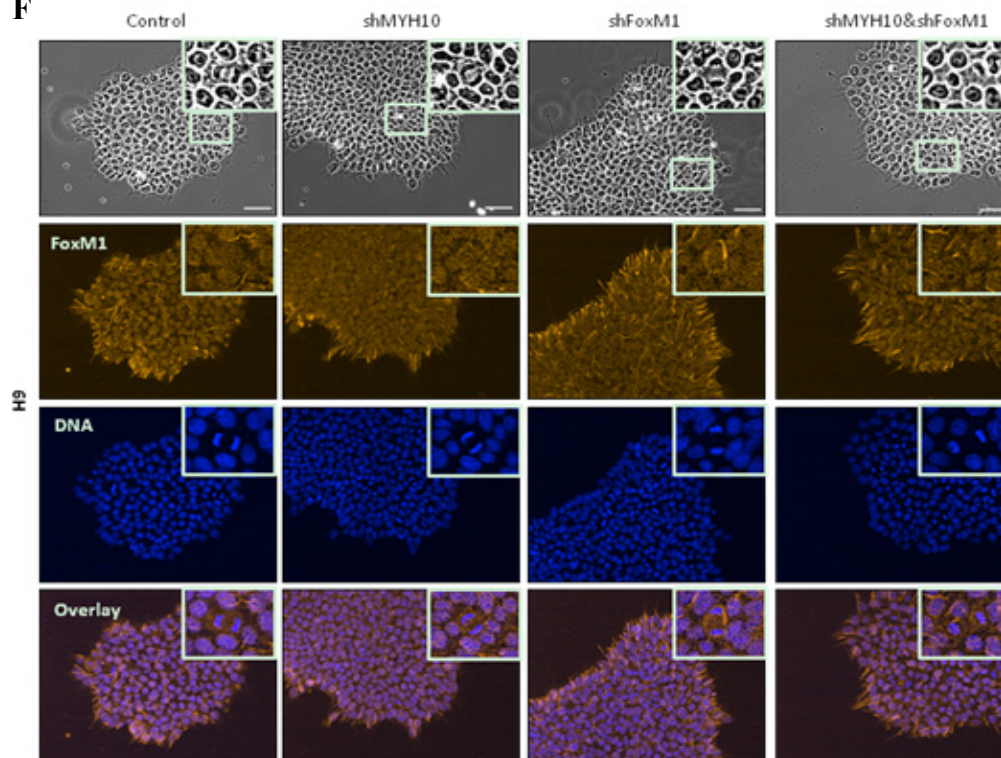


Figure 2.3.12 Specific knock-down of FOXM1 and MYH10 via retroviral gene transfer. (A) Western blot analysis of MYH10, FOXM1 and FOXO3A

proteins in H9 cells with or without FOXM1 depletion. **(B)** Western blot analysis of MYH10, MYH9 and FOXM1 proteins in H9 cells with or without MYH10 depletion. **(C)** Western blot analysis of MYH10, MYH9, FOXM1, E-CADHERIN and OCT4 proteins in H9 cells with or without MYH10 and FOXM1 knockdown. shRNAs targeting MYH10 or FOXM1 were used to double knock down the proteins in H9 cells. Cells without retrovirus infection or treated with nontargeting shControl were presented as negative controls. **(D)** Representative phase contrast images of H9 cells with or without depletion of FOXM1 or MYH10 compared with cells transfected with or without shControl (Scale bar=100 μ m). **(E, F)** Immunofluorescence staining of MYH10 **(E)** and FOXM1 **(F)** in H9 cells with MYH10 and FOXM1 depletion. Zoomed images from the indicated area were shown in the insets (Scale bar=100 μ m).

2.3.7 Knockdown of the FOXM1 and MYH10 complex affects pluripotency in H9 cells.

2.3.7.1 Genetic knockdown of FOXM1 downregulated OCT4, NANOG and SOX2 expression in human H9 cells.

Protein levels of OCT4, NANOG and SOX2 were examined in H9 cells transduced with shFoxM1. All three master pluripotent markers were found to be downregulated (Fig. 2.3.14A).

2.3.7.2 Genetic knockdown of MYH10 reduced OCT4, NANOG and SOX2 expression in H9 cells.

We obtained similar results on OCT4, NANOG and SOX2 expression when H9 cells were transduced with shMYH10, compared with cells transduced with shFoxM1 (Fig. 2.3.14B).

2.3.7.3 Pluripotency is further reduced in double knockdown of MYH10 and FOXM1 H9 cells

One of the master pluripotent markers, OCT4, was found to be largely downregulated when compared to the individual knockdown, suggesting a synergistic effect on pluripotency when this protein complex was depleted as a whole (Fig. 2.3.13C, 5th row).

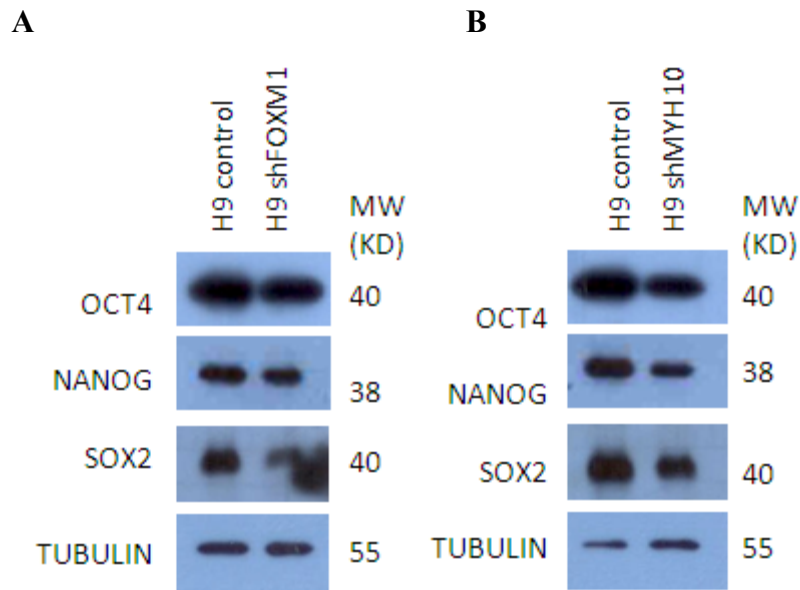


Figure 2.3.13 Depletion of MYH10 and FOXM1 induces the loss of pluripotency. (A) Western blot analysis of OCT4, NANOG and SOX2 proteins in H9 cells with or without FOXM1 depletion. (B) Western blot analysis of OCT4, NANOG and SOX2 proteins in H9 cells with or without MYH10 depletion.

2.3.8 Adhesive pathway was interfered in human embryonic stem cells depleted with FOXM1 and MYH10.

2.3.8.1 FOXM1 modulates ROCK1, E-CADHERIN and beta-CATENIN protein levels in H9 cells.

Compared with the thiostrepton-treated H9 cells where cell-death was observed after treatment, there was no significant cell death found in cells transduced with shFOXM1 (Fig. 2.3.4C & Fig. 2.3.13D, *3rd column*). However, we noted a downregulation of E-CADHERIN (Fig. 2.3.15A, *2nd row*). The reduced E-CADHERIN level after shFoxM1 transduction was further confirmed by immunofluorescence staining of E-CADHERIN (Fig. 2.3.15C, *3rd row*).

As mentioned in section 2.1.4, beta-catenin binds with the cytoplasmic domain of E-CADHERIN to stabilize the cell-cell interaction. In consistent with the lower protein level of E-CADHERIN, beta-CATENIN also exerts a declining pattern after FOXM1 was depleted (Fig. 2.3.15A, *3rd row*). As illustrated in Fig. 1.5, the instability of E-CADHERIN at the cell-cell junction can induce the activation of ROCK for actomyosin contraction. Therefore, the protein level of ROCK1 was found to be enhanced when E-CADHERIN was suppressed after FOXM1 depletion in H9 cells (Fig. 2.3.15A, *1st row*).

2.3.8.2 MYH10 regulates ROCK1, E-CADHERIN and beta-CATENIN expression levels in H9 cells.

In contrast with the treatment of blebbistatin, the colonies of H9 cells remained tightly-packed after specific knockdown of MYH10 (Fig. 2.3.7B & Fig. 2.3.13D, 4th column). Interestingly, from the result of Western blotting protein level of E-CADHERIN was increased and appeared to reinforce the adhesions among cells at the cell-cell junctions (Fig. 2.3.15B, 2nd row). However, the staining of E-CADHERIN with immunofluorescence showed that E-CADHERIN was mis-localized at the cell-cell junctions (Fig. 2.3.15C, 2nd column). It may indicate that the appearance of contact colonies of MYH10-depleted H9 cells was remained in the absence of E-CADHERIN at the cell-cell junctions.

2.3.8.3 E-CADHERIN was highly upregulated after double knockdown of FOXM1 and MYH10 in H9 cells.

Previously, we found that E-CADHERIN was dramatically downregulated in combined treatment of blebbistatin and thioestrepton (Fig. 2.3.10A, 4th column). However, in this double knockdown study, the expression level of E-CADHERIN did not reveal a declining trend after double knockdown, (Fig. 2.3.13C, 4th row). Instead, E-CADHERIN level was detected to be highly upregulated, suggesting that simultaneous depletion of FOXM1 and MYH10 may adversely promote cell adhesion via upregulation of E-CADHERIN.

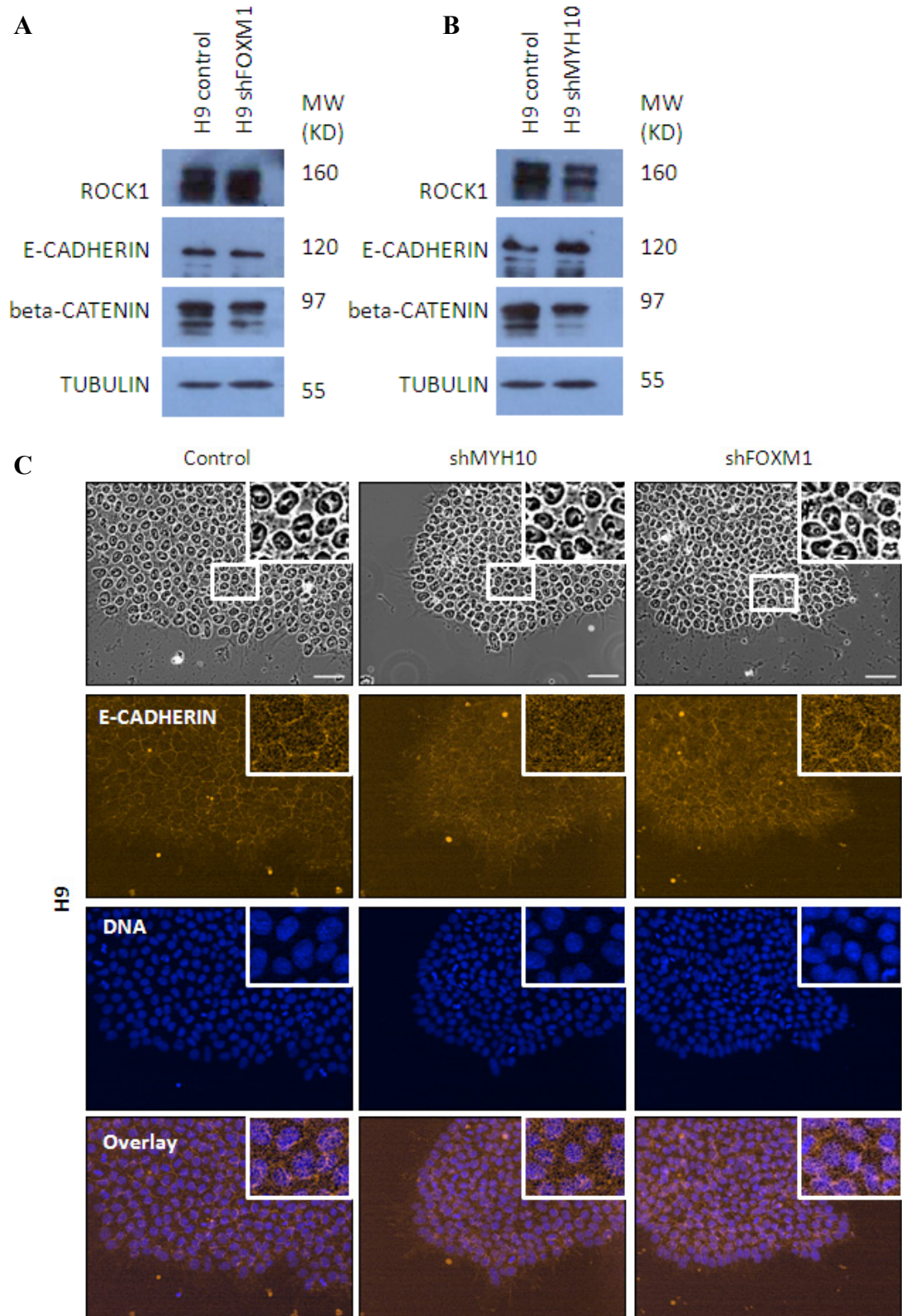


Figure 2.3.14 Depletion of MYH10 but FOXM1 increased the protein level of E-CADHERIN. (A) Western blot analysis of ROCK1, E-CADHERIN and beta-CATENIN proteins in H9 cells with or without FOXM1 depletion. (B)

Western blot analysis of ROCK1, E-CADHERIN and beta-CATENIN proteins in H9 cells with or without MYH10 depletion. (C) Immunofluorescence staining of E-CADHERIN in H9 cells with MYH10 or FOXM1 depletion. Zoomed images from the indicated area were shown in the insets (Scale bar=100 μm).

2.3.9 Knockdown of the FOXM1 and MYH10 protein complex induced cytokinesis defects

2.3.9.1 FOXM1 is required for expression of the mitotic regulators AURORA B kinase and KIF14.

Unlike the treatment of thiostrepton where AURORA B was downregulated, transduction of shFOXM1 in H9 cells increased the expression level of the mitotic regulator AURORA B kinase while the mitotic kinesin KIF14 was still downregulated (Fig. 2.3.16A, *1st & 2nd columns*). The staining of MYH10 at the cleavage furrow was reduced after FOXM1 knockdown (Fig. 2.3.16C, *3rd column*), suggesting that cytokinesis may be dysregulated in FOXM1-silenced H9 cells.

2.3.9.2 MYH10 monitors the proper expression of the mitotic regulators AURORA B kinase and KIF14.

H9 cells transduced with shMYH10 significantly down regulated FOXM1 (Fig. 2.3.13B, *3rd column*). In accordance with FOXM1 depletion, the protein level of KIF14 was suppressed by knockdown of MYH10 (Fig. 2.3.16B, *1st column*). And the protein level of AURORA B kinase was elevated after MYH10 depletion same as FOXM1 knockdown (Fig. 2.3.16B, *2nd column*). The recruitment of MYH10 at the cleavage furrow was correspondingly decreased after MYH10 knockdown (Fig. 2.3.16C, *2nd column*), suggesting a similar dysregulated cytokinesis process in FOXM1-depleted H9 cells was observed in

MYH10-depleted cells. In contrast, the protein level of KIF14 was increased during blebbistatin treatment (Fig. 2.11A, 2nd column), suggesting a distinctive mechanism involved in chemical inhibition of NMII other than depletion of MYH10 alone.

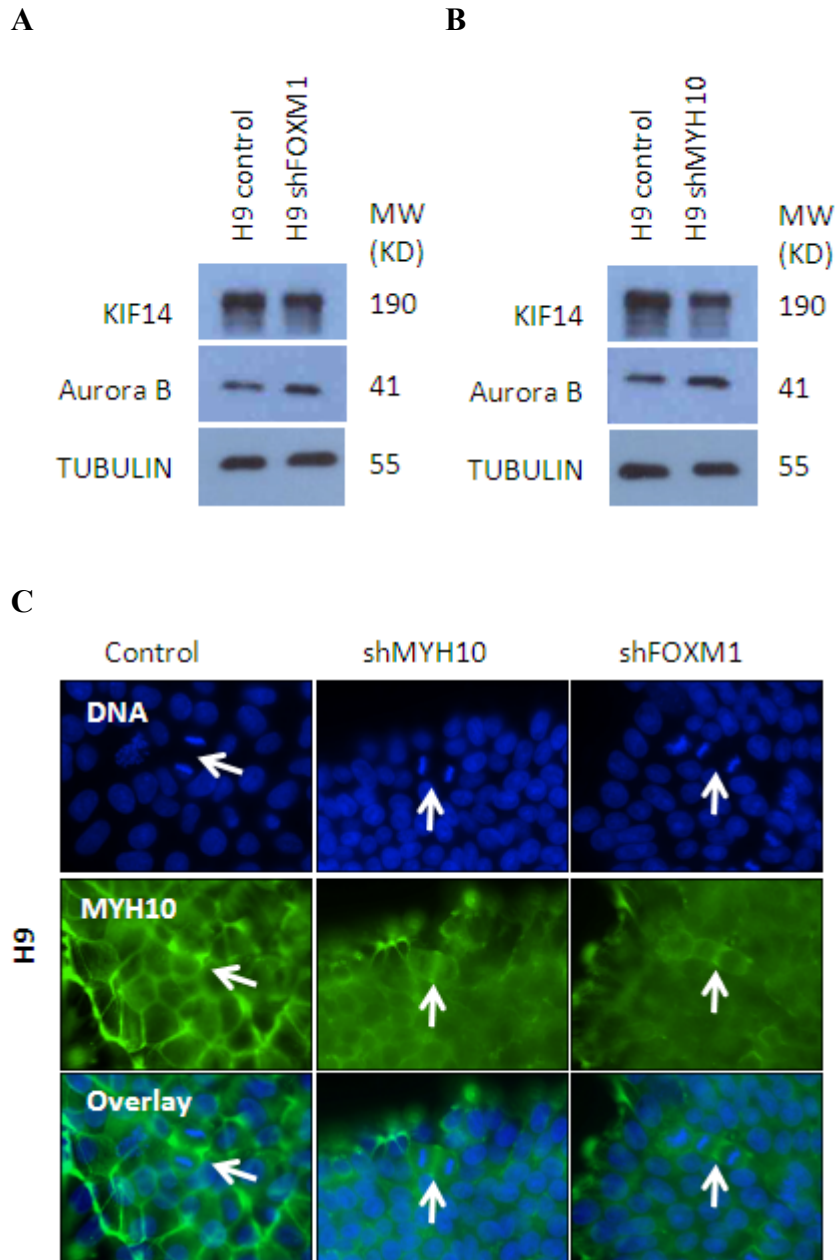


Figure 2.3.15 Depletion of MYH10 and FOXM1 deregulates cytokinesis and mitotic exit. (A) Western blot analysis of KIF14 and AURORA B proteins in H9 cells with or without FOXM1 depletion. (B) Western blot analysis of KIF14 and AURORA B proteins in H9 cells with or without MYH10 depletion. (C) Immunofluorescence staining of MYH10 in H9 cells at telophase with MYH10 and FOXM1 depletion.

2.3.10 Summary diagram

Protein	Category	Function
FOXM1	Protein bait of the study	Transcription factor involved in cell proliferation, cell survival and pluripotency
MYH10	Binding partner with FOXM1	Cytokinesis, cell-cell interaction, cell motility
MYH9	Protein isoform of MYH10	Cytokinesis, cell-cell interaction, cell motility
OCT4	Pluripotency marker	Transcription factor controlling embryonic development and stem cell pluripotency
NANOG		Transcription regulator monitor embryonic stem cell proliferation and self-renewal
SOX2		Transcription factor regulates embryonic development and differentiation
BCL-2	Apoptotic marker	Mitochondrial membrane protein suppressing apoptosis
ROCK1	Adhesive marker	Protein kinase regulates actin cytoskeleton, adhesion and cytokinesis via myosin
E-CADHERIN		Adhesion protein co-localized with F-actin for maintain junctional structure in hES cells
beta-CATENIN		Adhesion protein binds with E-CADHERIN to maintenance cell-cell adhesion in hES cells
KIF14	Mitotic marker	Mitotic kinesin directs cytokinesis by targeting to the central spindle
AURORAB		Kinase participates in the regulation of mitosis including spindle assembly and cleavage furrow formation
CEP170	Mother centriole marker	Protein localizes to the sub-distal appendages of mother centrioles

	Blebbistatin 5uM	Thiostrepton 0.5uM	Blebbistatin + Thiostrepton	shFOXM1	shMYH10
FOXM1	induced (++)	reduced (-)	induced (+)	reduced (--)	reduced (--)
MYH10	/	/	/	/	reduced (--)
OCT4	induced (++)	reduced (--)	reduced (--)	reduced (--)	reduced (--)
NANOG	induced (++)	reduced (--)	reduced (--)	reduced (--)	reduced (--)
SOX2	induced (++)	reduced (--)	reduced (--)	reduced (--)	reduced (--)
BCL-2	induced (++)	reduced (--)	induced (+)	unfinished	unfinished
ROCK1	induced (++)	induced (++)	induced (+)	reduced (-)	reduced (--)
E-CADHERIN	reduced (--)	reduced (--)	reduced (--)	reduced (-)	induced (+)
beta-CATENIN	reduced (--)	reduced (--)	reduced (--)	reduced (-)	reduced (-)
KIF14	induced (++)	reduced (--)	induced (+)	reduced (-)	reduced (-)
AURORAB	induced (++)	reduced (--)	induced (+)	induced (+)	induced (+)

Table 2.3.2 Summary diagram of MYH10 interacts with FOXM1 in human embryonic stem cells. Results were compared with control condition. (+) represents induced; (++) represents highly induced; (-) represents reduced; (--) represents highly reduced; / represents no obvious change were observed.

2.4 Discussion

2.4.1 MYH10 is a novel protein binding partner with FOXM1 in human embryonic stem cells.

As elucidated in section 1.2.3, FOXM1 is essential to promote cell proliferation in all dividing cells including human ES cells, which suggests the indispensable role of FOXM1 as an ageing factor in tissue homeostasis. Here, we demonstrate that FOXM1 endogenously binds with MYH10 in human ES cells out of other binding proteins from mass spectrometry screens with ageing factors (Fig. 2.3.2 A, B & Fig. 2.3.3 A, B). The interactions between MYH10 with FOXO3A and SIRT1 were also predicted and confirmed by co-immunoprecipitations (Fig. 2.3.2 & Fig. 2.3.3). The mutual bindings of FOXM1 with FOXO3A²¹⁹ and SIRT1 with FOXO3A²²⁴ were verified by other groups in cancer cell lines. In particular, the role of this novel complex of MYH10 and FOXM1 is unexplored in human ES cells. The role of MYH10 and FOXM1, on its own per se, has not been studied in human ES cells. Our results suggest that MYH10 may modulate multifaceted cellular activities including viability, adhesion, cytokinesis and eventually pluripotency together with FOXM1 in human ES cells.

2.4.2 Blebbistatin-treated cells exhibited increased viability.

The cellular protective function and mechanisms of blebbistatin on dissociated human ES cells were extensively studied^{170,172,185}. Blebbistatin,

which functions as the inhibitor for non-muscle myosin II, can efficiently block the ATPase activity of MYH9 and MYH10 to prevent the apoptosis caused by myosin hyperactivation in dissociated human ES cells¹⁷⁰. Apoptosis is triggered by myosin hyperactivation mediated by mitochondrial pathway involving BCL-2 family. This protective function by blebbistatin on dissociated human ES cells was found to be dosage dependent within the range of 1.25-10 μ M in long-term treatment¹⁷⁰. Hence, we evaluated the effect of blebbistatin on H9 cells for apoptosis within this dosage range by detection of the protein levels of MYH10 and FOXM1 correlating with BCL-2 level. Four days treatment of 2.5-20 μ M blebbistatin on H9 cells showed enhanced apoptosis (Fig. 2.3.7, B). It was found that blebbistatin treatment can slightly increase the protein level of MYH10 on a higher concentration with more dissociated colonies, indicating a possible compensation of MYH10 expression in response to the inhibition from blebbistatin (Fig. 2.3.7C, 1st row). Intriguing, the state of apoptosis depending on blebbistatin treatment is related to the protein level of BCL-2 showing higher anti-apoptotic level of blebbistatin below 10 μ M (Fig. 2.3.7C, 5th row). The protein level of FOXM1 is correspondingly elevated below 10 μ M blebbistatin treatment while higher concentration of blebbistatin treatment reduced the protein level of FOXM1 (Fig. 2.3.7C, 2nd row). Overexpression of FOXM1, in various tumors, could improve cellular proliferation by upregulation of the anti-apoptotic BCL-2 protein²²⁵⁻²²⁷. It is hereby plausible to correlate the expression of FOXM1 with BCL-2 protein level with respect to apoptosis in

human ES cells treated with blebbistatin. The inhibition of FOXM1 by proteasome inhibitor, thiostrepton, showed selective targeting of FOXM1 on multiple cell lines²¹⁴ and was tested on our IMR90 epithelial cells (Fig. 2.3.4 A&B) . The effect of thiostrepton on H9 human ES cells was shown to confer increased cellular toxic at the effective inhibitory concentration (Fig. 2.3.4, C). Although 0.5 μ M of thiostrepton treatment was tested to be efficient to inhibit the protein level of FOXM1 in H9 cells (Fig. 2.3.6A, 3rd column), adverse apoptosis was still observed (Fig. 2.3.4 C & Fig. 2.3.5 C) with downregulated BCL-2 (Fig. 2.3.9A, 3rd column). Taken together, a combined treatment was designed to investigate the survival threshold balanced by blebbistatin and thiostrepton (Fig. 2.3.6, B). In the presence of 5 μ M blebbistatin treatment for 48 hours, addition of 0.5 μ M thiostrepton, and subsequent 48hours with blebbistatin showed downregulated FOXM1 and BCL-2 compared with cells treated with blebbistatin alone (Fig. 2.3.6A, 4th column & Fig. 2.3.9A, 4th column). Our results showed that blebbistatin may upregulate FOXM1 to improve cellular survival under low dosage (2.5 μ M-5 μ M) mediated by mitochondrial pathway.

2.4.3 Cell-cell interactions were regulated by Myosin and FOXM1 in human ES cells via E-CADHERIN/beta-CATENIN and ROCK axis..

The selective ROCK inhibitor Y27632 was firstly identified to promote cellular survival of dissociated human ES cells in 2007¹⁸². Further investigations

found that the dissociation induced apoptosis in human ES cells was triggered by ROCK activation, which enhanced the phosphorylation of Myosin light chain 2 (MLC2) to activate myosin-actin hypertension and eventually caused cell death by blebbing¹⁷². We found elevated ROCK1 protein level from H9 cells treated with 5 μ M blebbistatin for 4 days (Fig. 2.3.10A, 1st row). This increased protein level of ROCK1 indicating an enhanced ROCK activity in response to blebbistatin-induced dissociation. However, increased ROCK1 activity was unable to induce apoptosis through MLC2 due to the chemical inhibition of blebbistatin on myosin heavy chains (refers to 2.1.7).

The effect of thiostrepton on H9 cells exerts enhanced cellular death with downregulation of E-CADHERIN and beta-CATENIN at cell-cell junctions (Fig. 2.3.4 and Fig. 2.3.10) inducing the upregulation of ROCK1 (Fig. 2.3.10A, 1st row). The downregulation of FOXM1 was not the trigger of apoptosis *per se* after we repeated all tests using genetic knockdown of FOXM1 by RNAi (Fig. 2.3.13 A & D). We postulated that there would be cytotoxicity on embryonic stem cells from thiostrepton either due to its antibiotic origin, or from non-specific targeting of proteosomes (refers to 2.1.8), or even from upregulation of ROCK. Comparing thiostrepton treatment alone with combined treatment of blebbistatin and thiostrepton, the cytotoxicity of thiostrepton was compromised by detection of upregulation of anti-apoptotic BCL-2 expression, which may be induced by upregulation of FOXM1 through blebbistatin (Fig. 2.3.6 & Fig. 2.3.9, 4th column). This protective effect of blebbistatin in the presence of combined

treatment may attenuate the protein level of ROCK1 (Fig. 2.3.10A, *1st row*). However, in contrast with control H9 cells, cells treated with chemical inhibitors of FOXM1 or MYH10 exhibited upregulated ROCK1 along with downregulated E-CADHERIN and beta-CATENIN indicated unstable cell-cell interactions in human ES cells (Fig. 2.3.10A). This instability of cell-cell interactions was also revealed by the IF staining of E-CADHERIN and beta-CATENIN at cell-cell junctions in iPS_{IMR90} (Fig. 2.3. 10A&B).

Considering the stimulation of ROCK1 protein level after genetic knockdown of FOXM1 (Fig. 2.3.14A, *1st row*), E-CADHERIN and beta-CATENIN were also found to be downregulated, showing the sign of instability of cell-cell interactions after FOXM1 depletion from H9 cells. (Fig. 2.3.14A, *2nd row 3rd row*). The punctate staining of E-CADHERIN confirmed the observation from Western blotting (Fig. 2.3.14 C, *3rd column*). We also found that MYH10-depletion in H9 cells showed dramatic downregulation of FOXM1 (Fig. 2.3.12B, *3rd row*). However, the protein levels of ROCK1 and E-CADHERIN from MYH10 knockdown are in conflicts with the findings from FOXM1 knockdown (Fig. 2.3.14A & B, *1st & 2nd rows*). There is no significant effect on protein levels of either MYH10 or MYH9 after FOXM1 knockdown (Fig. 2.3.15c, *2nd & 3rd row*). These findings suggested that reduced level of FOXM1 can stimulate ROCK1 protein level depending on MYH10 level and affecting cell-cell interactions through E-CADHERIN and beta-CATENIN.

2.4.4 MYH10 exerts distinctive functions from MYH9 in modulating E-CADHERIN mediated adhesion in human embryonic stem cells.

H9 cells treated with 5 μ M blebbistatin showed dissociated colonies within 24hours¹⁸⁴ and these poorly formed colonies can be maintained up to 4 days in our experiments (Fig. 2.3.5, B). The inhibition of blebbistatin targeting all isoforms of non-muscle myosin II heavy chain, including MYH9 and MYH10, caused discrete cell colonies without localization of MYH10 at the cell-cell junctions (Fig. 2.3.6C, 2nd column). The adhesion molecule E-CADHERIN was found to be lost at the junction and diffused in the cytoplasm under blebbistatin treatment (Fig. 2.3.10B, 2nd column). The protein level of E-CADHERIN was thereby decreased significantly with blebbistatin treatment compared with compact H9 cells (Fig. 2.3.10A, 2nd column). To access whether MYH9 or MYH10 is responsive to the loss of cell-cell junction integrity upon blebbistatin treatment, we generated specific shRNA oligonucleotide target MYH10 for knockdown experiments. Genetic knockdown of MYH10 but MYH9 showed tight colonies with small projections around the periphery, which is different from the morphology induced by blebbistatin (Fig. 2.3.13B & Fig. 2.2.5B). Furthermore, specific depletion of MYH9 with shRNA was carried out by several groups previously to support that MYH9 controls colony formation through E-CADHERIN^{170,184,185}. However, we found that depletion of MYH10 induced the protein level of E-CADHERIN (Fig. 2.3.15B, 2nd row). The increased protein

level of E-CADHERIN failed to enhance the localization at the junctions (Fig. 2.14, *2nd column*), suggesting the instability of cell-cell interactions in spite of a tight colony formation. The detection of downregulated beta-CATENIN suggested a reduced binding of the cytoplasmic domain of E-CADHERIN with beta-CATENIN to associated the CADHERIN-mediated cell-cell interaction ¹⁸⁵, after MYH10 knockdown. On the other hand, knockdown MYH10 in H9 cells showed reduced level of ROCK1 protein (Fig. 2.3.15B, *1st row*), indicating a lower activation of ROCK1 required for the phosphorylation of residual MYH10 and MYH9 to maintain a relatively low tension of actin-myosin in those cells for colony formation. Our results inferred an alternative pathway governed by MYH10 through E-CADHERIN other than adhesions.

2.4.5 FOXM1 serves downstream of the adhesion pathway to monitor pluripotency in human embryonic stem cells.

The role of E-CADHERIN in human ES cells was no longer restricted in the function of adhesion and survival, but also was related to the maintenance of pluripotency ^{181,185}. From previous studies, either genetic depletion of E-CADHERIN or long-term treatment of blebbistatin can despair the formation of colonies of human ES cells with profound pluripotent defect ¹⁸⁵. An exception to the inversely higher expression of pluripotent markers in H9 cells treated with 2.5-5 μ M of blebbistatin due to the fact of low level of E-CADHERIN protein in response to 5 μ M blebbistatin treatment (Fig. 2.3.10A, *2nd row* & Fig. 2.3.7A).

The improvements of cellular viability and pluripotency in human

embryonic cells treated with 5 μ M blebbistatin or 10 μ M Y27632 were discovered earlier and developed into routine culture condition into various applications^{170,182,228}. Therefore, there should be an alternative pathway downstream of myosin activity despite of the protein level of E-CADHERIN to regulate pluripotency in stem cells. We identified the correlation of FOXM1 with the protein level of OCT4 and NANOG in response to the dosage of blebbistatin treatments (Fig. 2.3.7C). The inhibition of FOXM1 by either thiostrepton or shRNA targeted FOXM1 knockdown showed repression of all three pluripotent markers (Fig. 2.3.7A, 3rd column & Fig. 2.3.13A). The findings of heterogeneous expression patterns of OCT4 and NANOG in stem cell populations, which exhibit distinct differentiation potential^{79,229}, were excluded from chemical inhibitions of FOXM1 or MYH10 by the observations of homogeneous staining of OCT4 (Fig. 2.3.7D). To further answer the role of FOXM1 on regulating pluripotency in human ES cells, we searched the promoter region of *OCT4*, NANOG and SOX2 for the FOXM1 binding sites. ChIP assay confirmed the direct binding of FOXM1 on *OCT4* promoter provided us concrete evidence on FOXM1 controlling pluripotency from transcriptional level (Fig. 2.3.8A&B). Quantitative analysis of FOXM1 occupancy on the *OCT4* promoter showed correlations between blebbistatin treatment on FOXM1's binding on *Oct4* promoter with the protein level of OCT4 (Fig. 2.3.7A & 2.3.8C, 2nd columns). However, adding thiostrepton alone has little effect on FoxM1's binding on *Oct4* promoter (Fig 2.3.8C, 3rd column) while the stemness markers were all decreased

(Fig. 2.3.7A, 2nd column). The plausible reason can be due to the nature of thiostrepton, which also acts as a proteasomal inhibitor. In this scenario, thiostrepton can, theoretically, stabilize other proteins so that the inhibition is not specific (refers to 2.1.8). In combined treatment, the occupancy of FOXM1 on *Oct4* promoter was greatly decreased (Fig 2.3.8C, 4th column). The protein levels of all stemness markers were also detected to be reduced (Fig 2.3.7A, 4th column). We postulate that thiostrepton may competitively bind to the FOXM1 protein in this condition to prevent the binding of FOXM1 with *OCT4* promoter independent of the high protein level of FOXM1 induced by blebbistatin for survival. This idea needs to be verified by competition electrophoretic mobility shift assays and mass spectrometric analysis in the future. The genetic knockdown of MYH10 displayed a compact colony with upregulated E-CADHERIN apart with the low level of OCT4 protein was also revealed with a low state of FOXM1 protein (Fig. 2.3.12C, 3rd column). Collectively, FOXM1 is firstly identified as the transcriptional regulator for pluripotency in response of myosin mediated adhesion pathway.

2.4.6 FOXM1 and MYH10 monitors the progression of cytokinesis in favor of symmetric division in human embryonic stem cells.

Apart from the functions from adhesion, actin-myosin contraction is also involved in the formation of cleavage furrow and cytokinesis^{230,231}. Thus, long-term or high dosage exposure to blebbistatin can inhibit cell proliferation²¹²

without improving colony efficiency¹⁸⁴. H9 cells treated with blebbistatin at the concentrations lower than 20 μ M was reported to exhibit no binucleated defect¹⁷⁰. And cytokinesis was proceeded under Y27632²³² treatment or in our experiment with 5 μ M of blebbistatin treatment and genetic knockdown of MYH10 (Fig. 2.3.11B, 2nd column & Fig. 2.3.15C, 2nd column), indicating the residual myosin heavy chain is presumably sufficient for cytokinesis.

However, base on the finding of FOXM1 on regulating pluripotency in response of adhesion pathway, we are speculating the foremost function of FOXM1 on mitotic progression will affect the symmetric division of stem cells in terms of pluripotent alteration. A progressively higher levels of AURORA B kinase activity was found to be essential for mitotic progression²³³. Our findings of upregulation of AURORA B after genetic knock-down of FOXM1 and MYH10 are related to the downregulation of FOXM1 (Fig. 2.3.15 A&B, 2nd row), suggesting a likely arrest of the mitotic progression due to less MYH10 recruitment at cleavage furrow (Fig. 2.3.15, C). The protein level of KIF14 on the other hand decreased in line with reduced FOXM1 protein level from knockdown FOXM1 and MYH10 (Fig. 2.3.15 A&B, 1st row). Because KIF14 was identified to co-localize with the midbody at late stage of mitosis for efficient cytokinesis from previous study²³⁴. And in a recent genome wide screen of protein-DNA interactions, KIF14 was identified positively regulated by FOXM1²³⁵. Therefore, the down regulation of KIF14 from our study indicated an impaired cell cycle progression suppressed by FOXM1 expression.

Depending on the phosphorylation site on myosin heavy chain by multiple kinases, including ROCK and myosin light chain kinase (MLCK), non-muscle myosin II can regulate adhesion, polarity in cell migration and cytokinesis differently for each isoform¹⁶⁹. AURORA B kinase was reported to be crucial for promoting non-muscle myosin II localization to the cleavage furrow by phosphorylation of MLC²³⁶. The upregulation of AURORA B in H9 cells treated with blebbistatin (Fig. 2.3.11 A, 2nd row) revealed a compensating effect resulting from the inhibition of non-muscle myosin II activity. And the protein level of KIF14 was hence induced to promote the commitment of cytokinesis (Fig. 2.3.11 A, 1st row). This promotion of cytokinesis induced by blebbistatin may facilitate the symmetric division for self-renewal in stem cells to maintain or further promote the pluripotency, which was supported by our finding of enhanced recruitment of CEP170 at the midbodies (Fig. 2.3.11 C, 2nd column).

The specific movement of the mother centriole, preferentially associated with CEP170, to the midbody was reported to terminate the mitosis by abscission of the parental cell into two equal daughter cells with identical polarity²⁰³. We detected that thiostrepton treated cells consist of supernumerary centrosomes and mis-localized centrioles at the mid-body, suggesting that FoxM1 may be important for the polarity required for asymmetric division (Fig. 2.3.11 C, 4th column), and further points to the direction that FoxM1 may contribute to stemness through its centrosomal function during cytokinesis. In contrast with genetic depletion of FOXM1, thiostrepton treated cells showed downregulated

AURORA B (Fig. 2.3.11A, 3rd column) and massive apoptotic cells, indicating the increased inaccurate chromosome segregations under thiostrepton treatment. Above all, we discovered that MYH10's association with FOXM1 in human ES cells may act as an important protein complex for mitotic progression and proper symmetric division.

Chapter 3 Functional role of MYH10 in breast cancer stem-like cells.

3.1 Introduction

3.1.1 The heterogeneity of breast cancer and cancer stem-like cells.

Breast cancer consists of heterogeneous cell populations. These different cell types within the tumor mass reveal various degrees of self-renewal capabilities. Due to the differences in cellular differentiation capabilities, these cells do exhibit differential angiogenic, invasive, clonogenic and metastatic properties²³⁷⁻²³⁹. Therefore, cancer cells within a tumor can be labeled with sets of markers revealing a pattern of heterogeneity²⁴⁰. When a small fraction of these cells were transplanted into immunodeficient mice, the xenografts formed would be resembled to their origins within the tumour²⁴¹. And those cancer initiating cells, which show the properties of self-renewal and differentiation for tumorigenesis, were defined as cancer stem-like cells²⁴². In the context of breast tumors, the combination of CD44 and CD24 revealed the heterogeneity within the tumor mass¹⁰¹. As few as 100 cells expressing CD44^{high}/CD24^{low} can establish xenografts in NOD/SCID mice models¹⁰¹. It was also found that CD44^{high}/CD24^{low} is enriched in basal subtype of cancer cell line, such as MDA-MB231²⁴³. Luminal derived cell line such as MCF7 is mainly expressing CD24, indicating its differentiated state²⁴³. Recent work showed that CD44^{high}/CD24^{low} was not the only markers for breast cancer stem-like cells.

More defined markers such as aldehyde dehydrogenase (ALDH)²⁴⁴, CD133²⁴⁵ and ABC transporter (ABCG2)²⁴⁶ could help to refine the concept of breast cancer stem-like cells. Because it was found that different subtypes of breast cancers from different origins shows diverse degrees of metastasis and invasion²⁴⁷⁻²⁴⁹. The signature of CD44^{high}/CD24^{low} was doubted to represent some, instead of all, for breast cancer stem-like cells within the tumour²⁵⁰. Indeed, it was reported that there may be no significant correlation between CD44^{high}/CD24^{low} prevalence and tumor progression from clinical investigations²⁴⁹, These studies posted an urgent need on identifying novel markers for breast CSCs.

3.1.2 Breast cancer stem-like cells are preferentially maintained in non-adherent spherical culture condition.

Human mammary progenitor cells were initially maintained in non-adherent condition to allow formation of spheroids called mammospheres²⁵¹. Single cell suspension of MCF7 cells carrying the CD44⁺/CD24⁻ phenotype can also form clonal non-adherent mammospheres in non-adherent condition. These mammospheres were found to be more resistant to radiation therapies²⁵² or chemical²⁵² insults compared to their parental cell lines in adherent condition. These mammospheres can also proliferate extensively and express the master pluripotent markers detected in embryonic stem cells such as OCT4²⁵³, NANOG²⁵⁴ and SOX2²⁵⁵. Thus, *in vitro* mammosphere formation assay is now widely used to study the underlying mechanisms and pathways of cancer

stem-like cell growth and survival.

3.1.3 The functional role of FOXM1 in cancer stem-like cells.

The oncogenic transcription factor FOXM1 was found elevated in the majority of solid tumors¹³⁵, including in breast cancer²⁵⁶. The expression was undetectable in normal epithelial cells with low rate of proliferation¹³⁷. It was reported that FOXM1 was downregulated in differentiated cells¹³¹. In the case of breast cancer, upregulation of FOXM1 was correlated with an undifferentiated state with poor clinical prognosis²⁵⁷. FOXM1 is able to act as a transcriptional repressor to suppress the differentiation of luminal epithelial progenitors²⁵⁸. Studies from other tissues uncovered that ectopic expression of *FOXM1* promoted epithelial mesenchymal transition (EMT) in pancreatic stem-like cells²⁵⁹ and induced the expansion of the stem/progenitor compartment in normal epithelial cells²⁶⁰. FOXM1 is also the direct downstream effector of the canonical WNT/ beta-CATENIN signaling pathway. The WNT pathway is one of the major signaling pathways in regulating the stem/progenitor cells (refers to 1.1.3), particularly in glioma stem cells¹⁹². Inhibition of FOXM1 with RNAi or with chemical inhibitors such as thiostrepton (refers to 2.1.8) could sensitize drug-resistant human cancer cells to chemotherapy. Thus, FoxM1 could act as a potential target for eliminating cancer stem-like cells²⁶¹⁻²⁶³.

3.1.4 Non-muscle myosin II plays important role in cancer stem-like cells metastasis.

One of the distinctive characteristics of cancer stem-like cells is the highly malignancy with high rates of morbidity and poor prognosis²³⁷. The process of metastasis was proposed to be initiated by metastatic colonization of cancer stem-like cells to reach distant sites and generate secondary tumors²⁶⁴. This process is usually triggered by the acquisition of epithelial to mesenchymal transition (EMT). These cells would obtain a mesenchymal phenotype for migration, and the process could be accomplished through colonization at a foreign site by another process called mesenchymal to epithelial transition (MET). MET is a step for the migrated cancer cells to adapt to the new niche²⁶⁵. Both processes would require the plasticity, and there are implications that the non-muscle myosin II isoforms are capable to confer plasticity²⁶⁶. For example, basal-derived tumors are usually more invasive and metastatic than luminal-derived tumours²⁶⁷, while non-muscle myosin II isoforms were mostly expressed in breast cell lines correlating to the basal type²⁶⁸. In the same study²⁶⁸, the author showed evidence that the switch of non-muscle myosin II from MYH14 to MYH10 contributes to breast cancer invasion in response to TGF- β . Moreover, it was found that different non-muscle myosin II isoforms could exert different functions in breast cancer migration²⁶⁹. For example, MYH9 was found to be preferentially upregulated in MCF7²⁶⁶ and MDA-MB231²⁷⁰ cells for invasion. On the other hand, MYH10 seems to be able to generate more durable

force with less energy usage than the other isoforms due to its kinetic properties^{209,271}, suggesting its role in tension maintenance for proper structure or microenvironment. Taken together, distinctive non-muscle myosin II isoforms may contribute to the cancer stem-like cell property of metastasis.

3.1.5 The approach to study the function of FOXM1 and MYH10 in breast cancer stem-like cells.

The proportions of CD44⁺/CD24⁻ expressing MCF7 and MDA-MB231 cells within each cell line, respectively, will be studied by Fluorescence-activated Cell Sorting (FACS) with anti-CD44 and anti-CD24 antibodies. The population of CD44⁺/CD24⁻ will be isolated and maintained in non-adherent condition to allow the formation of mammospheres. Properties of self-renewal and metastasis will be used as endpoints to evaluate the cancer stem-like characteristics of the sorted CD44⁺/CD24⁻ expressing MCF7 and MDA-MB231 cells.

Chemical inhibitors and genetic knockdown of FOXM1 and MYH10 will be used to study the functions of this novel protein complex in breast cancer stem-like cells. pSIREN-shFOXM1/shMYH10 generated from previous work (refers to 2.2.3) will be transfected into breast cancer cells and sorted for all functional studies of the cancer stem-like cells. Blebbistatin (inhibitor for MYH10, refers to 2.1.7) and thiostrepton (inhibitor for FOXM1, refers to 2.1.8) will also be used for parallel assays.

3.2 Materials and Methods.

3.2.1 Inhibitors and plasmids.

pCMV-GFP-MYH10 and pCMV-GFP-MYH9 were generously gifts from Prof. Robert S. Adelstein from National Heart, Lung and Blood Institute, NIH.

pcDNA3-FOXM1-ΔN was generously provided from Prof. Erick Lam from Imperial College London.

Chemicals unlisted refer to 2.2.1.

3.2.2 Cell culture and transfection.

Human breast cancer MCF7 and MDA-MB231 cells were purchased from American Type Culture Collection (ATCC) and cultured under ATCC recommendations (details refer to 2.2.2). For non-adherent spherical culture, 1×10^5 trypsinized single cells were seeded in a non tissue culture treated 60 mm polystyrene petri dish (SPL life sciences). Cells are maintained in conditional medium containing 90% MammoCult basal medium with 10% provided growth supplement (Stemcell Technologies), 0.2% heparine (Stemcell Technologies), 1% penicillin and streptomycin (Invitrogen) and 0.0048% w/v hydrocortisone (Sigma) filtered through 0.22 μm syringe filter. Cells were allowed to grow for 1 week to form mammospheres before subculture. Briefly, mammospheres were centrifuged at 1000 rpm for 3 minutes. Cells were dissociated with 1 ml of trypsin-EDTA (Invitrogen) with the assistant of vigorously pipetting and

neutralized with 2%FBS in PBS. Cells were centrifuged and resuspended with complete MammoCult medium for splitting.

Routinely, cells were transfected in adherent condition (refers to 2.2.2) and trypsinized after 48 hours to form mammospheres.

For specific gene knockdown in sorted CD44⁺/CD24⁻ MCF7 cells, cells were allowed to grow into healthy spheres at passage 2 and dissociated in single cell condition. 2µg pSIREN-shRNA plasmids (refers to 2.2.3) with 5 µl X-tremeGENE HP transfection reagent (Roche Diagnostics) were mixed with cells in 100ml MammoCult medium for 5mins before transfer to petri dish with complete MammoCult omitted antibiotics. Medium was replaced after 24 hours with complete MammoCult medium.

All cells were maintained in a humidified incubator (Thermo) supplied with 5% carbon dioxide at 37° C.

Pictures of mammospheres were obtained daily from an inverted microscope (Olympus CKX41) with a 10X/0.25 php objective. At least 4 fields of the mammospheres were recorded from each dish. And the diameters of mammospheres were calculated from 20 representative individuals from all fields for mean value and standard deviation.

3.2.3 Cell viability assay.

2X10⁴ of cells were seeded into 96-well plate with 200µl medium per well in triplets. 0-200µM of blebbistatin was administrated to cells for 24 hours. Cells

were washed once with PBS and replaced with medium containing 1% MTT w/v (Sigma) for 4 hours at 37 ° C. The substrate was dissolved in 100ml DMSO-Ethanol (1:1, Sigma) for 15 minutes at room temperature. The absorbance was measured at 570 nm by microplate reader (Bio-rad).

3.2.4 Flow cytometry and Fluorescence-activated Cell Sorting (FACS).

Cells were treated with trypsin to obtain single cell suspensions. Subsequently, cell pellet was washed with 3ml sorting buffer (refers to Appendix II) once and concentrated into 100µl sorting buffer, of which 10µl combinational fluorochrome conjugated antibodies (Table 3.2.1) against around 6×10^6 cells were added and incubated at 4 ° C for 7 minutes with gentle rocking. Isotype-matched mouse immunoglobulins were used as controls (Table 3.2.1). Stained cells were washed 3 times with 200µl sorting buffer and filtered through cell strainer (BD Biosciences). Cells were kept on ice and prevented from light before flow cytometric analysis.

For analysis, cells were sorted with FACS Aria I (BD Bioscience) under the following conditions: nozzle tip diameter (100µm) with the threshold rate (~1,000 events/s) and analyzed by FACS Diva software (BD Bioscience).

For sorting, CD44⁺/CD24⁻ population was gated according to isotypic controls and single staining of CD44 or CD24 and collected with drop deflection after configurations of stream deflection and drop delay following the protocol from the manufacturer (BD Biosciences).

Antibody	Catalog No.	Company	Species
APC-IgG	555745	BD Pharmingen	mouse
PE-IgG	555428	BD Pharmingen	mouse
APC-CD44	559942	BD Pharmingen	mouse
PE-CD24	555574	BD Pharmingen	mouse

Table 3. 2. 1 Fluorochrome conjugated antibodies for FACS analysis.

3.2.5 Western blot.

Details refer to 2.2.5. Primary antibodies unlisted from 2.2.5 are listed below for western blot analysis.

Antibody	Catalog No.	Company	MW	Species	Dilution
β-actin	ab3280	Abcam	42KD	mouse	1:1000
EPCAM	3599	Cell Signaling	40KD	Rabbit	1:500
TWIST1	Sc-15393	Santa Cruz	28KD	Rabbit	1:1000

Table 3. 2. 1 Primary antibodies for western blot analysis in breast cancer stem-like cell research. MW: Molecular Weight.

3.2.6 Immunofluorescence (IF).

Mammospheres were collected and washed with 1ml PBS. Cells were aliquot into 1.7ml Eppendorf tubes with 1ml 4% formaldehyde in PBS (Sigma) for 10 minutes at room temperature for fixation. Mammospheres were washed once with cold PBS and permeablized with 0.5% Triton X-100 and 2% BSA in

PBS for 20 minutes at room temperature. Spheres were washed for 3-4 times and stained with primary and secondary antibodies as described in 2.2.6 in Eppendorf tubes. Before mounting, spheres were concentrated into 100 μ l PBS, of which 10 μ l was dropped on a glass slide and sealed with nail polish. Details of microscope and imaging process refer to 2.2.6.

3.3 Results

3.3.1 Identification of distinctive MYH9 and MYH10 expression in multiple cell lines.

From western blot analysis, MYH10 was detected from all tested cell lines with the highest expression level in human ES H9 cells and iPS_{IMR90} induced pluripotent stem cells (Fig. 3.3.1 A, 1st row). The breast cancer cells, MCF7, cultured in non-adherent condition, would subsequently form spheroids; it was reported that these spheroids are enriched with more cancer stem-like cells^{251,272}. Here in this study, we detected a higher expression of MYH10 compared to their counterpart when cultured in conventional adherent condition (Fig. 3.3.1 A, 3rd & 4th columns). The expression pattern of MYH9 in various cell lines differed from the pattern of MYH10. MYH9 expression in hES and iPS cells was found to be lower compared to MYH10. MYH9 protein level was undetectable from MCF7 breast cancer cells, in both adherent and non-adherent culture conditions. MYH9 was found highly expressed in MDA-MB231 breast cancer cells. This cell line was originally derived from metastatic pleural effusion from the primary site²⁷³. HeLa cells (from ATCC), was used as positive control as these cells were known to express both MYH10 and MYH9 isoforms²⁷⁴ (Fig. 3.3.1 A, last column).

To examine the role(s) of non-muscle myosin II in breast cancer and breast cancer stem-like cells, blebbistatin was used to inhibit the ATPase binding site of non-muscle myosin II heavy chain (refers to 2.1.7). Methylthiazole tetrazolium (MTT) assay was carried out to determine the cytotoxicity of blebbistatin in

breast cancer cells. Blebbistatin was reported to exert minimal toxicity in various types of cancer cells at low concentrations. However, it could induce apoptosis when the concentration is too high. It was postulated that blebbistatin-induced cell death could be due to cytokinesis failure^{212,213}. We also revealed a dose-dependent growth inhibition of MCF7 and MDA-MB231 cells by blebbistatin from 1 μ M to 200 μ M (Fig. 3.3.1 B&C, *black dots*). However, MCF7 cells which were isolated with the surface markers for CD44^{high} and CD24^{low}, exhibit stem-like properties¹⁰¹ including enhanced drug resistance²⁷⁵. We found that CD44^{high}CD24^{low} MCF7 cells showed robust resistant against blebbistatin and increased viability at the range of 1 μ M to 50 μ M (Fig. 3.3.1 B, *red dots*).

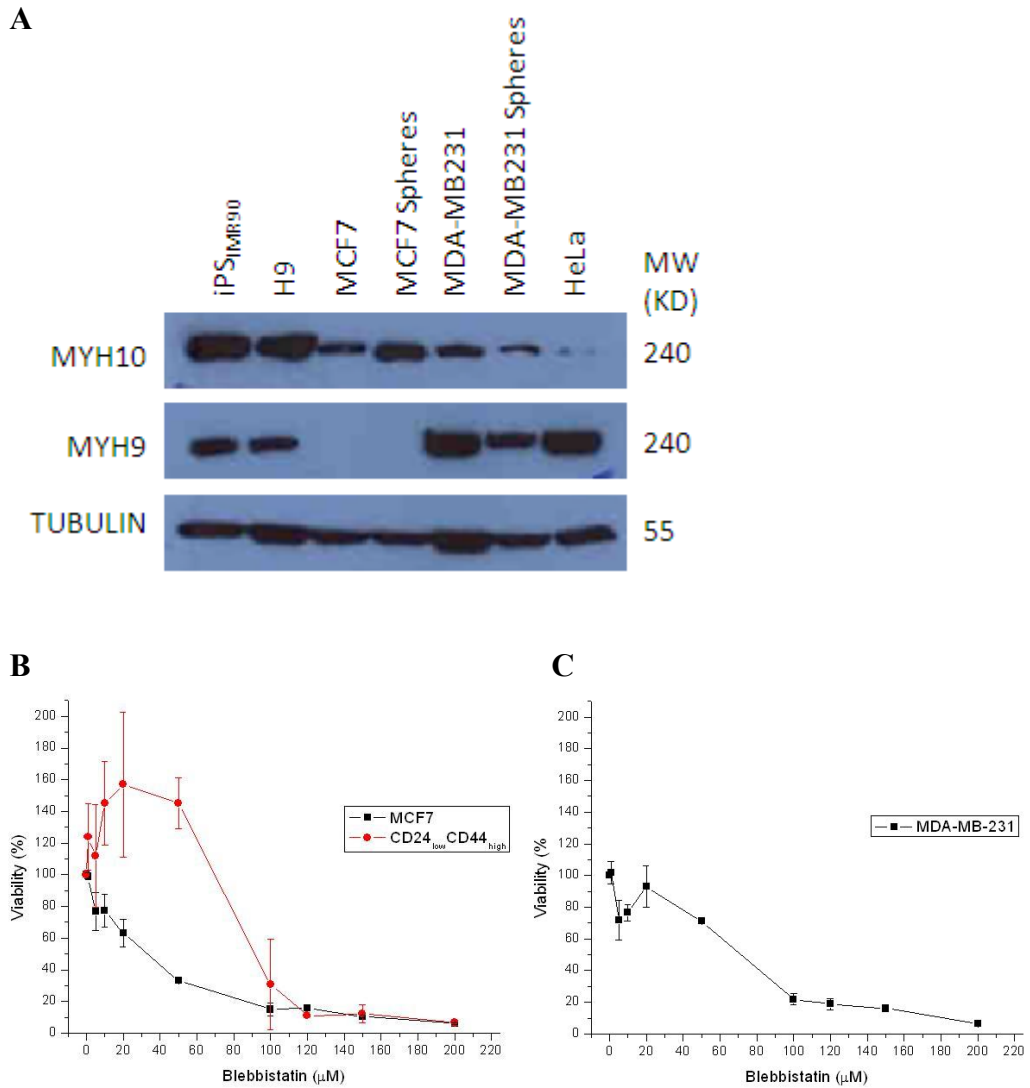


Figure 3.3.1 Expressions of non-muscle myosin II isoforms are distinctive in varied cell types. (A) Western blot analysis of non-muscle myosin II isoforms: MYH10 and MYH9 in multiple cell lines including, induced pluripotent stem cell (iPS_{IMR90}), human ES cell (H9), cervical cancer cell (HeLa) and breast cancer cells (MCF7 and MDA-MB231) which cultured in adherent condition or non-adherent suspension condition (indicated with spheres). (B) Methylthiazole tetrazolium (MTT) assay performed with MCF7 cells cultured in adherent condition (black dots) and FACS-sorted CD44^{high}/CD24^{low} MCF7 maintained in non-adherent suspension condition (red dots) treated for 24 hours with increasing

dosages of blebbistatin as indicated. (C) MTT assay performed with MDA-MB231 cells in adherent condition treated for 24 hours with increasing dosages of blebbistatin as indicated. Cell viability was presented as percentage of control cells which were untreated with blebbistatin.

3.3.2 Rho GTPase and ROCK were induced by FOXM1 expression.

Enhanced Rho GTPase and ROCK protein levels were detected in HeLa cells which were transiently overexpressed with the FOXM1 expression plasmid (Fig. 3.3.2, *2nd and 3rd rows*). However, upregulation of RhoGTPase and ROCK was not detected when a NH₂-terminal truncated FOXM1 mutant, instead of the wild-type, was transfected into the HeLa cells (Fig. 3.3.2, *2nd and 3rd rows*). We noted that the endogenous FOXM1 protein level was not altered after the transfection of mutant (Fig. 3.3.2, *arrows*). Upregulation of RhoGTPase and ROCK may suggest elevated activities of the upstream of non-muscle myosin II. Unfortunately, the endogenous expression of MYH10 was extremely low in HeLa cells (Fig. 3.3.1&3.2, *1st row*).

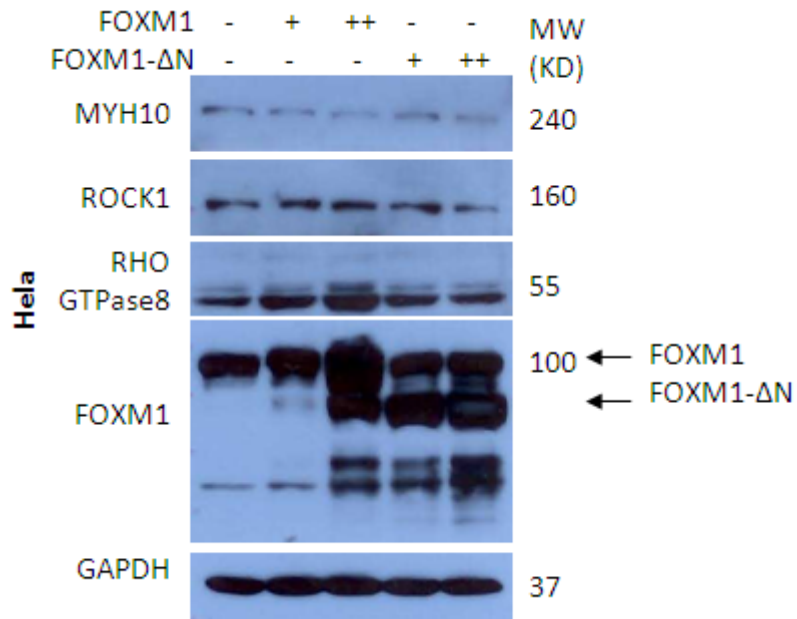


Figure 3.3.2 Expression of FOXM1 induces the protein level of Rho GTPase and its effector Rho-associated protein kinase. Western blot analysis of MYH10, ROCK1, Gho-GTPase8 and FOXM1 proteins in HeLa cells transfected with either 1 μ g (+) or 2 μ g (++) wild type FOXM1 vector or NH₂-terminal truncated FOXM1 mutant (FOXM1-ΔN).

3.3.3 Expression of MYH10 and FOXM1 is required to maintain CD44^{high}/CD24^{low} breast cancer stem-like cells.

3.3.3.1 Inhibition of FOXM1 reduced the CD44^{high}/CD24^{low} breast cancer stem-like population.

To further investigate the role of FOXM1 in regulating breast cancer stem-like cells, FACS was performed on the relatively non-metastatic MCF7 and metastatic MDA-MB231 breast cancer cells. Adherent and non-adherent culture conditions (refers to 3.2.2) were established to validate the effect of enrichment of breast cancer stem-like cells in non-adherent condition (refers to 3.1.2). MCF7 cells-derived mammospheres showed 10 times higher enrichment of CD44^{high}/CD24^{low} cancer stem-like population than adherent MCF7 cells (Fig. 3.3.3 B&D, 2nd rows). The metastatic MDA-MB231 cells has a very high proportion of CD44^{high}/CD24^{low} cells (99.2%), showing a predominant more cancer stem-like property compared to unsorted MCF7 cells (Fig. 3.3.3 F, 2nd row). The population of CD44^{high}/CD24^{low} cells was slightly altered (97.7%) in non-adherent culture condition, indicating that the change from adherent to non-adherent culture condition did minimal effect on CSC enrichment in MDA-MB231 cells (Fig. 3.3.3 H, 2nd row).

Genetic knockdown of FOXM1 by shRNA (refers to 3.2.2) showed a slight decline (-0.4%) of CD44^{high}/CD24^{low} population as compared to MCF7 cells (Fig. 3.3.3 B, 3rd row). MCF7 cells cultured in non-adherent condition showed more reduced (-1.3%) population of CD44^{high}/CD24^{low} as compared to

MCF7 cells without transfection in the same culture condition (Fig. 3.3.3 D, 3rd row). Nevertheless, there is no obvious shift of CD44^{high}/CD24^{low} population of MDA-MB231 cells in adherent condition while a drop of the population (-3%) was found in non-adherent condition after FOXM1 knockdown (Fig. 3.3.3 F&H, 3rd rows).

The chemical inhibitor of FOXM1, thiostrepton (refers to 2.1.8), exerts clear effect on cancer stem-like property by reducing the expression of CD44⁺/CD24⁻ on MCF7 cells with -0.7% in adherent and -6.9% in mammospheres respectively (Fig. 3.3.3 B&D, 4th rows). The scenarios for MDA-MB231 are more intense than MCF7. The population of CD44⁺/CD24⁻ dropped after thiostrepton treatment with -9.7% and -8.6% in adherent and non-adherent condition, respectively (Fig. 3.3.3 F&H, 4th rows).

3.3.3.2 Expression of MYH10 is essential for the support of CD44^{high}CD24^{low} breast cancer stem-like population.

MCF7 cells cultured in adherent condition form a monolayer supported by the polystyrene coating of the culture wares. In this specific culture condition, we detected only a rare cancer stem-like population of CD44⁺/CD24⁻ breast cancer cells (less than 2%) within the whole population^{276,277} (Fig. 3.3.3 A).

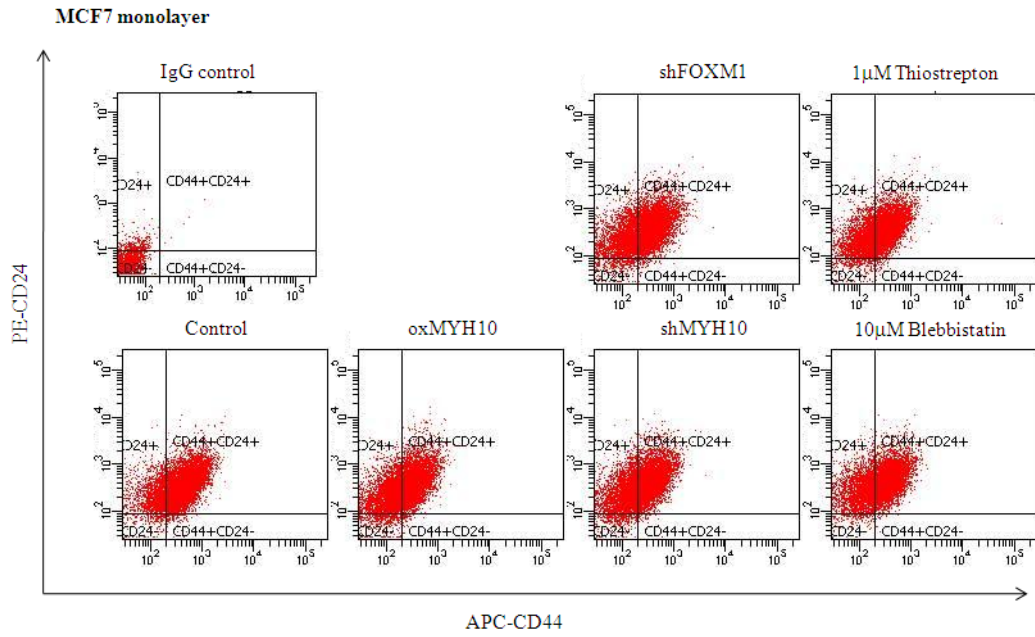
Specific targeting of MYH10 in MCF7 cells was achieved using shRNA as previous (refers to 3.2.2). The population of CD44⁺/CD24⁻ was reduced by 2-fold (from 1.6% to 0.8%) in MYH10-depleted cells compared to the control

cells transfected with control shRNA (Fig. 3.3.3 B, 6th row). On the contrary, our Flow Cytometry data revealed that overexpression of MYH10 in MCF7 cells failed to increase the population of CD44⁺/CD24⁻ (Fig. 3.3.3 B, 5th row). Mammospheres formed from MCF7 cells showed an increase of CD44⁺/CD24⁻ population after overexpressing MYH10 from 19.7% to 23.7% (Fig. 3.3.3 D, 5th row). Cells transfected with shMYH10 plasmid showed a diminished population (from 19.7% to 18.3%) of CD44⁺/CD24⁻ (Fig. 3.3.3 D, 6th row). We did a parallel experiment on MDA-MB231 cells in which the cell line comprises a majority of the CD44⁺/CD24⁻ population. In line with the MCF7 result, we also detected a decrease of CD44⁺/CD24⁻ population after MYH10 depletion in both adherent condition (-5.8%) and non-adherent condition (-1.6%) (Fig. 3.3.3 F&H, 5th rows).

The chemical inhibitor of MYH10, blebbistatin (refers to 2.1.7), exerts significant effect on cancer stem-like property by reducing the populations of CD44⁺/CD24⁻ in both MCF7 and MDA-231 cells. For MCF7 cells, blebbistatin treatment reduced the CD44⁺/CD24⁻ population by 1.3% in adherent and by 15.2% in mammospheres (Fig. 3.3.3 B&D, 7th rows). In MDA-MB231 cells, blebbistatin treatment reduced the CD44⁺/CD24⁻ population by 10.4% in adherent and by 15.2% in mammospheres (Fig. 3.3.3 F&H, 6th rows).

The unstained and isotypic controls for setting up the Flow Cytometry assays are attached in Appendix III, A-F.

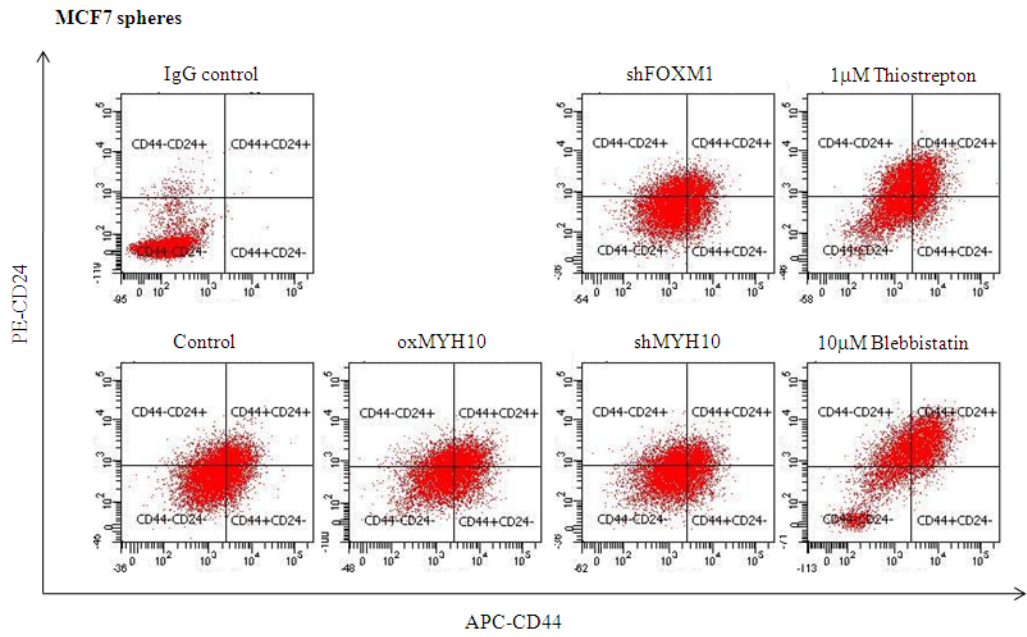
A



B

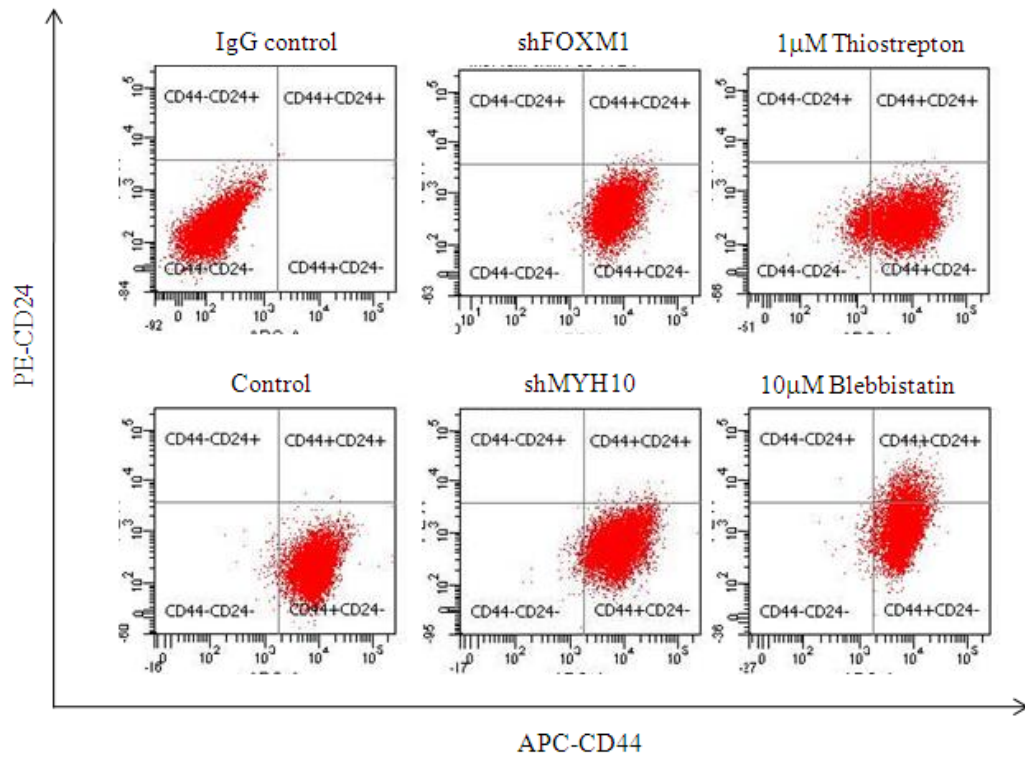
Cell line	Culture condition	Treatments	CD44 ⁺ /CD24 ⁻	CD44 ⁺ /CD24 ⁺	CD44 ⁻ /CD24 ⁺	CD44 ⁻ /CD24 ⁻
MCF7	monolayer	IgG control	0.0	0.1	3.6	96.3
MCF7	monolayer	Control	1.6	74.6	18.3	5.5
MCF7	monolayer	shFOXM1	1.2	60.1	31.4	7.2
MCF7	monolayer	Thiostrepton	0.9	61.0	32.6	5.5
MCF7	monolayer	oxMYH10	1.0	54.9	36.0	8.1
MCF7	monolayer	shMYH10	0.8	57.6	34.3	7.4
MCF7	monolayer	Blebbistatin	0.3	62.8	31.1	5.8

C



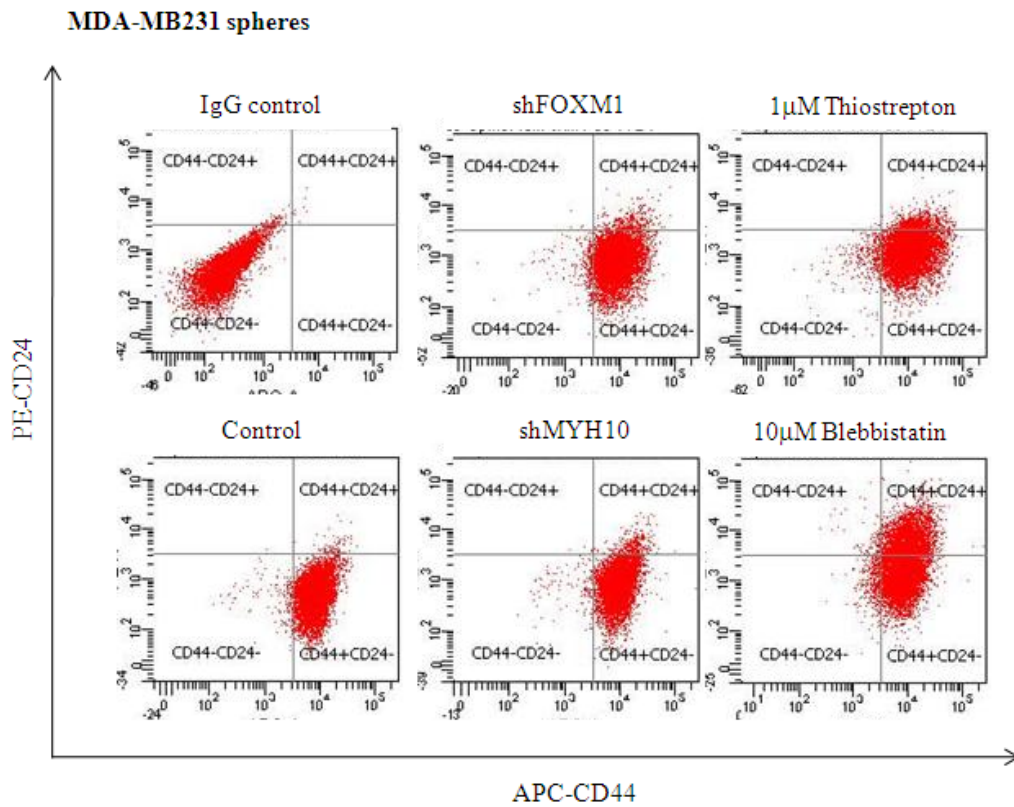
D

Cell line	Culture condition	Treatments	CD44 ⁺ /CD24 ⁻	CD44 ⁺ /CD24 ⁺	CD44 ⁻ /CD24 ⁺	CD44 ⁻ /CD24 ⁻
MCF7	sphere	IgG control	0.1	0.1	1.6	98.3
MCF7	sphere	Control	19.7	16.0	13.8	50.6
MCF7	sphere	shFOX M1	15.5	14.0	17.0	42.4
MCF7	sphere	Thiostrepton	12.8	29.0	22.9	35.3
MCF7	sphere	oxMYH10	23.7	21.5	15.2	39.6
MCF7	sphere	shMYH10	18.3	15.9	19.2	46.6
MCF7	sphere	Blebbistatin	4.5	44.2	24.6	26.7

E**MDA-MB231 monolayer****F**

Cell line	Culture condition	Treatments	CD44 ⁺ /CD24 ⁻	CD44 ⁺ /CD24 ⁺	CD44 ⁻ /CD24 ⁺	CD44 ⁻ /CD24 ⁻
MDA-MB231	monolayer	IgG control	0.0	0.0	0.0	99.9
MDA-MB231	monolayer	Control	99.2	0.0	0.0	0.7
MDA-MB231	monolayer	shFOXM1	99.4	0.2	0.0	0.4
MDA-MB231	monolayer	Thiostrepton	89.5	0.0	0.0	10.5
MDA-MB231	monolayer	shMYH10	93.4	0.4	0.0	1.3
MDA-MB231	monolayer	Blebbistatin	88.8	9.9	0.0	1.2

G



H

Cell line	Culture condition	Treatments	CD44 ⁺ /CD24 ⁻	CD44 ⁺ /CD24 ⁺	CD44 ⁻ /CD24 ⁺	CD44 ⁻ /CD24 ⁻
MDA-MB231	sphere	IgG control	0.0	0.1	0.5	99.4
MDA-MB231	sphere	Control	97.7	0.8	0.0	1.5
MDA-MB231	sphere	shFOX M1	94.7	3.2	0.0	2.0
MDA-MB231	sphere	Thioestrepton	89.1	8.0	0.0	2.8
MDA-MB231	sphere	shMYH10	96.1	2.8	0.0	1.0
MDA-MB231	sphere	Blebbistatin	67.2	28.7	0.7	3.4

Figure 3.3.3 Identifications of CD44⁺/CD24⁻ subpopulations in breast cancer cell lines after MYH10 and FOXM1 knock down by flow cytometry.

(A) Subpopulations identified by detections of APC-CD44 and PE-CD24 in monolayer MCF7 cells after MYH10 and FOXM1 knockdown by flow cytometry. (B) Percentages of the subpopulations from monolayer MCF7 cells

with distinctive treatments defined by flow cytometry. **(C)** Subpopulations identified by detections of APC-CD44 and PE-CD24 in spherical MCF7 cells after MYH10 and FOXM1 knockdown by flow cytometry. **(D)** Percentages of the subpopulations from spherical MCF7 cells with distinctive treatments defined by flow cytometry. **(E)** Subpopulations identified by detections of APC-CD44 and PE-CD24 in monolayer MDA-MB231 cells after MYH10 and FOXM1 knockdown by flow cytometry. **(F)** Percentages of the subpopulations from monolayer MDA-MB231 cells with distinctive treatments defined by flow cytometry. **(G)** Subpopulations identified by detections of APC-CD44 and PE-CD24 in monolayer MDA-MB231 cells after MYH10 and FOXM1 knockdown by flow cytometry. **(H)** Percentages of the subpopulations from monolayer MDA-MB231 cells with distinctive treatments defined by flow cytometry. Isotype controls were performed for each assay (not shown).

3.3.4 MYH10 knockdown improves sphere-forming efficiency in sorted CD44^{high}/CD24^{low} MCF7 cells.

To understand the function of MYH10 in facilitating breast cancer stem-like cell formation, MCF7 cells were stained with APC conjugated CD44 and PE conjugated CD24. The double-stained cells were sorted for the rare CD44⁺/CD24⁻ population and maintained in non-adherent spherical condition for further analysis. In the previous session, we reported that the CD44⁺/CD24⁻ population was reduced by 50% after MYH10 knockdown using FACS analysis (Fig. 3.3.3&3.4 A). The portion of CD44⁺/CD24⁻ cells was maintained in non-adherent condition for up to 7 days to facilitate mammosphere formation. By Western blotting analysis, MYH10 was efficiently downregulated in sorted CD44⁺/CD24⁻ mammospheres at day 7 after the transfection of shMYH10 plasmid into MCF7 cells. (Fig. 3.3.4, B). Knockdown of MYH10 facilitated the formation of mammospheres observed in a long-term period (up to 7 days) (Fig. 3.3.4, C). The enhancement of mammosphere formation is statistically significant compared with CD44⁺/CD24⁻ MCF7 mammospheres without transfection for the corresponding days (Fig. 3.3.4, D).

The unstained, isotypic, and single stained controls against APC-CD44 and PE-CD24 for the gating set up are attached in Appendix III, G&H.

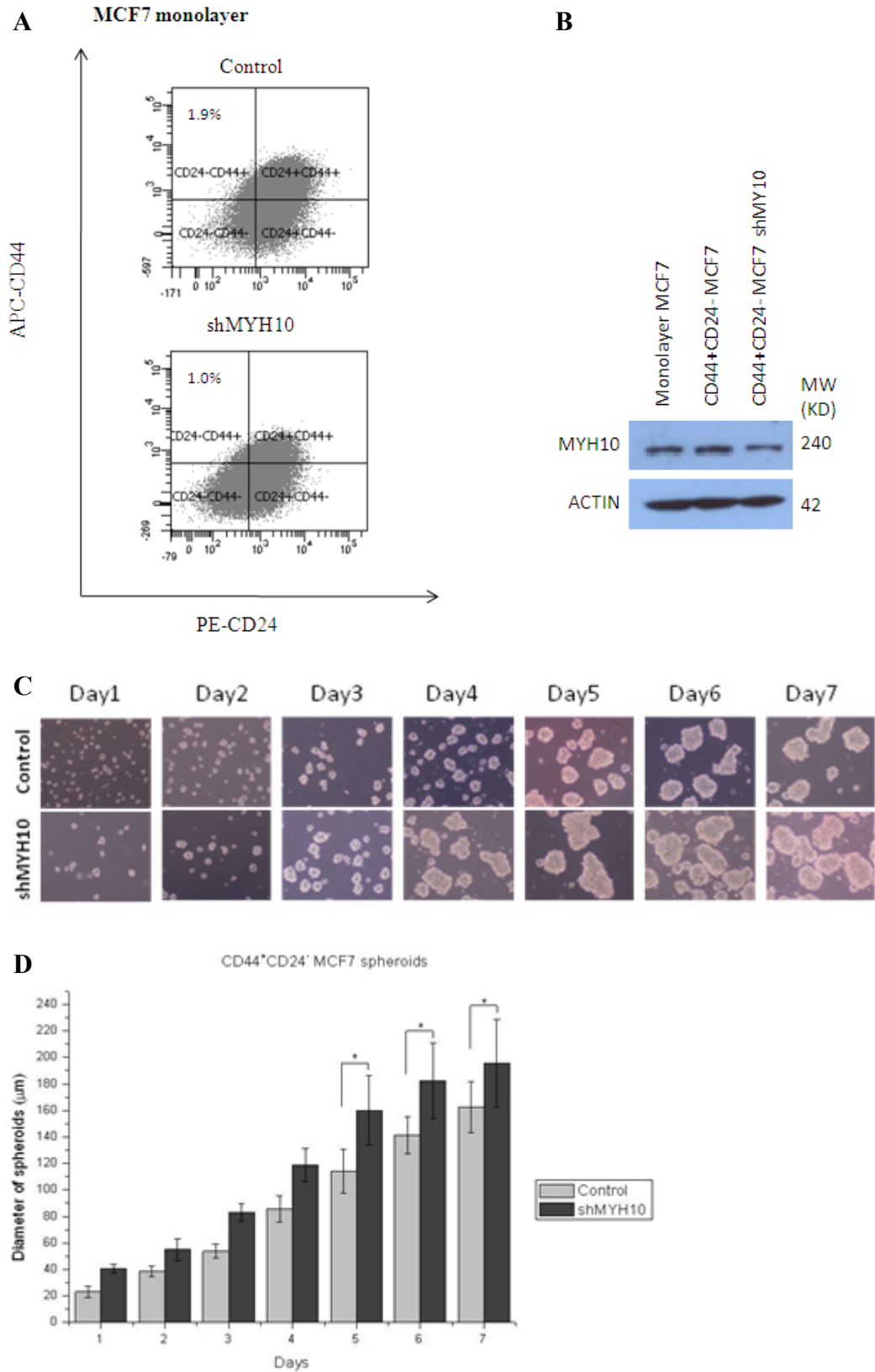


Figure 3.3.4 Inhibition of MYH10 improves sphere-forming efficiency from CD44^{high}/CD24^{low} breast cancer stem-like cells. (A) FACS reports of adherent

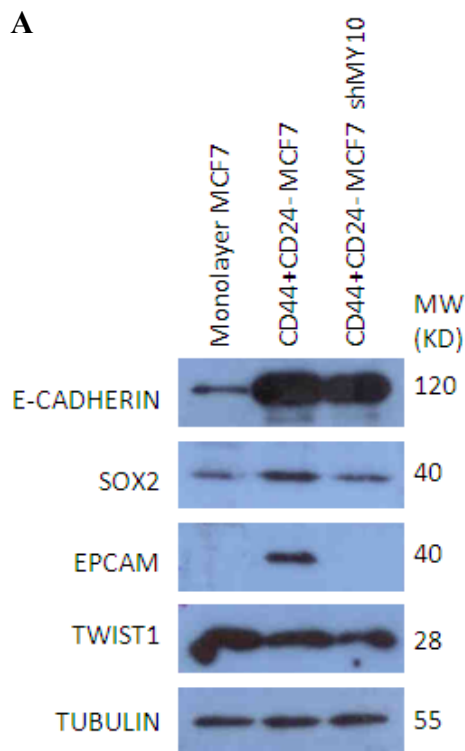
MCF7 cells non- or transfected with pSIREN-shMYH10 vector stained with anti-CD44 and anti-CD24 antibodies. Population of CD44⁺/CD24⁻ was collected for spheroids culture. **(B)** Western blot analysis of MYH10 protein from MCF7 cells non-transfected or transfected with pSIREN-shMYH10 vector and cultured in spheroid condition for 7 days after collection from the population of CD44^{high}/CD24^{low} by FACS. Lysate from MCF7 cells cultured in adherent condition was displayed for comparison. **(C)** Representative bright-phase images of MCF7 CD44⁺/CD24⁻ spheroids for 7 days with or without MYH10 knockdown. **(D)** Chart of the diameters of MCF7 CD44⁺/CD24⁻ spheroids with or without MYH10 knockdown in the indicated days. Diameters were measured from images recorded from 4 random fields. Mean \pm SD. Statistical analysis was done using Student's t test. *, P<0.01, significant.

3.3.5 CD44^{high}/CD24^{low} cells with MYH10 knockdown show decreased property of cancer stem-like cells.

Western blot analysis was performed to study the potential mechanisms of MYH10 in breast cancer stem-like cells. As a result of a more compact 3-dimensional structure, the protein level of E-CADHERIN was much higher in CD44⁺/CD24⁻ MCF7 mammospheres compared with MCF7 cells seeded in monolayer (Fig. 3.3.5 A, 1st row). The protein level of E-CADHERIN was reduced after MYH10 knockdown (Fig. 3.3.5 A, 1st row). The staining from immunofluorescence against MYH10 (Fig. 3.3.5 B, left) and E-CADHERIN (Fig.

3.3.5 B, *right*) revealed high expression levels of E-CADHERIN and MYH10 localized at the cell-cell junctions. However, MYH10 and E-CADHERIN was either reduced or completely not expressed at the cell-cell junctions after MYH10 knockdown (Fig. 3.3.5 B, *insets*).

The population of CD44^{high}/CD24^{low} sorted from MCF7 cells revealed cancer stem-like properties with enhanced protein levels of the pluripotent markers such as SOX2²⁵⁵ and EPCAM²⁷⁸ (Fig. 3.3.5 A, *2nd and 3rd rows*). The stemness was reduced when CD44^{high}/CD24^{low} MCF7 cells were depleted with MYH10 (Fig. 3.3.5 A, *3rd column*). Cancer stem-like cells exhibit higher potential for metastasis with increased protein level of TWIST1²⁷⁹. In agreement with the literature, we also detected a downregulation of TWIST1 after MYH10 knockdown (Fig. 3.3.5 A, *4th row*).



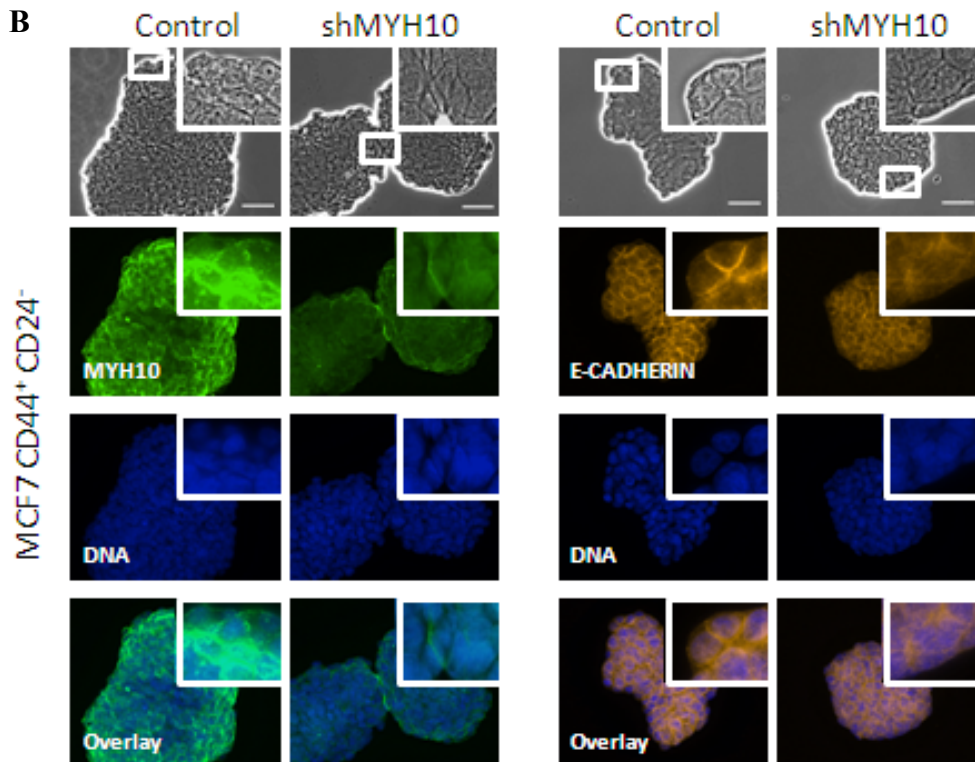
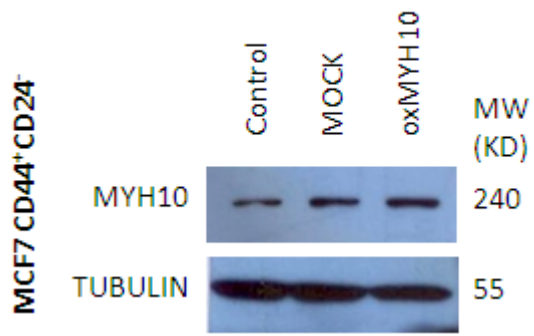


Figure 3.3.5 Inhibition of MYH10 in CD44^{high}/CD24^{low} MCF7 spheroids showed reduced characteristics of cancer stem-like cells.(A) Western blot analysis of E-CADHERIN, SOX2, EPCAM and TWIST1 proteins from MCF7 cells untransfected or transfected with pSIREN-shMYH10 vector and cultured in spheroid condition for 7 days after collection from the population of CD44^{high}/CD24^{low} by FACS. Lysate from MCF7 cells cultured in adherent condition was displayed for comparison. **(B)** Fluorescence images of MCF7 CD44⁺/CD24⁻ spheroids with or without MYH10 knockdown stained with antibody against MYH10 (*left*) or E-CADHERIN (*right*) at day 7 (Scale bar=100μm).

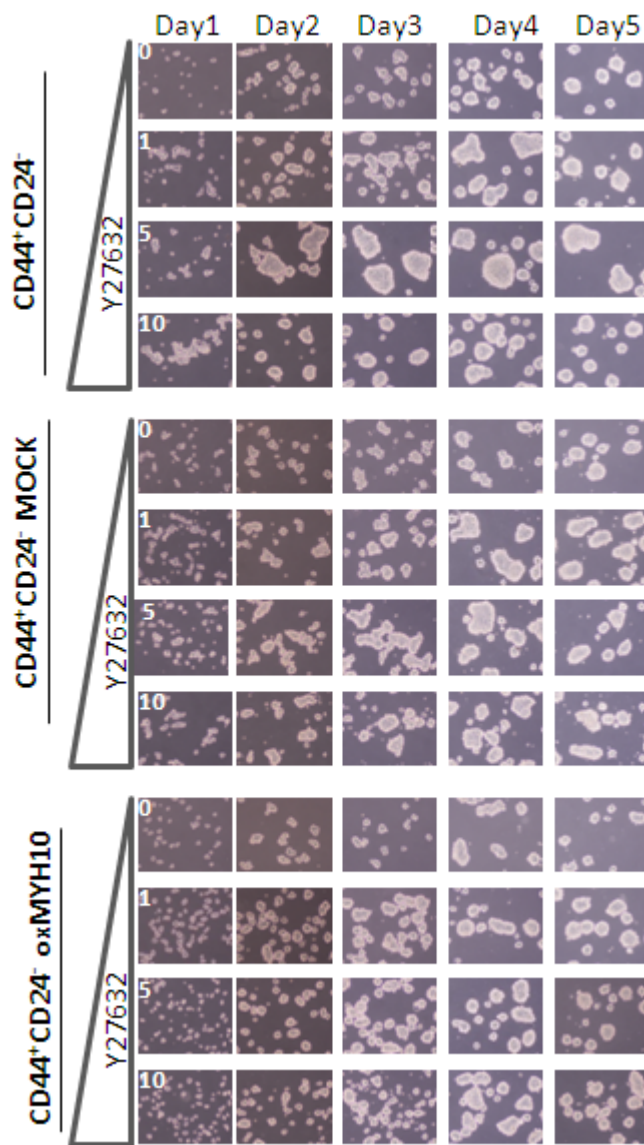
3.3.6 ROCK-MYH10 pathway is responsible for the increased efficiency of MCF7 CD44^{high}/CD24^{low} sphere formation.

MCF7 CD44⁺/CD24⁻ cells was transfected with the pCMV-GFP-MYH10 plasmid (refers to 3.2.2), and subsequently verified by western blot after mammosphere formation at day 5 (Fig. 3.3.6A, *1st row*). ROCK inhibitor (Y27632), which was reported to increase sphere-forming efficiency from primary colon cancer cells²⁸⁰ was used to verify if the MYH10-mediated mammosphere-forming ability was associated with the ROCK pathway. We verified that the exposure of CD44^{high}/CD24^{low} cells to Y27632 at a concentration of 5 μ M would facilitate mammosphere formation, suggesting that MYH10-mediated mammosphere formation capability is associated with ROCK (Fig. 3.3.6B, *top panel*, and Fig. 3.3.6C, *cyan bars*). Overexpression of MYH10 reversed the phenotype in which mammosphere formation ability was affected (Fig. 3.3.4C vs. Fig. 3.3.6B, *1st row of the bottom panel*), when cells were treated with 1-10 μ M of Y27632 (Fig. 3.3.6B, *bottom panel* and Fig. 3.3.6C, *purple bars*). No obvious size difference was observed between non-transfected cells and mock-transfected (transfection without plasmids) cells (Fig. 3.3.6B, *middle panel* and Fig. 3.3.6C, *navy blue bars*). The sizes of MCF7 mammosphere were more significantly decreased by overexpression of MYH10 compared with non-transfected and mock-transfected cells at 5 μ M Y27632 treatments from day 2 (Fig. 3.3.6C, *cross-line bars*).

A



B



C

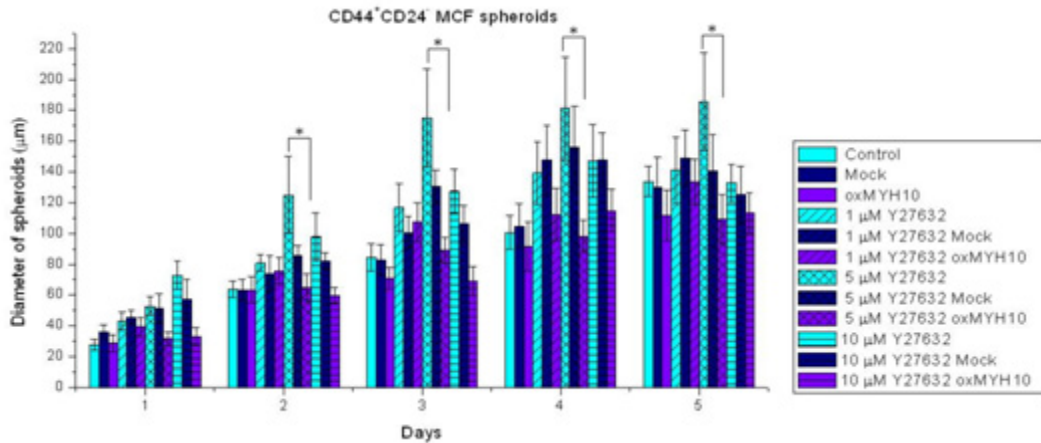


Figure 3.3.6 Expression of MYH10 can suppress the sphere-forming efficiency from breast cancer stem-like cells. (A) Western blot analysis of MYH10 protein from MCF7 cells untransfected or transfected with empty vector (Mock) or MYH10 vector (oxMYH10) and cultured in spheroid condition for 5 days after collection from the population of CD44^{high}/CD24^{low} by FACS. (B) Representative bright-phase images of MCF7 CD44⁺/CD24⁻ spheroids for 5 days with or without MYH10 overexpression, and treated with 0-10µM Y27632. Cells transfected with empty vector were cultured under same conditions and displayed for comparison (Mock). (C) Chart of the diameters of MCF7 CD44⁺/CD24⁻ spheroids with or without MYH10 overexpression and treated with 0-10µM Y27632 in the indicated days. Cells transfected with empty vector were cultured under same conditions and displayed for comparison. Diameters were measured from images recorded from 4 random fields. Mean ± SD. Statistical analysis was done using Student's t test. *, P<0.01, significant.

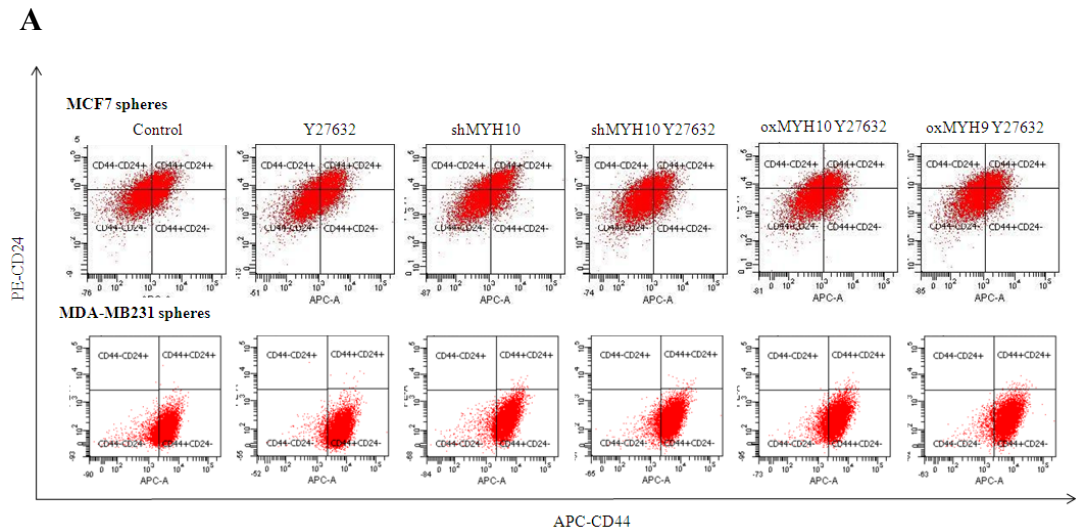
3.3.7 ROCK inhibitor promotes CD44^{high}/CD24^{low} cancer stem-like population in breast cancer cells, which requires non-muscle myosin II participation.

As mentioned, ROCK inhibitor (Y27632) improves the *in vitro* growth of ES cells by inhibition of ROCK to prevent myosin hyperactivation (refers to 2.1.3). The potential of inducing cancer stem-like population in breast cancer cells with Y27632 treatment was carried out in luminal MCF7 cells and basal MDA-MB231 cells. The proportions of CD44⁺/CD24⁻ expressing cells increased were markedly by the ROCK inhibitor, Y27632, with 3.3% increase in MCF7 cells and 11.6% increase in MDA-MB231 cells, respectively (Fig. 3.3.7 B&C).

For luminal derived MCF7 cells, genetic knockdown of MYH10 reduced the fraction of CD44⁺/CD24⁻ with around 1.5% from 19.7% to 18.3% and from 19.7% to 18.0% in two independent experiments (Fig. 3.3.3D, 6th row & Fig. 3.3.7B, 3rd row). Moreover, depletion of MYH10 from MCF7 can prevent the induction of the proportion of CD44⁺/CD24⁻ by Y27632 from 23.0% to 18.3% (Fig. 3.3.7B, 4th row). Notably, the proportion of CD44⁺/CD24⁻ in MYH10 knockdown alone (18.0%) remained similar level as (18.3%) MYH10 depleted cells in Y27632 (Fig. 3.3.7B, 3rd & 4th rows). Enforcing *MYH10* or *MYH9* expression can both restore the enrichments of CD44⁺/CD24⁻ cells in the presence of Y27632 from 19.7% to 22.1% for MYH10 overexpression and to 21.1% for MYH9 overexpression (Fig. 3.3.7B, 5th & 6th rows).

For basal derived MDA-MB231 cells, the scenario is different from MCF7

cells probably due to the high expression of MYH9 in MDA-MB231 cells (Fig. 3.3.1A, 2nd row). Knockdown of MYH10 in MDA-MB231 spheres showed increased population of CD44⁺/CD24⁻ compared with non-transfected cells from 83.4% to 91.0% (Fig. 3.3.7C, 3rd row). However, compared with cells treated with Y27632 alone, MYH10 depleted MDA-MB231 cells showed reduced proportion of CD44⁺/CD24⁻ from 95.0% to 89.5% (Fig. 3.3.7C, 2nd & 4th rows). Similar to MCF7 cells, the proportion of CD44⁺/CD24⁻ in MYH10 knockdown MDA-MB231 cells (91.0%) is as similar as (89.5%) the MYH10 depleted MDA-MB231 cells in Y27632 (Fig. 3.3.7C, 3rd & 4th rows). In contrast with MCF7 cells, overexpression of MYH10 only slightly induced the proportion of CD44⁺/CD24⁻ even in the presence of Y27632 compared with non-transfected MDA-MB231 cells from 83.4% to 84.0% (Fig. 3.3.7C, 5th row). Overexpression of MYH9, on the hand, greatly increased the population of CD44⁺/CD24⁻ MDA-MB231 cells in Y27632 from 83.4% to 93.2% (Fig. 3.3.7C, 6th row)



B

Cell line	Culture condition	Treatments	CD44 ⁻ /CD24 ⁻	CD44 ⁺ /CD24 ⁺	CD44 ⁻ /CD24 ⁺	CD44 ⁺ /CD24 ⁻
MCF7	sphere	Control	19.7	24.9	11.3	44.1
MCF7	sphere	Y27632	23.0	23.7	6.7	46.6
MCF7	sphere	shMYH10	18.0	26.3	8.7	46.9
MCF7	sphere	shMYH10& Y27632	18.3	15.5	9.8	56.3
MCF7	sphere	oxMYH10& Y27632	22.1	18.3	10.1	49.6
MCF7	sphere	oxMYH9& Y27632	21.1	19.2	10.7	48.9

C

Cell line	Culture condition	Treatments	CD44 ⁺ /CD24 ⁻	CD44 ⁻ /CD24 ⁺	CD44 ⁺ /CD24 ⁺	CD44 ⁻ /CD24 ⁻
MDA-MB231	sphere	Control	83.4	0.0	0.0	16.6
MDA-MB231	sphere	Y27632	95.0	0.1	0.0	5.0
MDA-MB231	sphere	shMYH10	91.0	0.2	0.0	8.9
MDA-MB231	sphere	shMYH10& Y27632	89.5	0.1	0.0	10.4
MDA-MB231	sphere	oxMYH10& Y27632	84.0	0.3	0.0	15.8
MDA-MB231	sphere	oxMYH9& Y27632	93.2	0.3	0.0	6.6

Figure 3.3.7 Identifications of CD44⁺/CD24⁻ subpopulations in breast cancer cell lines treated with Y27632 regarding to MYH10/MYH9 expression by flow cytometry. (A) Subpopulations identified by expression of APC-CD44 and

PE-CD24 in spherical MCF7 cells (*top*) or MDA-MB231 cells (*bottom*) without or with MYH10 knockdown (shMYH10) or overexpression (oxMYH10) in the presence with or without 10 μ M Y27632 by flow cytometry. Spherical cells transfected with MYH9 vector (oxMYH9) and cultured with 10 μ M Y27632 were displayed for comparison. **(B)** Percentages of the subpopulations from spherical MCF7 cells with distinctive treatments defined by flow cytometry. **(C)** Percentages of the subpopulations from spherical MDA-MB231 cells with distinctive treatments defined by flow cytometry.

3.4 Discussion

3.4.1 Verification and isolation of CD44^{high}/CD24^{low} breast cancer cells with cancer stem-like cell characteristics.

Pioneering work by Al-Hajj uncovered that human mammary tumors encompass stem cell and non-stem cell components, in which only the stem cell fraction can contribute to tumorigenesis upon transplantation into immunodeficient animals¹⁰¹. These cancer stem-like cells were described as a CD44⁺/CD24⁻ phenotype, showing enhanced invasiveness and multidrug resistance^{243,276}. We selected 2 types of typical breast cancer cell lines with different origin: luminal derived MCF7 cells and basal derived MDA-MB231 cells to study. Luminal breast cancer cell lines are mainly enriched with CD44^{-/low}CD24^{high} cells, while basal breast cancer cell lines are enriched in the CD44⁺/CD24^{-/low} cancer stem-like phenotype²⁴⁴. We used APC conjugated CD44 and PE conjugated CD24 antibodies to target MCF7 and analyzed with fluorescence-activated cell sorting (FACS) (Fig. 3.3.4, A). The population of CD44⁺/CD24⁻ was collected and maintained in non-adherent condition for sphere formation. *In vitro* assays, revealing an increased drug resistance of blebbistatin existed in sorted CD44⁺/CD24⁻ cell population (Fig. 3.3.1, B). Furthermore, marker for mammary stem progenitor (EPCAM)²⁷⁸ was found to be highly expressed in the CD44⁺/CD24⁻ cell population (Fig. 3.3.5A, 3rd row). CD44⁺/CD24⁻ population sorted from MCF7 cells also displayed an increased expression of one of the master embryonic pluripotent markers (SOX2)²⁵⁵ (Fig.

3.3.5A, 2nd row). The relatively high expression of the marker (TWIST1) for epithelial–mesenchymal transition (EMT)²⁷⁹, suggested a potentially more invasive CD44⁺/CD24⁻ sorted population (Fig. 3.3.5A, 4th row). A small number of sorted CD44⁺/CD24⁻ cells were successfully xeno-transplanted into NOC-SCID mice for *in vivo* tumor formation study (*animal work done by other team members, data not shown, refers to acknowledgment*). Collectively, our data provide us a reliable model to study and characterize breast cancer stem-like cells.

3.4.2 Justification of the potential role of FOXM1 in promoting the maintenance of cancer stem-like cells in breast cancer.

It was reported that *FOXM1* expression is elevated in multiple tumors with poor patient outcome including breast cancer^{256,257}, and corresponding to the cancer stem-like cell phenotype in pancreatic cancer cells²⁵⁹. Therefore, in this study, we have examined the potential role of FOXM1 in maintaining the cancer stem-like cells in MCF7 and MDA-MB231 breast cancer cells. This was achieved by chemical and genetic knockdown of FOXM1. The results from chemical and genetic knockdown of FOXM1 showed distinctively reduced CD44⁺/CD24⁻ populations (Fig. 3.3.3 B-H, 3rd and 4th rows) with a higher efficiency from chemical treatment. The more effective reduction of CD44⁺/CD24⁻ population from thiostrepton may partially due to its cytotoxicity on breast cancer cells²¹⁴. The less effective inhibition of CD44⁺/CD24⁻ population from genetic knockdown of FOXM1 may also due to the low

efficiency of transfection in MCF7 and MDA-MB231 cells (data not shown). A further investigation on HeLa cells, which was optimized for transfection in our lab, revealed that the expression of FOXM1 may well be responsible for mediating the Rho-GTPase and ROCK1 pathways (Fig. 3.3.2). The finding that overexpression of the Δ N-FOXM1 mutant alone, which lacks the NH₂-terminus of FOXM1, did not cause the upregulation of Rho-GTPase and ROCK1 (Fig. 3.3.2, *arrows*), suggesting the NH₂-terminus of FOXM1 is required for regulation of the Rho-GTPase and ROCK1 pathways.

3.4.3 MYH10 expression is essential to support the cancer stem-like component in breast cancer.

We found that MYH10 is highly expressed in human ES cells and MCF7 cells cultured in spherical condition, which enriches more breast cancer stem-like cells (Fig. 3.3.1A). Considering our finding of the protein complex of MYH10 and FOXM1 in human ES cells (Fig. 2.3.3) and the previous findings of the essential role of FOXM1 in cancer stem-like cells²⁸¹, we investigated the promising role of MYH10 in breast cancer stem-like cells. Similarly, genetic and chemical inhibitions were employed to study the role of MYH10 on the cancer stem-like CD44⁺/CD24⁻ cells. Significant reduction of the CD44⁺/CD24⁻ populations could be achieved by blebbistatin treatment (Fig. 3.3.3B-H, *last rows*). Genetic knockdown of MYH10 resulted in a decline of the CD44⁺/CD24⁻ population in MCF7 cells. In contrast, overexpression of MYH10 reinforced the

CD44⁺/CD24⁻ population in mammospheres (Fig. 3.3.3B&D, 6th rows), suggesting the promotion of cancer stem-like cells by MYH10 may require a microenvironment which mimics the intratumoural environment *in vivo*. Genetic knockdown of MYH10 alone, in MDA-MB231 cells, did not exert the same efficiency as blebbistatin treatment (Fig. 3.3.3F&H, 5th & 6th rows), which may be due to the existence of MYH9 in MDA-MB231 cells (Fig. 3.3.1 A, 2nd row). The expression of MYH9 may compensate the function of MYH10 after MYH10 knockdown in MDA-MB231 cells. It is also possible that MYH9 exhibits different function from MYH10 in basal derived breast cancer cells²⁶⁹. Some signature markers for cancer stem-like cells, including SOX2, EPCAM and TWIST1, were all reduced after MYH10 knockdown in CD44⁺/CD24⁻ cells, supporting that downregulation of MYH10 can induce the cells to shift to a more differentiated state. Moreover, the loss of E-CADHERIN expression and proper location at cell-cell junctions, suggesting a loose aggregation of the sphere with differentiated cells. Based on those findings, we can conclude that MYH10 is essential for the maintenance of breast cancer stem-like cells.

3.4.4 Rho kinase inhibitor facilitating mammosphere formation is associated with MYH10 expression.

The finding of ROCK inhibitor that promotes the formation of spheroids and survival of colon cancer stem-like cells²⁸⁰, assists us to unravel the underlying mechanism of the inhibition of ROCK in cancer stem-like cells. After

we found that the knockdown of MYH10, which is the direct effector of ROCK1, can mimic Y27632 treatment in breast cancer stem like cells by increasing spheroid formation in CD44⁺/CD24⁻ MCF7 cells (Fig. 3.3.4). The direct connection was confirmed by a rescue experiment when CD44⁺/CD24⁻ MCF7 cells were ectopically expressed with MYH10 and co-treated with Y27632 (Fig. 3.3.6). The promotions of sphere formation by Y27632 were correlated to its enhancement on the population of CD44⁺/CD24⁻ in breast cancer (Fig. 3.3.7 B&C, 2nd rows). However, the increased size of MCF7 mammospheres after MYH10 knockdown showed decreased proportion of CD44⁺/CD24⁻ (Fig. 3.3.7 B, 3rd row), which also reduced the proportion of CD44⁺/CD24⁻ cells induced by Y27632 (Fig. 3.3.7 B, 4th row). The introduction of ectopic MYH10 or MYH9 only shifted the stem-like component slightly, indicating the presence of MYH10 is required for the maintenance of cancer stem-like population and sphere formation. In contrast with MCF7 cells, overexpression of MYH9 but MYH10 can greatly increase the cancer stem-like population in the presence of Y27632 in MDA-MB231 cells. This opposite effect in MDA-MB231 cells, offered us to consider the distinctive role of MYH9 in basal derived cancer stem-like cells again (Fig. 3.3.7 C). Taken together, the expression of non-muscle myosin II may be critical in the maintenance of breast cancer stem-like cells *in vitro*.

Chapter 4 Conclusion and suggestions for future study

4.1 Conclusion

Two of my projects started with the novel identification of protein interactions between FOXM1 and MYH10. In human embryonic stem (ES) cells, we used chemical inhibitors of MYH10 (blebbistatin) and FOXM1 (thiostrepton) to investigate the effects of suppression of the identified targets. We found that blebbistatin treated cells can induce FOXM1 expression, and subsequently facilitate viability and self-renewal in human ES cells. In this study, we deduced that FOXM1 can directly regulate pluripotency through binding onto the *OCT4* promoter. *OCT4* expression could thus be regulated in response to blebbistatin. The induction could be detected by Chromatin Immunoprecipitation (ChIP) assay. The inhibition of the MYH10 and FOXM1 complex can affect AURORA KINASE B and KIF14 expression; resulted in supernumerary centrioles. The presence of extra copies of centrioles affected mitosis in hES cells. By using retroviral mediated shRNA knockdown, which represents specific targeting, we found that the chemical toxicity of thiostrepton on human ES cells may not be due to FOXM1-silencing. It also proved that the presence of this newly identified protein complex: FOXM1 and MYH10 may be essential for self-renewal and pluripotency. We deduced that the modulation of ROCK, E-CADHERIN and beta-CATENIN by FOXM1, may involve MYH10. The phenotype after MYH10 knockdown differs from blebbistatin-treated cells. The difference in phenotype

prompted us to investigate the differential functions between MYH9 and MYH10, together with FoxM1, in human ES cells.

In the cancer stem cell study, we also evaluated the roles of MYH10 and FOXM1 in cancer stem cells. After successful isolation and identification of cancer stem-like cells, we used genetic knockdown and chemical treatments to suppress the MYH10 and FOXM1 complex in cancer stem-like cells. We found that the identified complex, MYH10/FOXM1, may be critical for the maintenance of cancer stem-like cells, particularly in non-adherent culture condition which favors the formation of mammospheres. Knockdown MYH10 as well as inhibition of Rho kinase can efficiently induce mammospheres formation in MCF7 cancer stem-like cells, of which the induction of size is independent on its stem-like population for MYH10. MYH10 and MYH9 contribute differentially in cancer stem-like cell maintenance depending on their cancer origin.

4.2 Suggestions for future study.

4.2.1 Potential binding of MYH10 with FOXO3A and SIRT1 in human embryonic stem cells.

As one of the initial three ageing factors for screening, SIRT1 and FOXO3A probed out a common band at 225KD as same molecular weight as the one from FOXM1 (Fig. 2.3.1 A). The result from mass spectrometry also predicted that

band from SIRT1 as MYH10 with a score of 80 for high identity (Fig. 2.3.2 C, D & Table 2.3.1). Moreover, *in vitro* assay also showed endogenous binding of MYH10 with FOXO3A and SIRT1 in H9 and iPS_{IMR90} cells (Fig. 3.3.1 C-F). We only focused on the study of the interaction between FOXM1 and MYH10 in stem cell research. However, both SIRT1 and FOXO3A are significant in ageing; it will be our great interests to investigate their potential crosstalk with MYH10 for hES cells survival and maintenance.

4.2.2 Clarification of a differential function of MYH10 from MYH9 in human embryonic stem cell.

After the discovery of using Y27632 to dissociate hES cells¹⁸², further investigations using Y27632-mediated actin-myosin contractility could induce apoptosis in human embryonic cells. The actin-myosin contractility may involve both MYH9 and MYH10¹⁷⁰; however, the precise role of MYH10 in the induction of this phenotype is still unclear. From Walker's study, rescue experiment was designed to prove that MYH9 instead of MYH10 is responsible for the enhanced survival in mouse ES cells¹⁷⁰. The weakness of this study may lie on the fact that, unlike hES cells, mouse ES cells are resistant to dissociation-induced apoptosis¹⁸¹. Therefore, the conclusion derived from Walker's report¹⁷⁰ is debatable. Detailed investigations from Li's report¹⁸⁵ showed specific gene depletion of MYH9 by shRNA targeting. They revealed that colony dissociation in human ES cells after MYH9 depletion, similar to blebbistatin treatment¹⁸⁵. In contrast, report from Chen using siRNA targeting

against MYH9/MYH10 in human ES cells did not show colony dissociation¹⁸⁴. Instead, Chen et al observed cell spreading, which is another phenotype from blebbistatin treatment¹⁸⁴. Both articles tried to show evidence of the role of MYH9 as the sole reason for cell blebbing. And association with various phenotypes by same targeting of MYH9. They also reached the ambivalent conclusions for pluripotency from blebbistatin treatment. The data from us showed that MYH10 knockdown retains the colony integrity with protrusions at the periphery, which matched with Chen and Li's descriptions for cell spreading and projections^{184,185}. We hypothesized that MYH10 may act differently from MYH9 on stem cell spreading, where genetic knockdown of MYH9 is urgent for further study. We connected the change in pluripotency induced by blebbistatin with FOXM1 expression and binding on OCT4 promoter. The discrepancy from previous findings is, at least in part, due to the technical difficulty regarding gene manipulations in human ES cell. A more reliable gene transfer system may be required.

4.2.3 Validation the function of MYH10 and FOXM1 during mitosis for determination of symmetric or asymmetric division.

Our findings of poor locations of centrioles at the midbody after thiostrepton treatment showed a sign of asymmetric division, more details of work are required to elaborate by genetic depletion of FOXM1. Moreover, to justify whether the process is undergoing symmetric or asymmetric division, markers to define the parental and daughter cells are essential, of which limited

work was explored in human ES cells. Inspiration from the proper location of the mitotic spindle for the determination of asymmetric division in cancer,²⁸² may offer us an opportunity to study in stem cells by tracking the movement of centrioles by staining of CEP170, CEP120 or PLK2 for discrimination of mother and daughter centrioles. It might also offer us the chance to get insights of the cancer stem cell model by better understand the faithful control of ES cell mitosis.

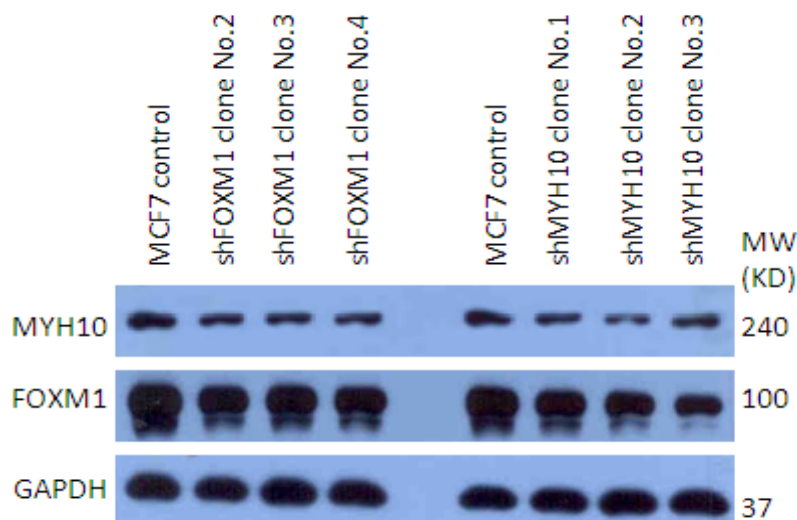
4.2.4 Mechanisms of MYH10 and FOXM1 in cancer stem-like cells.

Our data showed that MYH10 and FOXM1 are both essential to maintain the CD44^{high}/CD24^{low} cancer stem-like property in MCF7 breast cancer cells. However, we did not find direct connection between those two proteins in breast cancer cells by lacking the evidence of protein to protein or protein to DNA direct interactions. Our finding of FOXM1 (N terminus) positively regulates non-muscle myosin II in HeLa cells needs to be further demonstrated in breast cancer cells as well as the immunoprecipitation assay. More efficient gene targeting of MYH10 and FOXM1 may be required to rectify the uncertainty of stem-like populations in MDA-MB231 cells. The study from Ohata revealed that CD44 was induced by Rho kinase inhibition as well as blebbistatin in colon cancer stem-like cells, which increases the size of spheroids²⁸⁰. However, in our observation there is no size induction by blebbistatin in primary MCF7 spheroids without CD44⁺/CD24⁻ sorting (data not shown). And the CD44⁺/CD24⁻

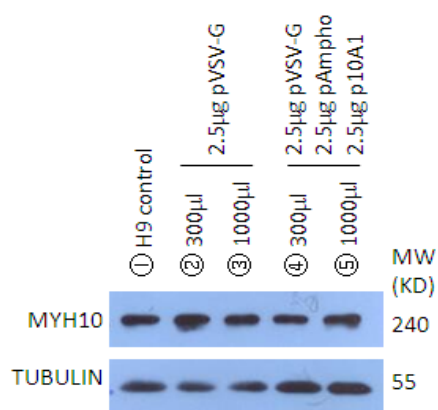
populations were dramatically suppressed after blebbistatin treatment in 2 breast cancer cell lines in either adherent or non-adherent condition. Based on our finding that CD44⁺/CD24⁻ MCF7 and MDA-MB231 cells positively response to Y27632 treatment as Ohata's report, and MYH10 and MYH9 showing distinctively properties in two cell lines in response of Y27632. Detailed investigations by gene knock down of MYH10 and MYH9 together with blebbistatin treatment in CD44⁺/CD24⁻ MCF7 and MDA-MB231 cells are necessary to explain whether this effect is cell line dependent. The finding that sphere forming ability is not equivalent to tumorigenic recently²⁸³ has provided us an alternative explanation for induced sphere-size with lower cancer stem-like population in our model for MYH10 knockdown. However, animal experiment for tumor transplantation in NOD/SCID mouse is essential and more stringent *in vivo* assay for testing the self-renewal and tumorigenic properties of cancer stem-like cells.

Appendix I

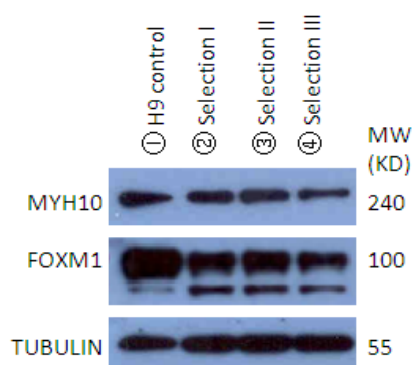
A



B



C



Appendix I Conditions for retroviral production, infection and selection of target cells.

(A) Western blot analysis of FOXM1 and MYH10 proteins in MCF7 cells after transfection of varied clone of pSIREN-shFOXM1 (left) or pSIREN-shMYH10 (right) plasmids. (B) Western blot analysis of MYH10 protein in H9 cells after infection of 300 μ l (②,④) or 1000 μ l (③,⑤) virus collected from GP2-293 packing cells co-transfected with 5 μ g pSIREN-shMYH10 and 2.5 μ g pVSV-G (②,③) or 2.5 μ g pVSV-G, 2.5 μ g

pAmpho and 2.5 μ g 10A1 (④,⑤). (C) Western blots analysis of MYH10 and FOXM1 proteins in H9 cells. GP2-293 packing cells were transfected with 8 μ g pSIREN-shMYH10 and were supplied with 1 μ g/ml (②), 2 μ g/ml (③) and 3 μ g/ml (④) puromycin for 8 days for selection of stable packing cell lines before transfection of 2.5 μ g pVSV-G, 2.5 μ g pAmpho and 2.5 μ g 10A1 to produce virus to infect H9 cells.

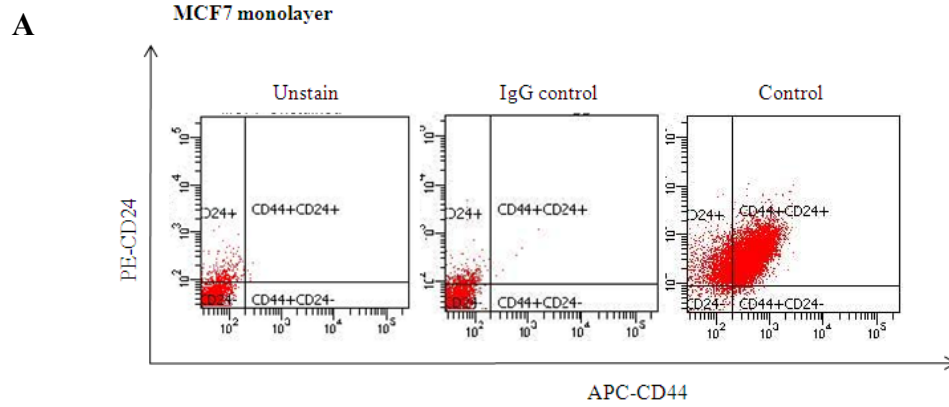
Appendix II

The formulas of buffer from section 2.2 and 3.2 are listed as below:

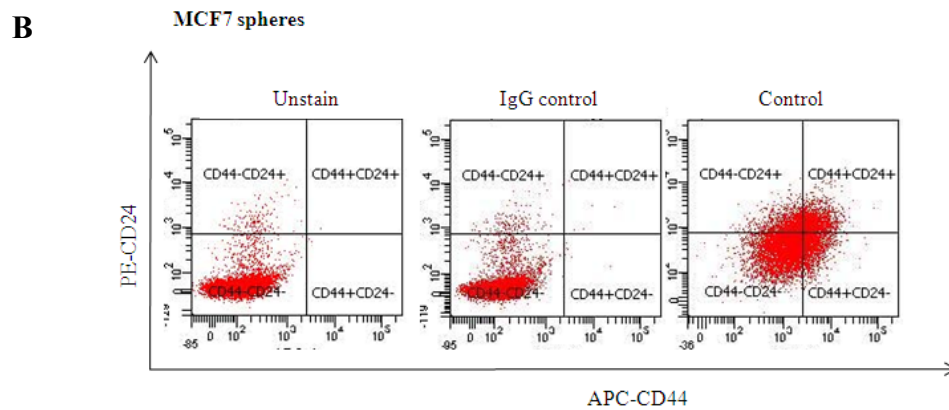
RIPA buffer		IP buffer	
NaCl	150mM	NaCl	150mM
Tris-HCl, pH8.0	50mM	Tris-HCl, pH7.5	50mM
NP-40	1%	EDTA	5mM
Sodium deoxycholate	0.5%	NP-40	0.5%
SDS	0.1%	Triton X-100	1%
Coomassie Brilliant Blue Staining		Destaining Solution	
Methanol	40%	Methanol	30%
Acetic acid	10%	Acetic acid	10%
Coomassie Brilliant Blue R-250	0.025%		
SDS-PAGE 10% running gel (2 minigels)		SDS-PAGE 4% stacking gel (2 minigels)	
30% Polyacrylamide	5ml	30% Polyacrylamide	750µl
Milli-Q water	4.3ml	Milli-Q water	4.4ml
1.0 M Tris-HCl, pH 8.8	5.6ml	1.0 M Tris-HCl, pH 6.8	750µl
10% SDS	75µl	10% SDS	30µl
10% Ammonium Persulfate	75µl	10% Ammonium Persulfate	30µl
TEMED	15µl	TEMED	6µl

Cell sorting buffer for FACS		Cell fixation for IF	
HEPES	25mM	3.7% Paraformaldehyde*	5ml
EDTA	5mM	2X PHEM buffer	5ml
1% FBS	5ml	*Boil 0.2g paraformaldehyde in 5 ml water with 10µl NaOH (5N)	
1% Penicillin and Streptomycin	5ml	2X PHEM buffer	
Autoclaved PBS	460 ml	PIPES	120mM
Filter through 0.22 µm filter		HEPES	50mM
		EGTA	100mM
		MgSO ₄	100mM

Appendix III

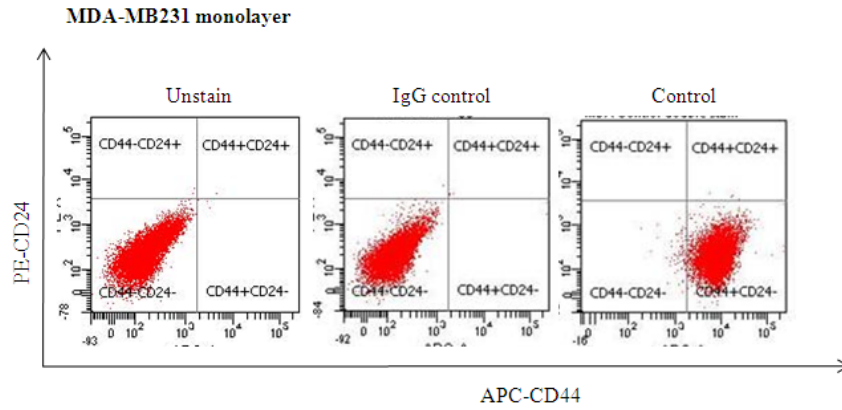


Cell line	Culture condition	Treatments	CD44 ⁺ /CD24 ⁻	CD44 ⁺ /CD24 ⁺	CD44 ⁻ /CD24 ⁺	CD44 ⁻ /CD24 ⁻
MCF7	monolayer	Unstain	0.0	0.2	3.4	96.4
MCF7	monolayer	IgG control	0.0	0.1	3.6	96.3
MCF7	monolayer	Control	1.6	74.6	18.3	5.5

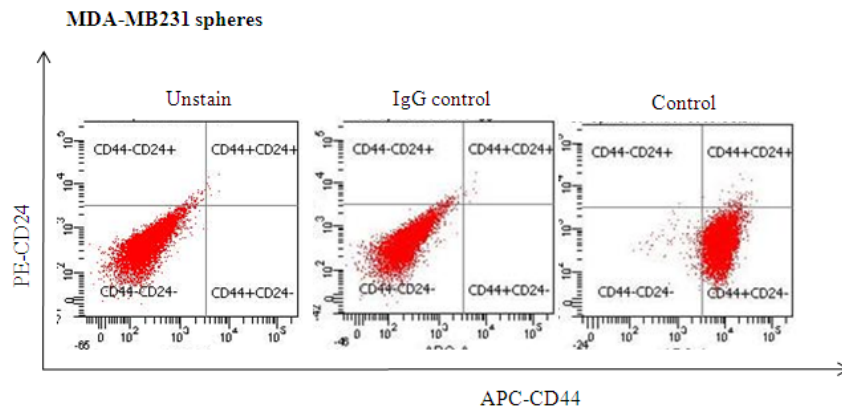


Cell line	Culture condition	Treatments	CD44 ⁺ /CD24 ⁻	CD44 ⁺ /CD24 ⁺	CD44 ⁻ /CD24 ⁺	CD44 ⁻ /CD24 ⁻
MCF7	sphere	Unstain	0.0	0.0	1.3	98.6
MCF7	sphere	IgG control	0.1	0.1	1.6	98.3
MCF7	sphere	Control	19.7	16.0	13.8	50.6

Appendix III A, B refer to the unstained and IgG control of Fig. 3.3A-D

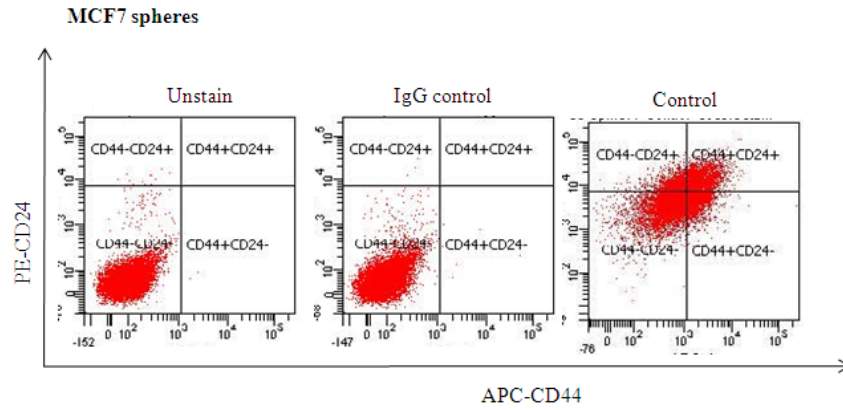
C

Cell line	Culture condition	Treatments	CD44 ⁺ /CD24 ⁻	CD44 ⁺ /CD24 ⁺	CD44 ⁻ /CD24 ⁺	CD44 ⁻ /CD24 ⁻
MDA-MB231	monolayer	Unstain	0.0	0.0	0.0	99.9
MDA-MB231	monolayer	IgG control	0.0	0.0	0.0	99.9
MDA-MB231	monolayer	Control	99.2	0.0	0.0	0.7

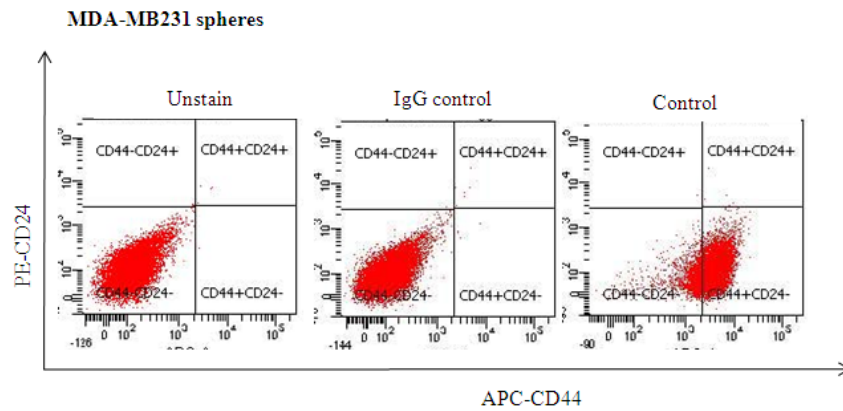
D

Cell line	Culture condition	Treatments	CD44 ⁺ /CD24 ⁻	CD44 ⁺ /CD24 ⁺	CD44 ⁻ /CD24 ⁺	CD44 ⁻ /CD24 ⁻
MDA-MB231	sphere	Unstain	0.0	0.1	0.5	99.4
MDA-MB231	sphere	IgG control	0.0	0.1	0.5	99.4
MDA-MB231	sphere	Control	97.7	0.8	0.0	1.5

Appendix III C, D refer to the unstained and IgG control of Fig. 3.3E-H

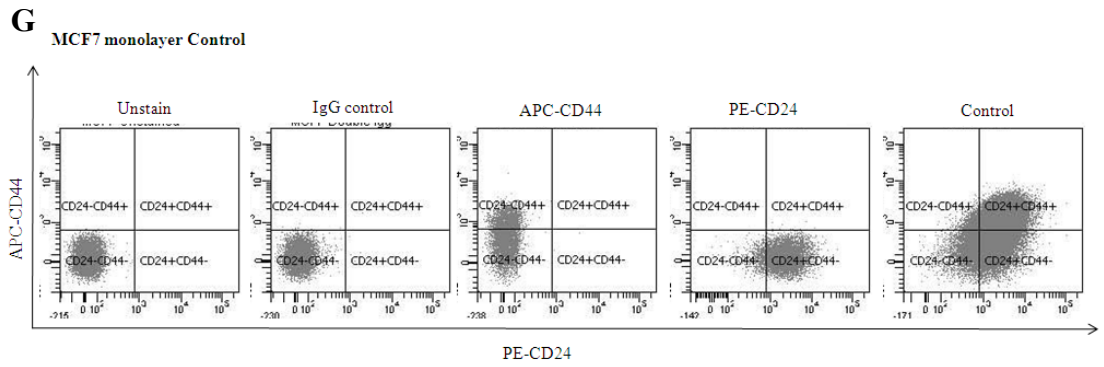
E

Cell line	Culture condition	Treatments	CD44 ⁺ /CD24 ⁻	CD44 ⁺ /CD24 ⁺	CD44 ⁻ /CD24 ⁺	CD44 ⁻ /CD24 ⁻
MCF7	sphere	Unstain	0.0	0.0	0.1	99.9
MCF7	sphere	IgG control	0.1	0.0	0.0	99.9
MCF7	sphere	Control	19.7	24.9	11.3	44.1

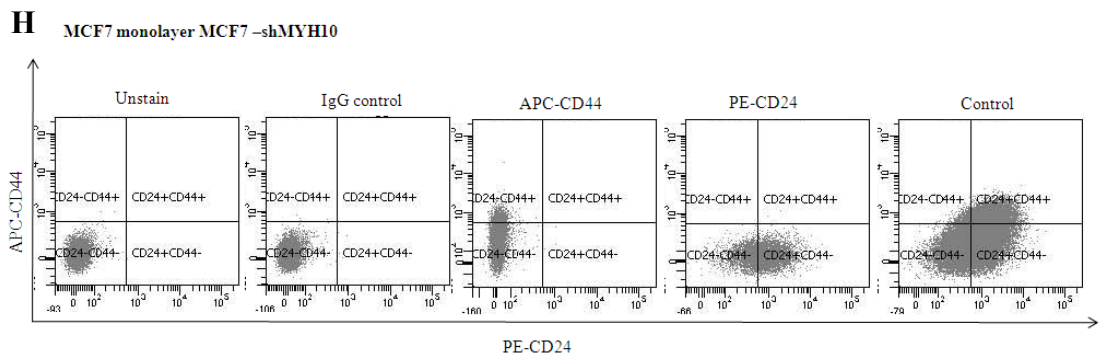
F

Cell line	Culture condition	Treatments	CD44 ⁺ /CD24 ⁻	CD44 ⁺ /CD24 ⁺	CD44 ⁻ /CD24 ⁺	CD44 ⁻ /CD24 ⁻
MDA-MB231	sphere	Unstain	0.0	0.0	0.0	99.9
MDA-MB231	sphere	IgG control	0.0	0.0	0.0	100.0
MDA-MB231	sphere	Control	83.4	0.0	0.0	16.6

Appendix III E, F refer to the unstained and IgG control of Fig. 3.7.



Cell line	Culture condition	Treatments	CD44 ⁺ /CD24 ⁻	CD44 ⁺ /CD24 ⁺	CD44 ⁻ /CD24 ⁺	CD44 ⁻ /CD24 ⁻
MCF7	monolayer	Unstain	0.0	0.0	0.0	100.0
MCF7	monolayer	IgG control	0.1	0.0	0.1	99.8
MCF7	monolayer	APC-CD44	33.6	0.0	0.0	66.3
MCF7	monolayer	PE-CD24	0.0	0.1	90.8	9.0
MCF7	monolayer	Control	1.9	54.0	35.9	8.2



Cell line	Culture condition	Treatments	CD44 ⁺ /CD24 ⁻	CD44 ⁺ /CD24 ⁺	CD44 ⁻ /CD24 ⁺	CD44 ⁻ /CD24 ⁻
MCF7 -shMYH10	monolayer	Unstain	0.0	0.0	0.0	99.9
MCF7 -shMYH10	monolayer	IgG control	0.1	0.0	0.1	99.9
MCF7 -shMYH10	monolayer	APC-CD44	13.0	0.0	0.1	86.9
MCF7 -shMYH10	monolayer	PE-CD24	0.0	0.0	63.3	36.7
MCF7 -shMYH10	monolayer	Control	1.0	17.2	53.9	27.9

Appendix III G, H refer to the unstained, IgG control and single stain of APC-CD44 and PE-CD24 for gating the FACS of Fig. 3.4A.

References

1. Kiessling, A.A. Timing is everything in the human embryo. *Nat Biotechnol* **28**, 1025-6 (2010).
2. Beddington, R.S. & Robertson, E.J. Axis development and early asymmetry in mammals. in *Cell*, Vol. 96 195-209 (United States, 1999).
3. Jenkins, G.W. & Tortora, G.J. *Anatomy and Physiology from Science to Life*, 964-975 (WILEY, Hoboken, USA, 2013).
4. Gilbert, S.F. *Developmental Biology*, 300-308 (Sinauer Associates, Inc., Massachusetts, USA, 2010).
5. Stevens, L.C. & Little, C.C. Spontaneous Testicular Teratomas in an Inbred Strain of Mice. *Proc Natl Acad Sci U S A* **40**, 1080-7 (1954).
6. Martin, G.R. Isolation of a pluripotent cell line from early mouse embryos cultured in medium conditioned by teratocarcinoma stem cells. *Proc Natl Acad Sci U S A* **78**, 7634-8 (1981).
7. Evans, M.J. & Kaufman, M.H. Establishment in culture of pluripotential cells from mouse embryos. *Nature* **292**, 154-6 (1981).
8. Thomson, J.A. et al. Embryonic stem cell lines derived from human blastocysts. *Science* **282**, 1145-7 (1998).
9. Stojkovic, M. et al. Derivation of human embryonic stem cells from day-8 blastocysts recovered after three-step in vitro culture. in *Stem Cells*, Vol. 22 790-7 (United States, 2004).
10. Klimanskaya, I., Chung, Y., Becker, S., Lu, S.J. & Lanza, R. Human embryonic stem cell lines derived from single blastomeres. in *Nature*, Vol. 444 481-5 (England, 2006).
11. Lin, G. et al. A highly homozygous and parthenogenetic human embryonic stem cell line derived from a one-pronuclear oocyte following in vitro fertilization procedure. in *Cell Res*, Vol. 17 999-1007 (China, 2007).
12. Hoffman, L.M. & Carpenter, M.K. Characterization and culture of human embryonic stem cells. *Nat Biotechnol* **23**, 699-708 (2005).
13. Thomson, J.A. & Odorico, J.S. Human embryonic stem cell and embryonic germ cell lines. in *Trends Biotechnol*, Vol. 18 53-7 (England, 2000).
14. Amit, M. et al. Clonally derived human embryonic stem cell lines maintain pluripotency and proliferative potential for prolonged periods of culture. in *Dev Biol*, Vol. 227 271-8 (2000 Academic Press., United States, 2000).
15. Williams, R.L. et al. Myeloid leukaemia inhibitory factor maintains the developmental potential of embryonic stem cells. *Nature* **336**, 684-7 (1988).
16. Ying, Q.L., Nichols, J., Chambers, I. & Smith, A. BMP induction of Id proteins suppresses differentiation and sustains embryonic stem cell self-renewal in collaboration with STAT3. in *Cell*, Vol. 115 281-92 (United States, 2003).
17. Yoshida, K. et al. Maintenance of the pluripotential phenotype of embryonic stem cells through direct activation of gp130 signalling pathways. in *Mech Dev*, Vol. 45 163-71

- (Ireland, 1994).
18. Takahashi-Tezuka, M. et al. Gab1 acts as an adapter molecule linking the cytokine receptor gp130 to ERK mitogen-activated protein kinase. *Mol Cell Biol* **18**, 4109-17 (1998).
 19. Burdon, T., Stracey, C., Chambers, I., Nichols, J. & Smith, A. Suppression of SHP-2 and ERK signalling promotes self-renewal of mouse embryonic stem cells. in *Dev Biol*, Vol. 210 30-43 (1999 Academic Press., United States, 1999).
 20. Escary, J.L., Perreau, J., Dumenil, D., Ezine, S. & Brulet, P. Leukaemia inhibitory factor is necessary for maintenance of haematopoietic stem cells and thymocyte stimulation. *Nature* **363**, 361-4 (1993).
 21. Yoshida, K. et al. Targeted disruption of gp130, a common signal transducer for the interleukin 6 family of cytokines, leads to myocardial and hematological disorders. *Proc Natl Acad Sci U S A* **93**, 407-11 (1996).
 22. Takeda, K. et al. Targeted disruption of the mouse Stat3 gene leads to early embryonic lethality. *Proc Natl Acad Sci U S A* **94**, 3801-4 (1997).
 23. Miyabayashi, T. et al. Wnt/beta-catenin/CBP signaling maintains long-term murine embryonic stem cell pluripotency. in *Proc Natl Acad Sci U S A*, Vol. 104 5668-73 (United States, 2007).
 24. Sato, N., Meijer, L., Skaltsounis, L., Greengard, P. & Brivanlou, A.H. Maintenance of pluripotency in human and mouse embryonic stem cells through activation of Wnt signaling by a pharmacological GSK-3-specific inhibitor. in *Nat Med*, Vol. 10 55-63 (United States, 2004).
 25. Nichols, J., Silva, J., Roode, M. & Smith, A. Suppression of Erk signalling promotes ground state pluripotency in the mouse embryo. in *Development*, Vol. 136 3215-22 (England, 2009).
 26. Hanna, J. et al. Metastable pluripotent states in NOD-mouse-derived ESCs. in *Cell Stem Cell*, Vol. 4 513-24 (United States, 2009).
 27. Nichols, J. et al. Validated germline-competent embryonic stem cell lines from nonobese diabetic mice. in *Nat Med*, Vol. 15 814-8 (United States, 2009).
 28. Daheron, L. et al. LIF/STAT3 signaling fails to maintain self-renewal of human embryonic stem cells. in *Stem Cells*, Vol. 22 770-8 (United States, 2004).
 29. Humphrey, R.K. et al. Maintenance of pluripotency in human embryonic stem cells is STAT3 independent. in *Stem Cells*, Vol. 22 522-30 (United States, 2004).
 30. Brandenberger, R. et al. Transcriptome characterization elucidates signaling networks that control human ES cell growth and differentiation. in *Nat Biotechnol*, Vol. 22 707-16 (United States, 2004).
 31. Xu, R.H. et al. BMP4 initiates human embryonic stem cell differentiation to trophoblast. in *Nat Biotechnol*, Vol. 20 1261-4 (United States, 2002).
 32. Rho, J.Y. et al. Transcriptional profiling of the developmentally important signalling pathways in human embryonic stem cells. in *Hum Reprod*, Vol. 21 405-12 (England, 2006).
 33. Wang, G. et al. Noggin and bFGF cooperate to maintain the pluripotency of human embryonic stem cells in the absence of feeder layers. in *Biochem Biophys Res Commun*, Vol. 330 934-42 (United States, 2005).

34. Xu, C. et al. Basic fibroblast growth factor supports undifferentiated human embryonic stem cell growth without conditioned medium. in *Stem Cells*, Vol. 23 315-23 (United States, 2005).
35. Vallier, L., Alexander, M. & Pedersen, R.A. Activin/Nodal and FGF pathways cooperate to maintain pluripotency of human embryonic stem cells. in *J Cell Sci*, Vol. 118 4495-509 (England, 2005).
36. Wang, L. et al. Self-renewal of human embryonic stem cells requires insulin-like growth factor-1 receptor and ERBB2 receptor signaling. in *Blood*, Vol. 110 4111-9 (United States, 2007).
37. Li, J. et al. MEK/ERK signaling contributes to the maintenance of human embryonic stem cell self-renewal. in *Differentiation*, Vol. 75 299-307 (England, 2007).
38. Kang, H.B. et al. Basic fibroblast growth factor activates ERK and induces c-fos in human embryonic stem cell line MizhES1. *Stem Cells Dev* **14**, 395-401 (2005).
39. Xiao, L., Yuan, X. & Sharkis, S.J. Activin A maintains self-renewal and regulates fibroblast growth factor, Wnt, and bone morphogenic protein pathways in human embryonic stem cells. in *Stem Cells*, Vol. 24 1476-86 (United States, 2006).
40. Greber, B., Lehrach, H. & Adjaye, J. Fibroblast growth factor 2 modulates transforming growth factor beta signaling in mouse embryonic fibroblasts and human ESCs (hESCs) to support hESC self-renewal. in *Stem Cells*, Vol. 25 455-64 (United States, 2007).
41. Ludwig, T.E. et al. Derivation of human embryonic stem cells in defined conditions. in *Nat Biotechnol*, Vol. 24 185-7 (United States, 2006).
42. Pera, M.F. & Tam, P.P. Extrinsic regulation of pluripotent stem cells. *Nature* **465**, 713-20 (2010).
43. Boiani, M. & Scholer, H.R. Regulatory networks in embryo-derived pluripotent stem cells. in *Nat Rev Mol Cell Biol*, Vol. 6 872-84 (England, 2005).
44. Buecker, C. & Geijsen, N. Different flavors of pluripotency, molecular mechanisms, and practical implications. *Cell Stem Cell* **7**, 559-64 (2010).
45. Brons, I.G. et al. Derivation of pluripotent epiblast stem cells from mammalian embryos. in *Nature*, Vol. 448 191-5 (England, 2007).
46. Tesar, P.J. et al. New cell lines from mouse epiblast share defining features with human embryonic stem cells. in *Nature*, Vol. 448 196-9 (England, 2007).
47. Rossant, J. Stem cells and early lineage development. in *Cell*, Vol. 132 527-31 (United States, 2008).
48. Nichols, J. & Smith, A. Naive and primed pluripotent states. in *Cell Stem Cell*, Vol. 4 487-92 (United States, 2009).
49. Guo, G. et al. Klf4 reverts developmentally programmed restriction of ground state pluripotency. in *Development*, Vol. 136 1063-9 (England, 2009).
50. Hanna, J. et al. Human embryonic stem cells with biological and epigenetic characteristics similar to those of mouse ESCs. in *Proc Natl Acad Sci U S A*, Vol. 107 9222-7 (United States, 2010).
51. Sj., K. Studies of the developmental potential of four and eight-cell stage mouse blastomeres. *J Exp Zool* **200**, 365-376 (1977).
52. Yu, J. & Thomson, J.A. Pluripotent stem cell lines. *Genes Dev* **22**, 1987-97 (2008).
53. Prokhorova, T.A. et al. Teratoma formation by human embryonic stem cells is site

- dependent and enhanced by the presence of Matrigel. *Stem Cells Dev* **18**, 47-54 (2009).
54. Kang, L., Wang, J., Zhang, Y., Kou, Z. & Gao, S. iPS cells can support full-term development of tetraploid blastocyst-complemented embryos. in *Cell Stem Cell*, Vol. 5 135-8 (United States, 2009).
 55. Jaenisch, R. & Young, R. Stem cells, the molecular circuitry of pluripotency and nuclear reprogramming. in *Cell*, Vol. 132 567-82 (United States, 2008).
 56. Wilmut, I., Schnieke, A.E., McWhir, J., Kind, A.J. & Campbell, K.H. Viable offspring derived from fetal and adult mammalian cells. *Nature* **385**, 810-3 (1997).
 57. Gurdon, J.B., Byrne, J.A. & Simonsson, S. Nuclear reprogramming and stem cell creation. in *Proc Natl Acad Sci U S A*, Vol. 100 Suppl 1 11819-22 (United States, 2003).
 58. Zhou, Q., Brown, J., Kanarek, A., Rajagopal, J. & Melton, D.A. In vivo reprogramming of adult pancreatic exocrine cells to beta-cells. in *Nature*, Vol. 455 627-32 (England, 2008).
 59. Tokuzawa, Y. et al. Fbx15 is a novel target of Oct3/4 but is dispensable for embryonic stem cell self-renewal and mouse development. *Mol Cell Biol* **23**, 2699-708 (2003).
 60. Takahashi, K. & Yamanaka, S. Induction of pluripotent stem cells from mouse embryonic and adult fibroblast cultures by defined factors. *Cell* **126**, 663-76 (2006).
 61. Takahashi, K. et al. Induction of pluripotent stem cells from adult human fibroblasts by defined factors. *Cell* **131**, 861-72 (2007).
 62. Yu, J. et al. Induced pluripotent stem cell lines derived from human somatic cells. *Science* **318**, 1917-20 (2007).
 63. Giorgetti, A. et al. Generation of induced pluripotent stem cells from human cord blood using OCT4 and SOX2. in *Cell Stem Cell*, Vol. 5 353-7 (United States, 2009).
 64. Aoki, T. et al. Generation of induced pluripotent stem cells from human adipose-derived stem cells without c-MYC. *Tissue Eng Part A* **16**, 2197-206 (2010).
 65. Stadtfeld, M. & Hochedlinger, K. Induced pluripotency: history, mechanisms, and applications. *Genes Dev* **24**, 2239-63 (2010).
 66. Bird, A. Perceptions of epigenetics. in *Nature*, Vol. 447 396-8 (England, 2007).
 67. Li, X. & Zhao, X. Epigenetic regulation of mammalian stem cells. *Stem Cells Dev* **17**, 1043-52 (2008).
 68. Ivanova, N. et al. Dissecting self-renewal in stem cells with RNA interference. in *Nature*, Vol. 442 533-8 (England, 2006).
 69. Freberg, C.T., Dahl, J.A., Timoskainen, S. & Collas, P. Epigenetic reprogramming of OCT4 and NANOG regulatory regions by embryonal carcinoma cell extract. in *Mol Biol Cell*, Vol. 18 1543-53 (United States, 2007).
 70. Chambers, I. et al. Functional expression cloning of Nanog, a pluripotency sustaining factor in embryonic stem cells. in *Cell*, Vol. 113 643-55 (United States, 2003).
 71. Nichols, J. et al. Formation of pluripotent stem cells in the mammalian embryo depends on the POU transcription factor Oct4. *Cell* **95**, 379-91 (1998).
 72. Boyer, L.A. et al. Core transcriptional regulatory circuitry in human embryonic stem cells. in *Cell*, Vol. 122 947-56 (United States, 2005).
 73. Catena, R. et al. Conserved POU binding DNA sites in the Sox2 upstream enhancer regulate gene expression in embryonic and neural stem cells. in *J Biol Chem*, Vol. 279 41846-57 (United States, 2004).
 74. Kuroda, T. et al. Octamer and Sox elements are required for transcriptional cis

- regulation of Nanog gene expression. in *Mol Cell Biol*, Vol. 25 2475-85 (United States, 2005).
75. Okumura-Nakanishi, S., Saito, M., Niwa, H. & Ishikawa, F. Oct-3/4 and Sox2 regulate Oct-3/4 gene in embryonic stem cells. in *J Biol Chem*, Vol. 280 5307-17 (United States, 2005).
 76. Pesce, M., Gross, M.K. & Scholer, H.R. In line with our ancestors: Oct-4 and the mammalian germ. in *Bioessays*, Vol. 20 722-32 (England, 1998).
 77. Scholer, H.R., Hatzopoulos, A.K., Balling, R., Suzuki, N. & Gruss, P. A family of octamer-specific proteins present during mouse embryogenesis: evidence for germline-specific expression of an Oct factor. *EMBO J* **8**, 2543-50 (1989).
 78. Niwa, H. et al. Interaction between Oct3/4 and Cdx2 determines trophectoderm differentiation. in *Cell*, Vol. 123 917-29 (United States, 2005).
 79. Niwa, H., Miyazaki, J. & Smith, A.G. Quantitative expression of Oct-3/4 defines differentiation, dedifferentiation or self-renewal of ES cells. *Nat Genet* **24**, 372-6 (2000).
 80. Fong, H., Hohenstein, K.A. & Donovan, P.J. Regulation of self-renewal and pluripotency by Sox2 in human embryonic stem cells. in *Stem Cells*, Vol. 26 1931-8 (United States, 2008).
 81. Kopp, J.L., Ormsbee, B.D., Desler, M. & Rizzino, A. Small increases in the level of Sox2 trigger the differentiation of mouse embryonic stem cells. in *Stem Cells*, Vol. 26 903-11 (United States, 2008).
 82. Mitsui, K. et al. The homeoprotein Nanog is required for maintenance of pluripotency in mouse epiblast and ES cells. in *Cell*, Vol. 113 631-42 (United States, 2003).
 83. Darr, H., Mayshar, Y. & Benvenisty, N. Overexpression of NANOG in human ES cells enables feeder-free growth while inducing primitive ectoderm features. in *Development*, Vol. 133 1193-201 (England, 2006).
 84. Chambers, I. et al. Nanog safeguards pluripotency and mediates germline development. in *Nature*, Vol. 450 1230-4 (England, 2007).
 85. Chen, X. et al. Integration of external signaling pathways with the core transcriptional network in embryonic stem cells. in *Cell*, Vol. 133 1106-17 (United States, 2008).
 86. Cole, M.F., Johnstone, S.E., Newman, J.J., Kagey, M.H. & Young, R.A. Tcf3 is an integral component of the core regulatory circuitry of embryonic stem cells. in *Genes Dev*, Vol. 22 746-55 (United States, 2008).
 87. Zhang, J. et al. Sall4 modulates embryonic stem cell pluripotency and early embryonic development by the transcriptional regulation of Pou5f1. in *Nat Cell Biol*, Vol. 8 1114-23 (England, 2006).
 88. van den Berg, D.L. et al. An Oct4-centered protein interaction network in embryonic stem cells. in *Cell Stem Cell*, Vol. 6 369-81 (2010 Elsevier Inc, United States, 2010).
 89. Rossi, D.J., Jamieson, C.H. & Weissman, I.L. Stem cells and the pathways to aging and cancer. *Cell* **132**, 681-96 (2008).
 90. Sharpless, N.E. & DePinho, R.A. How stem cells age and why this makes us grow old. *Nat Rev Mol Cell Biol* **8**, 703-13 (2007).
 91. Rando, T.A. Stem cells, ageing and the quest for immortality. *Nature* **441**, 1080-6 (2006).
 92. Saretzki, G., Armstrong, L., Leake, A., Lako, M. & von Zglinicki, T. Stress defense in murine embryonic stem cells is superior to that of various differentiated murine cells.

- Stem Cells* **22**, 962-71 (2004).
93. Tichy, E.D. & Stambrook, P.J. DNA repair in murine embryonic stem cells and differentiated cells. *Exp Cell Res* **314**, 1929-36 (2008).
 94. Kirkwood, T.B. Understanding the odd science of aging. *Cell* **120**, 437-47 (2005).
 95. Finkel, T., Serrano, M. & Blasco, M.A. The common biology of cancer and ageing. in *Nature*, Vol. 448 767-74 (England, 2007).
 96. Shackleton, M., Quintana, E., Fearon, E.R. & Morrison, S.J. Heterogeneity in cancer: cancer stem cells versus clonal evolution. in *Cell*, Vol. 138 822-9 (United States, 2009).
 97. O'Brien, C.A., Kreso, A. & Jamieson, C.H. Cancer stem cells and self-renewal. in *Clin Cancer Res*, Vol. 16 3113-20 (2010 Aacr., United States, 2010).
 98. Bomken, S., Fiser, K., Heidenreich, O. & Vormoor, J. Understanding the cancer stem cell. in *Br J Cancer*, Vol. 103 439-45 (England, 2010).
 99. Kleinsmith, L.J. & Pierce, G.B., Jr. MULTIPOTENTIALITY OF SINGLE EMBRYONAL CARCINOMA CELLS. *Cancer Res* **24**, 1544-51 (1964).
 100. Bonnet, D. & Dick, J.E. Human acute myeloid leukemia is organized as a hierarchy that originates from a primitive hematopoietic cell. *Nat Med* **3**, 730-7 (1997).
 101. Al-Hajj, M., Wicha, M.S., Benito-Hernandez, A., Morrison, S.J. & Clarke, M.F. Prospective identification of tumorigenic breast cancer cells. in *Proc Natl Acad Sci U S A*, Vol. 100 3983-8 (United States, 2003).
 102. Cho, R.W. et al. Isolation and molecular characterization of cancer stem cells in MMTV-Wnt-1 murine breast tumors. in *Stem Cells*, Vol. 26 364-71 (United States, 2008).
 103. Singh, S.K. et al. Identification of human brain tumour initiating cells. in *Nature*, Vol. 432 396-401 (England, 2004).
 104. Ricci-Vitiani, L. et al. Identification and expansion of human colon-cancer-initiating cells. in *Nature*, Vol. 445 111-5 (England, 2007).
 105. Dalerba, P. et al. Phenotypic characterization of human colorectal cancer stem cells. in *Proc Natl Acad Sci U S A*, Vol. 104 10158-63 (United States, 2007).
 106. Huang, E.H. et al. Aldehyde dehydrogenase 1 is a marker for normal and malignant human colonic stem cells (SC) and tracks SC overpopulation during colon tumorigenesis. in *Cancer Res*, Vol. 69 3382-9 (United States, 2009).
 107. Schatton, T. et al. Identification of cells initiating human melanomas. in *Nature*, Vol. 451 345-9 (England, 2008).
 108. Li, C. et al. Identification of pancreatic cancer stem cells. in *Cancer Res*, Vol. 67 1030-7 (United States, 2007).
 109. Hermann, P.C. et al. Distinct populations of cancer stem cells determine tumor growth and metastatic activity in human pancreatic cancer. in *Cell Stem Cell*, Vol. 1 313-23 (United States, 2007).
 110. Collins, A.T., Berry, P.A., Hyde, C., Stower, M.J. & Maitland, N.J. Prospective identification of tumorigenic prostate cancer stem cells. in *Cancer Res*, Vol. 65 10946-51 (United States, 2005).
 111. Curley, M.D. et al. CD133 expression defines a tumor initiating cell population in primary human ovarian cancer. *Stem Cells* **27**, 2875-83 (2009).
 112. Yang, Z.F. et al. Significance of CD90+ cancer stem cells in human liver cancer. in *Cancer Cell*, Vol. 13 153-66 (United States, 2008).

113. Eramo, A. et al. Identification and expansion of the tumorigenic lung cancer stem cell population. in *Cell Death Differ*, Vol. 15 504-14 (England, 2008).
114. Hochedlinger, K., Yamada, Y., Beard, C. & Jaenisch, R. Ectopic expression of Oct-4 blocks progenitor-cell differentiation and causes dysplasia in epithelial tissues. in *Cell*, Vol. 121 465-77 (United States, 2005).
115. Zhang, F. et al. Cancer is a disease of unregulated expansion of somatic stem cells resulting from disrupted asymmetric division. in *Med Hypotheses*, Vol. 70 208-9 (Scotland, 2008).
116. Sperger, J.M. et al. Gene expression patterns in human embryonic stem cells and human pluripotent germ cell tumors. in *Proc Natl Acad Sci U S A*, Vol. 100 13350-5 (United States, 2003).
117. Calvanese, V. et al. Cancer genes hypermethylated in human embryonic stem cells. *PLoS One* **3**, e3294 (2008).
118. Eilers, M. & Eisenman, R.N. Myc's broad reach. in *Genes Dev*, Vol. 22 2755-66 (United States, 2008).
119. Evans, P.M. & Liu, C. Roles of Krupel-like factor 4 in normal homeostasis, cancer and stem cells. *Acta Biochim Biophys Sin (Shanghai)* **40**, 554-64 (2008).
120. Gutierrez-Aranda, I. et al. Human induced pluripotent stem cells develop teratoma more efficiently and faster than human embryonic stem cells regardless the site of injection. *Stem Cells* **28**, 1568-70 (2010).
121. Ben-David, U. & Benvenisty, N. The tumorigenicity of human embryonic and induced pluripotent stem cells. in *Nat Rev Cancer*, Vol. 11 268-77 (England, 2011).
122. Voog, J. & Jones, D.L. Stem cells and the niche: a dynamic duo. *Cell Stem Cell* **6**, 103-15 (2010).
123. Borovski, T., De Sousa, E.M.F., Vermeulen, L. & Medema, J.P. Cancer stem cell niche: the place to be. in *Cancer Res*, Vol. 71 634-9 (United States, 2011).
124. Espada, J., Calvo, M.B., Diaz-Prado, S. & Medina, V. Wnt signalling and cancer stem cells. in *Clin Transl Oncol*, Vol. 11 411-27 (Spain, 2009).
125. He, X.C., Zhang, J. & Li, L. Cellular and molecular regulation of hematopoietic and intestinal stem cell behavior. in *Ann N Y Acad Sci*, Vol. 1049 28-38 (United States, 2005).
126. He, X.C. et al. BMP signaling inhibits intestinal stem cell self-renewal through suppression of Wnt-beta-catenin signaling. in *Nat Genet*, Vol. 36 1117-21 (United States, 2004).
127. Ming Kwan, K., Li, A.G., Wang, X.J., Wurst, W. & Behringer, R.R. Essential roles of BMPRII signaling in differentiation and growth of hair follicles and in skin tumorigenesis. *Genesis* **39**, 10-25 (2004).
128. Pierrou, S., Hellqvist, M., Samuelsson, L., Enerback, S. & Carlsson, P. Cloning and characterization of seven human forkhead proteins: binding site specificity and DNA bending. *EMBO J* **13**, 5002-12 (1994).
129. Yao, K.M., Sha, M., Lu, Z. & Wong, G.G. Molecular analysis of a novel winged helix protein, WIN. Expression pattern, DNA binding property, and alternative splicing within the DNA binding domain. *J Biol Chem* **272**, 19827-36 (1997).
130. Laoukili, J. et al. FoxM1 is required for execution of the mitotic programme and chromosome stability. in *Nat Cell Biol*, Vol. 7 126-36 (England, 2005).

131. Ahn, J.I. et al. Temporal expression changes during differentiation of neural stem cells derived from mouse embryonic stem cell. *J Cell Biochem* **93**, 563-78 (2004).
132. Korver, W. et al. Uncoupling of S phase and mitosis in cardiomyocytes and hepatocytes lacking the winged-helix transcription factor Trident. in *Curr Biol*, Vol. 8 1327-30 (England, 1998).
133. Chen, Y.J. et al. A conserved phosphorylation site within the forkhead domain of FoxM1B is required for its activation by cyclin-CDK1. in *J Biol Chem*, Vol. 284 30695-707 (United States, 2009).
134. Kalinichenko, V.V., Lim, L., Shin, B. & Costa, R.H. Differential expression of forkhead box transcription factors following butylated hydroxytoluene lung injury. *Am J Physiol Lung Cell Mol Physiol* **280**, L695-704 (2001).
135. Pilarsky, C., Wenzig, M., Specht, T., Saeger, H.D. & Grutzmann, R. Identification and validation of commonly overexpressed genes in solid tumors by comparison of microarray data. *Neoplasia* **6**, 744-50 (2004).
136. Park, H.J. et al. FoxM1, a critical regulator of oxidative stress during oncogenesis. in *EMBO J*, Vol. 28 2908-18 (England, 2009).
137. Korver, W., Roose, J. & Clevers, H. The winged-helix transcription factor Trident is expressed in cycling cells. in *Nucleic Acids Res*, Vol. 25 1715-9 (England, 1997).
138. Barsotti, A.M. & Prives, C. Pro-proliferative FoxM1 is a target of p53-mediated repression. in *Oncogene*, Vol. 28 4295-305 (England, 2009).
139. Dykstra, B. & de Haan, G. Hematopoietic stem cell aging and self-renewal. *Cell Tissue Res* **331**, 91-101 (2008).
140. Rossi, D.J. et al. Cell intrinsic alterations underlie hematopoietic stem cell aging. *Proc Natl Acad Sci U S A* **102**, 9194-9 (2005).
141. Kim, M., Moon, H.B. & Spangrude, G.J. Major age-related changes of mouse hematopoietic stem/progenitor cells. *Ann N Y Acad Sci* **996**, 195-208 (2003).
142. Iwama, A. et al. Enhanced self-renewal of hematopoietic stem cells mediated by the polycomb gene product Bmi-1. *Immunity* **21**, 843-51 (2004).
143. Molofsky, A.V. et al. Bmi-1 dependence distinguishes neural stem cell self-renewal from progenitor proliferation. *Nature* **425**, 962-7 (2003).
144. Lessard, J. & Sauvageau, G. Bmi-1 determines the proliferative capacity of normal and leukaemic stem cells. *Nature* **423**, 255-60 (2003).
145. Oguro, H. et al. Differential impact of Ink4a and Arf on hematopoietic stem cells and their bone marrow microenvironment in Bmi1-deficient mice. *J Exp Med* **203**, 2247-53 (2006).
146. Li, S.K. et al. FoxM1c counteracts oxidative stress-induced senescence and stimulates Bmi-1 expression. *J Biol Chem* **283**, 16545-53 (2008).
147. van der Horst, A. & Burgering, B.M. Stressing the role of FoxO proteins in lifespan and disease. *Nat Rev Mol Cell Biol* **8**, 440-50 (2007).
148. Jacobs, F.M. et al. FoxO6, a novel member of the FoxO class of transcription factors with distinct shuttling dynamics. in *J Biol Chem*, Vol. 278 35959-67 (United States, 2003).
149. Furuyama, T., Nakazawa, T., Nakano, I. & Mori, N. Identification of the differential distribution patterns of mRNAs and consensus binding sequences for mouse DAF-16 homologues. *Biochem J* **349**, 629-34 (2000).

150. Tothova, Z. et al. FoxOs are critical mediators of hematopoietic stem cell resistance to physiologic oxidative stress. *Cell* **128**, 325-39 (2007).
151. Castrillon, D.H., Miao, L., Kollipara, R., Horner, J.W. & DePinho, R.A. Suppression of ovarian follicle activation in mice by the transcription factor Foxo3a. in *Science*, Vol. 301 215-8 (United States, 2003).
152. Brunet, A. et al. Akt promotes cell survival by phosphorylating and inhibiting a Forkhead transcription factor. *Cell* **96**, 857-68 (1999).
153. Essers, M.A. et al. FOXO transcription factor activation by oxidative stress mediated by the small GTPase Ral and JNK. *Embo J* **23**, 4802-12 (2004).
154. Brunet, A. et al. Stress-dependent regulation of FOXO transcription factors by the SIRT1 deacetylase. *Science* **303**, 2011-5 (2004).
155. van der Horst, A. et al. FOXO4 transcriptional activity is regulated by monoubiquitination and USP7/HAUSP. *Nat Cell Biol* **8**, 1064-73 (2006).
156. Vogt, P.K., Jiang, H. & Aoki, M. Triple layer control: phosphorylation, acetylation and ubiquitination of FOXO proteins. *Cell Cycle* **4**, 908-13 (2005).
157. Tothova, Z. & Gilliland, D.G. FoxO transcription factors and stem cell homeostasis: insights from the hematopoietic system. *Cell Stem Cell* **1**, 140-52 (2007).
158. Miyamoto, K. et al. Foxo3a is essential for maintenance of the hematopoietic stem cell pool. *Cell Stem Cell* **1**, 101-12 (2007).
159. Kikushige, Y. et al. Self-renewing hematopoietic stem cell is the primary target in pathogenesis of human chronic lymphocytic leukemia. in *Cancer Cell*, Vol. 20 246-59 (2011 Elsevier Inc, United States, 2011).
160. Sauve, A.A., Wolberger, C., Schramm, V.L. & Boeke, J.D. The biochemistry of sirtuins. *Annu Rev Biochem* **75**, 435-65 (2006).
161. Cohen, H.Y. et al. Calorie restriction promotes mammalian cell survival by inducing the SIRT1 deacetylase. *Science* **305**, 390-2 (2004).
162. McBurney, M.W. et al. The absence of SIR2alpha protein has no effect on global gene silencing in mouse embryonic stem cells. *Mol Cancer Res* **1**, 402-9 (2003).
163. Imai, S., Armstrong, C.M., Kaerberlein, M. & Guarente, L. Transcriptional silencing and longevity protein Sir2 is an NAD-dependent histone deacetylase. *Nature* **403**, 795-800 (2000).
164. Vaquero, A. et al. Human SirT1 interacts with histone H1 and promotes formation of facultative heterochromatin. in *Mol Cell*, Vol. 16 93-105 (United States, 2004).
165. Spivakov, M. & Fisher, A.G. Epigenetic signatures of stem-cell identity. *Nat Rev Genet* **8**, 263-71 (2007).
166. Han, M.K. et al. SIRT1 regulates apoptosis and Nanog expression in mouse embryonic stem cells by controlling p53 subcellular localization. *Cell Stem Cell* **2**, 241-51 (2008).
167. Calvanese, V. et al. Sirtuin 1 regulation of developmental genes during differentiation of stem cells. in *Proc Natl Acad Sci U S A*, Vol. 107 13736-41 (United States, 2010).
168. Calvanese, V. & Fraga, M.F. SirT1 brings stemness closer to cancer and aging. *Aging (Albany NY)* **3**, 162-7 (2011).
169. Vicente-Manzanares, M., Ma, X., Adelstein, R.S. & Horwitz, A.R. Non-muscle myosin II takes centre stage in cell adhesion and migration. *Nat Rev Mol Cell Biol* **10**, 778-90 (2009).

170. Walker, A. et al. Non-muscle myosin II regulates survival threshold of pluripotent stem cells. *Nat Commun* **1**, doi:10.1038/ncomms1074 (2010).
171. Bresnick, A.R. Molecular mechanisms of nonmuscle myosin-II regulation. *Curr Opin Cell Biol* **11**, 26-33 (1999).
172. Ohgushi, M. et al. Molecular pathway and cell state responsible for dissociation-induced apoptosis in human pluripotent stem cells. in *Cell Stem Cell*, Vol. 7 225-39 (2010 Elsevier Inc, United States, 2010).
173. Even-Ram, S. et al. Myosin IIA regulates cell motility and actomyosin-microtubule crosstalk. *Nat Cell Biol* **9**, 299-309 (2007).
174. Ivanov, A.I., Hunt, D., Utech, M., Nusrat, A. & Parkos, C.A. Differential roles for actin polymerization and a myosin II motor in assembly of the epithelial apical junctional complex. in *Mol Biol Cell*, Vol. 16 2636-50 (United States, 2005).
175. Sharpless, N.E. & DePinho, R.A. How stem cells age and why this makes us grow old. in *Nat Rev Mol Cell Biol*, Vol. 8 703-13 (England, 2007).
176. Scott, C.T., McCormick, J.B. & Owen-Smith, J. And then there were two: use of hESC lines. in *Nat Biotechnol*, Vol. 27 696-7 (United States, 2009).
177. Adewumi, O. et al. Characterization of human embryonic stem cell lines by the International Stem Cell Initiative. in *Nat Biotechnol*, Vol. 25 803-16 (United States, 2007).
178. Jones, D.L. & Rando, T.A. Emerging models and paradigms for stem cell ageing. *Nat Cell Biol* **13**, 506-12 (2011).
179. Wood, J.G. et al. Sirtuin activators mimic caloric restriction and delay ageing in metazoans. in *Nature*, Vol. 430 686-9 (England, 2004).
180. Ito, K. et al. Regulation of oxidative stress by ATM is required for self-renewal of haematopoietic stem cells. in *Nature*, Vol. 431 997-1002 (England, 2004).
181. Ohgushi, M. & Sasai, Y. Lonely death dance of human pluripotent stem cells: ROCKing between metastable cell states. in *Trends Cell Biol*, Vol. 21 274-82 (2011 Elsevier Ltd, England, 2011).
182. Watanabe, K. et al. A ROCK inhibitor permits survival of dissociated human embryonic stem cells. in *Nat Biotechnol*, Vol. 25 681-6 (United States, 2007).
183. Ma, Y., Lin, H. & Qiu, C. High-efficiency transfection and siRNA-mediated gene knockdown in human pluripotent stem cells. *Curr Protoc Stem Cell Biol* **Chapter 2**, Unit 5C 2 (2012).
184. Chen, G., Hou, Z., Gulbranson, D.R. & Thomson, J.A. Actin-myosin contractility is responsible for the reduced viability of dissociated human embryonic stem cells. *Cell Stem Cell* **7**, 240-8 (2010).
185. Li, D. et al. Integrated biochemical and mechanical signals regulate multifaceted human embryonic stem cell functions. *J Cell Biol* **191**, 631-44 (2010).
186. Flynn, P.G. & Helfman, D.M. Non-muscle myosin IIB helps mediate TNF cell death signaling independent of actomyosin contractility (AMC). *J Cell Biochem* **110**, 1365-75 (2010).
187. D'Amour, K.A. et al. Efficient differentiation of human embryonic stem cells to definitive endoderm. in *Nat Biotechnol*, Vol. 23 1534-41 (United States, 2005).
188. Oda, H. & Takeichi, M. Evolution: structural and functional diversity of cadherin at the

- adherens junction. in *J Cell Biol*, Vol. 193 1137-46 (United States, 2011).
189. Heasman, J. et al. Overexpression of cadherins and underexpression of beta-catenin inhibit dorsal mesoderm induction in early *Xenopus* embryos. in *Cell*, Vol. 79 791-803 (United States, 1994).
 190. Li, L., Bennett, S.A. & Wang, L. Role of E-cadherin and other cell adhesion molecules in survival and differentiation of human pluripotent stem cells. in *Cell Adh Migr*, Vol. 6 59-70 (United States, 2012).
 191. Maretzky, T. et al. ADAM10 mediates E-cadherin shedding and regulates epithelial cell-cell adhesion, migration, and beta-catenin translocation. in *Proc Natl Acad Sci U S A*, Vol. 102 9182-7 (United States, 2005).
 192. Zhang, N. et al. FoxM1 promotes beta-catenin nuclear localization and controls Wnt target-gene expression and glioma tumorigenesis. in *Cancer Cell*, Vol. 20 427-42 (2011 Elsevier Inc, United States, 2011).
 193. Kim, I.M. et al. The forkhead box m1 transcription factor is essential for embryonic development of pulmonary vasculature. in *J Biol Chem*, Vol. 280 22278-86 (United States, 2005).
 194. Ramakrishna, S. et al. Myocardium defects and ventricular hypoplasia in mice homozygous null for the Forkhead Box M1 transcription factor. *Dev Dyn* **236**, 1000-13 (2007).
 195. Wierstra, I. The transcription factor FOXM1c binds to and transactivates the promoter of the tumor suppressor gene E-cadherin. *Cell Cycle* **10**, 760-6 (2011).
 196. Xie, Z. et al. Foxm1 transcription factor is required for maintenance of pluripotency of P19 embryonal carcinoma cells. in *Nucleic Acids Res*, Vol. 38 8027-38 (England, 2010).
 197. Schonegg, S. & Hyman, A.A. CDC-42 and RHO-1 coordinate acto-myosin contractility and PAR protein localization during polarity establishment in *C. elegans* embryos. in *Development*, Vol. 133 3507-16 (England, 2006).
 198. Werner, M., Munro, E. & Glotzer, M. Astral signals spatially bias cortical myosin recruitment to break symmetry and promote cytokinesis. in *Curr Biol*, Vol. 17 1286-97 (England, 2007).
 199. Grill, S.W., Howard, J., Schaffer, E., Stelzer, E.H. & Hyman, A.A. The distribution of active force generators controls mitotic spindle position. in *Science*, Vol. 301 518-21 (United States, 2003).
 200. Dean, S.O., Rogers, S.L., Stuurman, N., Vale, R.D. & Spudich, J.A. Distinct pathways control recruitment and maintenance of myosin II at the cleavage furrow during cytokinesis. in *Proc Natl Acad Sci U S A*, Vol. 102 13473-8 (United States, 2005).
 201. Murata-Hori, M. et al. Myosin II regulatory light chain as a novel substrate for AIM-1, an aurora/Ipl1p-related kinase from rat. *J Biochem* **128**, 903-7 (2000).
 202. Smith, T.C., Fang, Z. & Luna, E.J. Novel interactors and a role for supervillin in early cytokinesis. *Cytoskeleton (Hoboken)* **67**, 346-64 (2010).
 203. Guarguaglini, G. et al. The forkhead-associated domain protein Cep170 interacts with Polo-like kinase 1 and serves as a marker for mature centrioles. in *Mol Biol Cell*, Vol. 16 1095-107 (United States, 2005).
 204. Maliga, Z. et al. A genomic toolkit to investigate kinesin and myosin motor function in cells. in *Nat Cell Biol*, Vol. 15 325-34 (England, 2013).

205. Kalin, T.V., Ustiyanyan, V. & Kalinichenko, V.V. Multiple faces of FoxM1 transcription factor: Lessons from transgenic mouse models. *Cell Cycle* **10**, 396-405 (2010).
206. Leung, T.W. et al. Over-expression of FoxM1 stimulates cyclin B1 expression. in *FEBS Lett*, Vol. 507 59-66 (Netherlands, 2001).
207. Wang, I.C. et al. Forkhead box M1 regulates the transcriptional network of genes essential for mitotic progression and genes encoding the SCF (Skp2-Cks1) ubiquitin ligase. in *Mol Cell Biol*, Vol. 25 10875-94 (United States, 2005).
208. Gemenetzidis, E. et al. FOXM1 upregulation is an early event in human squamous cell carcinoma and it is enhanced by nicotine during malignant transformation. *PLoS One* **4**, e4849 (2009).
209. Wang, F. et al. Kinetic mechanism of non-muscle myosin IIB: functional adaptations for tension generation and maintenance. in *J Biol Chem*, Vol. 278 27439-48 (United States, 2003).
210. Murphy, C.T., Rock, R.S. & Spudis, J.A. A myosin II mutation uncouples ATPase activity from motility and shortens step size. *Nat Cell Biol* **3**, 311-5 (2001).
211. Allingham, J.S., Smith, R. & Rayment, I. The structural basis of blebbistatin inhibition and specificity for myosin II. in *Nat Struct Mol Biol*, Vol. 12 378-9 (United States, 2005).
212. Straight, A.F. et al. Dissecting temporal and spatial control of cytokinesis with a myosin II Inhibitor. *Science* **299**, 1743-7 (2003).
213. Kovacs, M., Toth, J., Hetenyi, C., Malnasi-Csizmadia, A. & Sellers, J.R. Mechanism of blebbistatin inhibition of myosin II. in *J Biol Chem*, Vol. 279 35557-63 (United States, 2004).
214. Kwok, J.M. et al. Thioestrepton selectively targets breast cancer cells through inhibition of forkhead box M1 expression. *Mol Cancer Ther* **7**, 2022-32 (2008).
215. Hegde, N.S., Sanders, D.A., Rodriguez, R. & Balasubramanian, S. The transcription factor FOXM1 is a cellular target of the natural product thioestrepton. in *Nat Chem*, Vol. 3 725-31 (England, 2011).
216. Bhat, U.G., Halasi, M. & Gartel, A.L. FoxM1 is a general target for proteasome inhibitors. *PLoS One* **4**, e6593 (2009).
217. Gartel, A.L. Thioestrepton, proteasome inhibitors and FOXM1. in *Cell Cycle*, Vol. 10 4341-2 (United States, 2011).
218. Gonczy, P. Mechanisms of asymmetric cell division: flies and worms pave the way. in *Nat Rev Mol Cell Biol*, Vol. 9 355-66 (England, 2008).
219. Madureira, P.A. et al. The Forkhead box M1 protein regulates the transcription of the estrogen receptor alpha in breast cancer cells. in *J Biol Chem*, Vol. 281 25167-76 (United States, 2006).
220. Yusuf, D. et al. The transcription factor encyclopedia. in *Genome Biol*, Vol. 13 R24 (England, 2012).
221. Nelson, J.D., Denisenko, O. & Bomsztyk, K. Protocol for the fast chromatin immunoprecipitation (ChIP) method. in *Nat Protoc*, Vol. 1 179-85 (England, 2006).
222. Xu, Y. et al. Revealing a core signaling regulatory mechanism for pluripotent stem cell survival and self-renewal by small molecules. in *Proc Natl Acad Sci U S A*, Vol. 107 8129-34 (United States, 2010).
223. Cabernard, C., Prehoda, K.E. & Doe, C.Q. A spindle-independent cleavage furrow

- positioning pathway. in *Nature*, Vol. 467 91-4 (England, 2010).
224. Motta, M.C. et al. Mammalian SIRT1 represses forkhead transcription factors. in *Cell*, Vol. 116 551-63 (United States, 2004).
 225. Bhat, U.G., Halasi, M. & Gartel, A.L. Thiazole antibiotics target FoxM1 and induce apoptosis in human cancer cells. *PLoS One* **4**, e5592 (2009).
 226. Bhat, U.G., Zipfel, P.A., Tyler, D.S. & Gartel, A.L. Novel anticancer compounds induce apoptosis in melanoma cells. in *Cell Cycle*, Vol. 7 1851-5 (United States, 2008).
 227. Halasi, M. & Gartel, A.L. Suppression of FOXM1 sensitizes human cancer cells to cell death induced by DNA-damage. in *PLoS One*, Vol. 7 e31761 (United States, 2010).
 228. Pakzad, M. et al. Presence of a ROCK inhibitor in extracellular matrix supports more undifferentiated growth of feeder-free human embryonic and induced pluripotent stem cells upon passaging. *Stem Cell Rev* **6**, 96-107 (2010).
 229. Karwacki-Neisius, V. et al. Reduced Oct4 expression directs a robust pluripotent state with distinct signaling activity and increased enhancer occupancy by Oct4 and Nanog. *Cell Stem Cell* **12**, 531-45 (2013).
 230. von Dassow, G. Concurrent cues for cytokinetic furrow induction in animal cells. in *Trends Cell Biol*, Vol. 19 165-73 (England, 2009).
 231. Zang, J.H. & Spudich, J.A. Myosin II localization during cytokinesis occurs by a mechanism that does not require its motor domain. *Proc Natl Acad Sci U S A* **95**, 13652-7 (1998).
 232. Riento, K. & Ridley, A.J. Rocks: multifunctional kinases in cell behaviour. in *Nat Rev Mol Cell Biol*, Vol. 4 446-56 (England, 2003).
 233. Xu, Z., Vagnarelli, P., Ogawa, H., Samejima, K. & Earnshaw, W.C. Gradient of increasing Aurora B kinase activity is required for cells to execute mitosis. in *J Biol Chem*, Vol. 285 40163-70 (United States, 2010).
 234. Carleton, M. et al. RNA interference-mediated silencing of mitotic kinesin KIF14 disrupts cell cycle progression and induces cytokinesis failure. in *Mol Cell Biol*, Vol. 26 3853-63 (United States, 2006).
 235. Lefebvre, C. et al. A human B-cell interactome identifies MYB and FOXM1 as master regulators of proliferation in germinal centers. in *Mol Syst Biol*, Vol. 6 377 (England, 2010).
 236. Kondo, T. et al. Aurora B but Not Rho/MLCK Signaling Is Required for Localization of Diphosphorylated Myosin II Regulatory Light Chain to the Midzone in Cytokinesis. in *PLoS One*, Vol. 8 e70965 (United States, 2013).
 237. Hanahan, D. & Weinberg, R.A. The hallmarks of cancer. in *Cell*, Vol. 100 57-70 (United States, 2000).
 238. Hanahan, D. & Weinberg, R.A. Hallmarks of cancer: the next generation. in *Cell*, Vol. 144 646-74 (2011 Elsevier Inc, United States, 2011).
 239. Polyak, K. Breast cancer: origins and evolution. *J Clin Invest* **117**, 3155-63 (2007).
 240. Polyak, K. Heterogeneity in breast cancer. *J Clin Invest* **121**, 3786-8 (2011).
 241. Clevers, H. The cancer stem cell: premises, promises and challenges. in *Nat Med*, Vol. 17 313-9 (United States, 2011).
 242. Wang, J.C. Good cells gone bad: the cellular origins of cancer. in *Trends Mol Med*, Vol. 16 145-51 (2010 Elsevier Ltd, England, 2010).

243. Mine, T. et al. Breast cancer cells expressing stem cell markers CD44+ CD24 lo are eliminated by Numb-1 peptide-activated T cells. *Cancer Immunol Immunother* **58**, 1185-94 (2009).
244. Ricardo, S. et al. Breast cancer stem cell markers CD44, CD24 and ALDH1: expression distribution within intrinsic molecular subtype. in *J Clin Pathol*, Vol. 64 937-46 (England, 2011).
245. Wright, M.H. et al. Brca1 breast tumors contain distinct CD44+/CD24- and CD133+ cells with cancer stem cell characteristics. in *Breast Cancer Res*, Vol. 10 R10 (England, 2008).
246. Zhou, S. et al. The ABC transporter Bcrp1/ABCG2 is expressed in a wide variety of stem cells and is a molecular determinant of the side-population phenotype. in *Nat Med*, Vol. 7 1028-34 (United States, 2001).
247. Sotiriou, C. et al. Breast cancer classification and prognosis based on gene expression profiles from a population-based study. in *Proc Natl Acad Sci U S A*, Vol. 100 10393-8 (United States, 2003).
248. Honeth, G. et al. The CD44+/CD24- phenotype is enriched in basal-like breast tumors. in *Breast Cancer Res*, Vol. 10 R53 (England, 2008).
249. Abraham, B.K. et al. Prevalence of CD44+/CD24-/low cells in breast cancer may not be associated with clinical outcome but may favor distant metastasis. in *Clin Cancer Res*, Vol. 11 1154-9 (United States, 2005).
250. Jaggupilli, A. & Elkord, E. Significance of CD44 and CD24 as cancer stem cell markers: an enduring ambiguity. *Clin Dev Immunol* **2012**, 708036 (2012).
251. Dontu, G. et al. In vitro propagation and transcriptional profiling of human mammary stem/progenitor cells. in *Genes Dev*, Vol. 17 1253-70 (United States, 2003).
252. Li, X. et al. Intrinsic resistance of tumorigenic breast cancer cells to chemotherapy. in *J Natl Cancer Inst*, Vol. 100 672-9 (United States, 2008).
253. Ponti, D. et al. Isolation and in vitro propagation of tumorigenic breast cancer cells with stem/progenitor cell properties. in *Cancer Res*, Vol. 65 5506-11 (United States, 2005).
254. Jeter, C.R. et al. NANOG promotes cancer stem cell characteristics and prostate cancer resistance to androgen deprivation. in *Oncogene*, Vol. 30 3833-45 (England, 2011).
255. Leis, O. et al. Sox2 expression in breast tumours and activation in breast cancer stem cells. in *Oncogene*, Vol. 31 1354-65 (England, 2012).
256. Wonsey, D.R. & Follettie, M.T. Loss of the forkhead transcription factor FoxM1 causes centrosome amplification and mitotic catastrophe. in *Cancer Res*, Vol. 65 5181-9 (United States, 2005).
257. Bektas, N. et al. Tight correlation between expression of the Forkhead transcription factor FOXM1 and HER2 in human breast cancer. in *BMC Cancer*, Vol. 8 42 (England, 2008).
258. Carr, J.R. et al. FoxM1 regulates mammary luminal cell fate. in *Cell Rep*, Vol. 1 715-29 (2012 The Authors. Published by Elsevier Inc, United States, 2012).
259. Bao, B. et al. Over-expression of FoxM1 leads to epithelial-mesenchymal transition and cancer stem cell phenotype in pancreatic cancer cells. *J Cell Biochem* **112**, 2296-306 (2011).
260. Gemenetzidis, E. et al. Induction of human epithelial stem/progenitor expansion by FOXM1. in *Cancer Res*, Vol. 70 9515-26 (2010 Acr., United States, 2010).

261. Pandit, B. & Gartel, A.L. FoxM1 knockdown sensitizes human cancer cells to proteasome inhibitor-induced apoptosis but not to autophagy. in *Cell Cycle*, Vol. 10 3269-73 (2011 Landes Bioscience, United States, 2011).
262. Zhang, N. et al. FoxM1 inhibition sensitizes resistant glioblastoma cells to temozolomide by downregulating the expression of DNA-repair gene Rad51. in *Clin Cancer Res*, Vol. 18 5961-71 (2012 Aacr., United States, 2012).
263. Halasi, M. & Gartel, A.L. Suppression of FOXM1 sensitizes human cancer cells to cell death induced by DNA-damage. in *PLoS One*, Vol. 7 e31761 (United States, 2012).
264. Malanchi, I. et al. Interactions between cancer stem cells and their niche govern metastatic colonization. in *Nature*, Vol. 481 85-9 (England, 2011).
265. Sampieri, K. & Fodde, R. Cancer stem cells and metastasis. *Semin Cancer Biol* **22**, 187-93 (2012).
266. Derycke, L. et al. The role of non-muscle myosin IIA in aggregation and invasion of human MCF-7 breast cancer cells. in *Int J Dev Biol*, Vol. 55 835-40 (Spain, 2011).
267. Badve, S. et al. Basal-like and triple-negative breast cancers: a critical review with an emphasis on the implications for pathologists and oncologists. in *Mod Pathol*, Vol. 24 157-67 (United States, 2011).
268. Beach, J.R. et al. Myosin II isoform switching mediates invasiveness after TGF-beta-induced epithelial-mesenchymal transition. in *Proc Natl Acad Sci U S A*, Vol. 108 17991-6 (United States, 2011).
269. Betapudi, V. Myosin II motor proteins with different functions determine the fate of lamellipodia extension during cell spreading. *PLoS One* **5**, e8560 (2010).
270. Betapudi, V., Licate, L.S. & Egelhoff, T.T. Distinct roles of nonmuscle myosin II isoforms in the regulation of MDA-MB-231 breast cancer cell spreading and migration. in *Cancer Res*, Vol. 66 4725-33 (United States, 2006).
271. Kovacs, M., Thirumurugan, K., Knight, P.J. & Sellers, J.R. Load-dependent mechanism of nonmuscle myosin 2. in *Proc Natl Acad Sci U S A*, Vol. 104 9994-9 (United States, 2007).
272. Grimshaw, M.J. et al. Mammosphere culture of metastatic breast cancer cells enriches for tumorigenic breast cancer cells. in *Breast Cancer Res*, Vol. 10 R52 (England, 2008).
273. Minn, A.J. et al. Distinct organ-specific metastatic potential of individual breast cancer cells and primary tumors. *J Clin Invest* **115**, 44-55 (2005).
274. Wei, Q. & Adelstein, R.S. Pitx2a expression alters actin-myosin cytoskeleton and migration of HeLa cells through Rho GTPase signaling. *Mol Biol Cell* **13**, 683-97 (2002).
275. Fillmore, C.M. & Kuperwasser, C. Human breast cancer cell lines contain stem-like cells that self-renew, give rise to phenotypically diverse progeny and survive chemotherapy. in *Breast Cancer Res*, Vol. 10 R25 (England, 2008).
276. Sheridan, C. et al. CD44+/CD24- breast cancer cells exhibit enhanced invasive properties: an early step necessary for metastasis. in *Breast Cancer Res*, Vol. 8 R59 (England, 2006).
277. Murohashi, M. et al. Gene set enrichment analysis provides insight into novel signalling pathways in breast cancer stem cells. in *Br J Cancer*, Vol. 102 206-12 (England, 2010).
278. Stingl, J., Eaves, C.J., Zandieh, I. & Emerman, J.T. Characterization of bipotent mammary epithelial progenitor cells in normal adult human breast tissue. *Breast Cancer Res Treat* **67**, 93-109 (2001).

279. Vesuna, F., Lisok, A., Kimble, B. & Raman, V. Twist modulates breast cancer stem cells by transcriptional regulation of CD24 expression. *Neoplasia* **11**, 1318-28 (2009).
280. Ohata, H. et al. Induction of the stem-like cell regulator CD44 by Rho kinase inhibition contributes to the maintenance of colon cancer-initiating cells. in *Cancer Res*, Vol. 72 5101-10 (2012 Aacr., United States, 2012).
281. Myatt, S.S. & Lam, E.W. The emerging roles of forkhead box (Fox) proteins in cancer. *Nat Rev Cancer* **7**, 847-59 (2007).
282. Bello, B., Reichert, H. & Hirth, F. The brain tumor gene negatively regulates neural progenitor cell proliferation in the larval central brain of *Drosophila*. in *Development*, Vol. 133 2639-48 (England, 2006).
283. Barrett, L.E. et al. Self-renewal does not predict tumor growth potential in mouse models of high-grade glioma. in *Cancer Cell*, Vol. 21 11-24 (2012 Elsevier Inc, United States, 2012).